Fabrication of personalised medicines using additive printing technologies

---

UEA

University of East Anglia

Chak Hin Tam

MPharm

Thesis submitted to the School of Pharmacy, University of East Anglia
in fulfilment of the requirement for the degree of Doctor of Philosophy

February 2024

Acknowledgements

I would like to express my sincere appreciation to the following individuals for their guidance and support during my PhD journey.

First and foremost, I extend my gratitude to my supervisors Professor Sheng Qi and Dr Lazlo Fabian for their constant encouragement, invaluable advice and assistance throughout my research. I am also grateful to Dr Matthew Alexander for sharing his expertise on nanoelectrospray and to Professor Peter Belton for his insightful discussions and feedback on my thesis. I would like to acknowledge Mr Bertrand Leze for his technical support and assistance for the electronic microscope imaging during the project.

My fellow PhD students in the drug delivery group have been a great source of support and I would like to thank them for their help and camaraderie. Special thanks to Sherif Hamdallah for sharing his knowledge on HPLC, Dr Randa Zoqlam for her supportive chats and coffee, and Dr Xin Yi Teoh for her contributions to challenge my experiment plannings. I also appreciate the mentorship and guidance provided by the postdoctoral staff, especially Dr Janine Wilkinson for her support in the lab and Dr Rahul Tiwari for his teaching on polymer chemistry. Dr Bin Zhang introduced me to the world of 3D printing, and I am grateful for her support and guidance.

Finally, I would like to express my deepest gratitude to my family for their unwavering support and encouragement throughout my research journey. Their love and support have been my driving force, and I cannot thank them enough.

Abstract

Personalised medicines, tailored to the specific needs of each patient, have emerged as a potential solution for improving therapeutic outcomes. This thesis explores two additive printing technologies using model drugs and polymers stated blow to fabricate drug delivery systems with the potential of personalisation. Additionally, characterisation of the printing parameters of each printing system was performed to understand their influence on the printing volume.

The microdispensing technology was used to fabricate personalised orodispersible films by on-demand printing of viscous ink containing paracetamol-hydroxypropyl methylcellulose onto a releasing substrate. Orodispersible films with personalised dosage were fabricated by changing the printing areas, which showed a linear relationship with the drug loading. The tensile strength of the printed film was comparable to that of the cast film and showed good handling propertied compared to the marketed product.

The nanoelectrospray (nES) technology was another printing method explored, which enables on-demand and layer-by-layer coating to deposit drug-loaded coatings on contact lenses. Zein, the model polymer, was used to characterise the spraying parameters of the custom-build nES system. This work showed that the contact lenses maintained an excellent vision zone after the nES coating process, and the spray volume was predictable using established scaling laws.

Polylactic-co-glycolic acid and three model drugs, ketotifen fumarate, bimatoprost and latanoprost, were coated in the peripheral region on commercially available contact lenses to assess the *in vitro* drug release and the influence of steam sterilisation to the coating. The drug loading of ketotifen fumarate and bimatoprost, was independent of *in vitro* drug release. Steam sterilisation was used to sterile the nES-coated contact lenses, and results showed that the method significantly damaged the drug-polymer coating. Gamma rays could be used as an alternative to minimize the damage to the drug-polymer coating.

Table of Contents

List of publications

J. Wilkinson, **C.H. Tam**, A. Askounis, S. Qi, Suppression of the coffee-ring effect by tailoring the viscosity of pharmaceutical sessile drops, Colloids Surfaces A Physicochem. Eng. Asp. 614 (2021). https://doi.org/10.1016/j.colsurfa.2021.126144.

C.H. Tam, M. Alexander, P. Belton, S. Qi, Drop-on-demand printing of personalised orodispersible films fabricated by precision micro-dispensing, Int. J. Pharm. 610 (2021). https://doi.org/10.1016/j.ijpharm.2021.121279.

C.H. Tam, M.S. Alexander, S. Qi, Precision coating of ocular devices/contact lenses by nanoelectrospray additive printing, Mater. Des. 219 (2022). https://doi.org/10.1016/j.matdes.2022.110782.

C.H. Tam, M. Alexander, J. Sanderson, S. Qi, Selectively coated contact lenses by nanoelectrospray (nES) to fabricate drug-eluting contact lenses for treating ocular diseases, Medical Engineering and Physics. 124 (2024). https://doi.org/10.1016/j.medengphy.2024.104110.

List of Figures

14

List of Tables

Abbreviations

3D   Three-dimensional

API   Active pharmaceutical ingredients

ATR-FTIR Attenuated total reflectance Fourier transform infrared spectroscopy

BIM   Bimatoprost

CLs   Contact lenses

DECLs   Drug-eluting contact lenses

DSC   Differential scanning calorimetry

DSC   Differential scanning calorimetry

EHDA   Electrohydrodynamic atomisation

FDA   Food and Drug Administration

GRAS   Generally recognised as safe

HPLC   High-performance liquid chromatography

HPMC   Hydroxypropyl Methylcellulose

KF   Ketotifen fumarate

LN   Latanoprost

MD   Micro-dispensing

nES   Nanoelectrospray

NSD   Nozzle substrate distance

ODFs   Orodispersible film

PAR   Paracetamol

PBS   Phosphate buffer saline

PET   Polyethylene terephthalate

PLGA   Polylactic-co-glycolic acid

PMMA   Polymethyl methacrylate

SEM   Scanning electron microscope

Tg   Glass transition temperature

Chapter 1 Introduction

1.1. The need for personalised medicines

In modern pharmaceutical manufacturing, medications are typically produced in standardised strengths to meet the need of most patients. This one-size-fits-all model was based on clinical data from clinical trials that determine the therapeutic dosage of medications. While mass production of medications is a cost-effective way to meet demand, it fails to account for individual variations in response to medications. Patients may experience unwanted side effects from prescribed medications due to the limitations of this approach[1]. Personalised medicines, therefore, offer a solution to achieve a better therapeutic outcome by using optimised and tailored therapies, potentially resulting in fewer side effects.

The concept of personalised medicines was commonly used in pharmacogenomics to offer tailored pharmaceutical treatments based on the patient's genetic information[2]. For example, patients with human epidermal growth factor receptor 2 (HER2)-positive breast cancer would receive a different treatment than those who are HER2-negative[3]. However, this concept should not be restricted to matching the patient's genetic profile with gene therapy. It should also cover the selection of the correct choice of medications with tailorable doses and formulations at appropriate timings[4]. As individuals react differently to the same medication due to physiological differences and genetic factors, some patients may require a higher dose to achieve optimal therapeutic outcomes, while others may require less (Figure 1.1). Hence, individualising medications is key to helping patients achieve the best therapeutic outcome while reducing the potential of experiencing unwanted side effects.
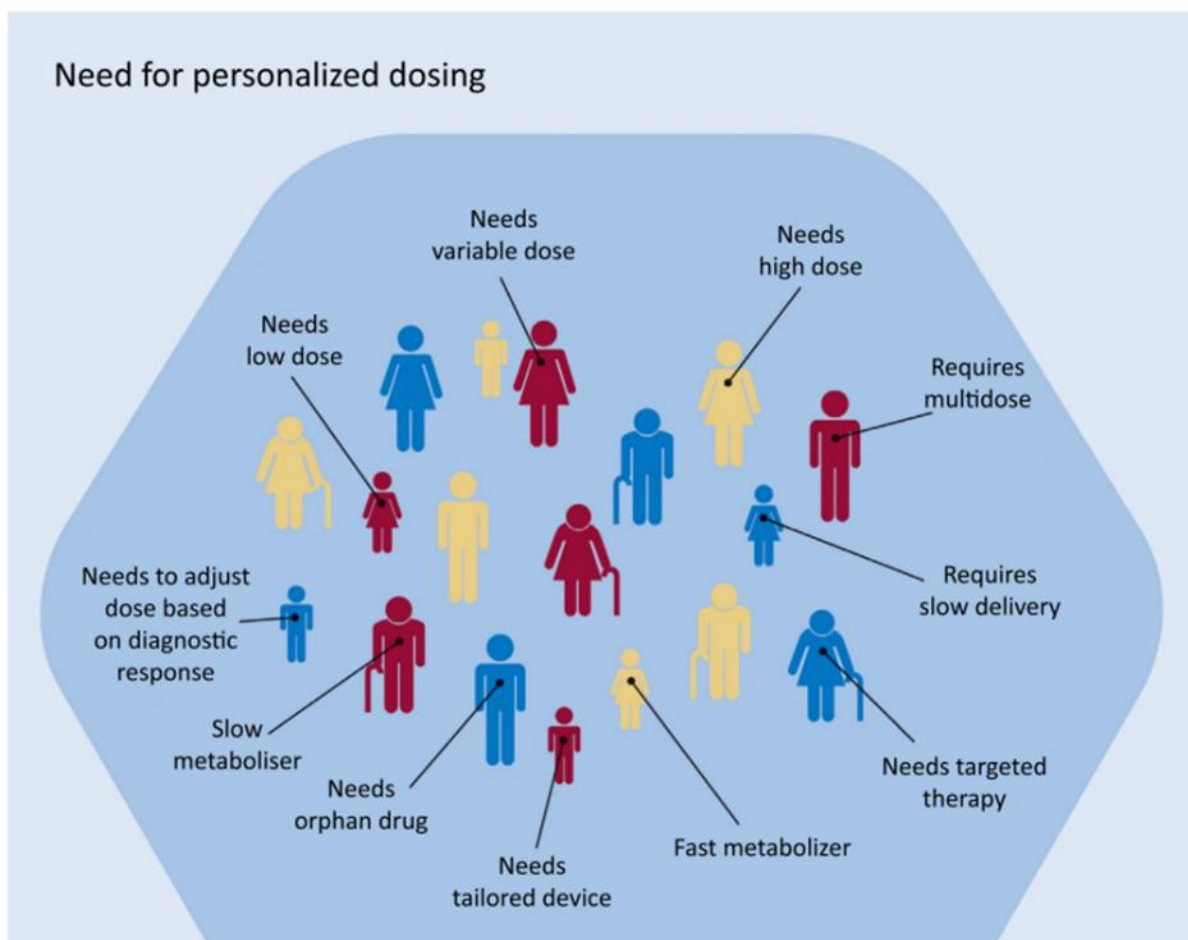
Figure 1.1. The importance of personalised medicines to accommodate the individual need. (Figure is adapted from[2] with permission.)

1.2. How can additive manufacturing be adapted to fabricate personalised medicines?

With the advancements in technology and the development of additive manufacturing (AM) technology, it may become possible to produce personalised medicines at hospital pharmacies or at the point-of-care in the future, as suggested by Sandler et al.[2]. The new model begins with obtaining personal information such as age, body weight, medical conditions and genetic information. The pharmacogenomics information obtained from the patient could provide insights on any dose adjustments of particular medications to achieve optimal therapeutic effect (Figure 1.2). This information is stored in the computer system of the point-of-care, mainly in the hospital, to create a comprehensive treatment profile for the patient. Once the patient receives a diagnosis from the doctor, the genetic information is shared with the on-site

pharmacy to produce personalised medicines with the help of artificial intelligence, which designs the ideal dosage form and appropriate dose. The individualised medications are printed on-demand once the patient information is received. The patient then collects the tailor-made medications and undergo a review if necessary. Any dose adjustments are recorded and implemented in the following collection, and this information can be fed back to the personal medication profile. To achieve a high level of flexibility in manufacturing medications, new equipment with a relatively small footprint and high precision is needed. Additive manufacturing is recognised by researchers as a highly suitable technology to accommodate the need for fabricating personalised medicines[5,6].
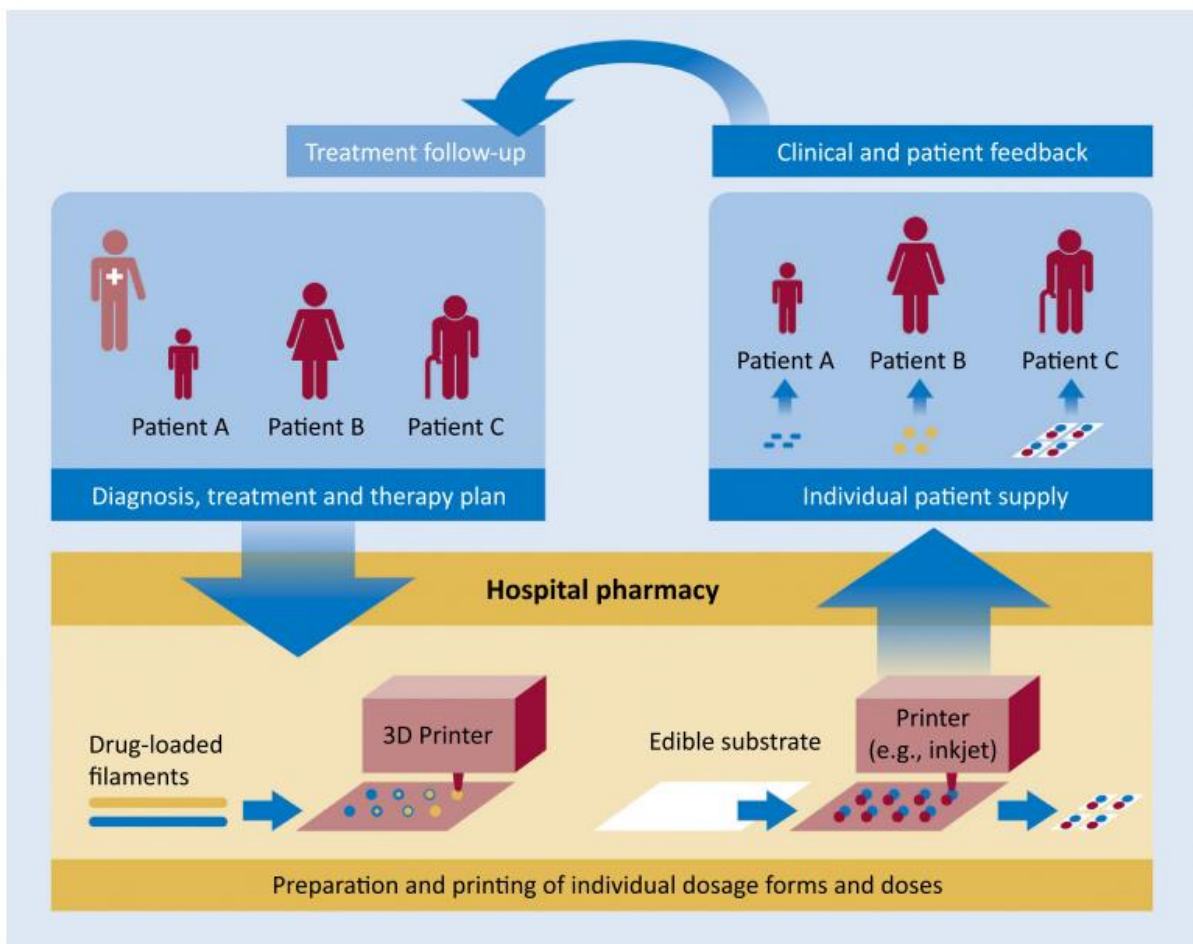
Figure 1.2. *The proposed model for implementing personalise medicines using printing technologies. (Figure is adapted from*[2] *with permission.)*

1.3. Who is going to benefit from personalised medicines?

Personalised medicine offers flexible dosing tailored to the patient's specific needs, providing particular benefits to patient groups that often require dose adjustments, such as paediatric and geriatric patients. Personalised medicine can also improve medicine compliance by reducing the likelihood of suffering from side effects.

Paediatric patients experience rapid metabolic changes during physiological development, necessitating a dose based on age or body weight range. Therefore, the required dose for paediatric patients is given according to age or body weight range. Although paediatric medications are commonly available in liquid form to facilitate swallowing and flexible dosage, measurement errors in liquid formulation leading may occur due to unclear graduations on syringes, spoons or measuring cups, and counting errors from droppers[7,8].

Geriatric patient is another patient group who may benefit from personalised medicine. The physiological degeneration of geriatric patients leads to slower metabolism, declining renal function and liver function with age. Dose adjustments are frequently necessary to avoid side effects while maintaining therapeutic efficacy, particularly to avoid interactions in polypharmacy[2]. Splitting tablets by carers to achieve the targeted dose is a common practice, but this increases the risk of dosing variation, especially for those film-coated tablets or modified-release formulations[9,10]. Polypharmacy is also common in geriatric patients and can lead to compliance issue. As medical advancements provide better healthcare through early disease detection, an increasing number of medications are prescribed to patients at their early age as prevention for age-related diseases, such as cardiovascular diseases and neurological disorders. Florence and Lee reported that patients aged 65 or older take thirteen medications on average[4]. It can be challenging for elderly patients to manage their medication regimen when they have to take four to six medications daily, of which one or two require administration three to four times daily. Although compliance aids are available in community pharmacies to help elderly patients to manage their medications, the increasing number of ageing populations implies a growing workload for healthcare professionals. It would benefit both patients and

healthcare professionals if the medication regimen could be simplified by combining medications with tailored doses in a few formulations, which could be achieved by printing multiple active pharmaceutical ingredients (APIs) in the same drug carrier.

1.4. Additive manufacturing as a mean to fabricate personalised medicines.

The use of AM has surged in recent years, pushing the boundaries of the research and development in the pharmaceutical industry[1,11]. AM techniques can be used to print various formulations, including tablets, oral films, medical implants, and even biomedical applications like tissue engineering. For examples, Gottschalk et al. used binder jetting technology to produce tablets containing different drug loadings (20% and 40%) of the poorly water-soluble drug ketoconazole[12]. The tablets with a 20% drug loading remained amorphous after 12 weeks of accelerated stability studies. Fused deposition modelling (FDM) was used to print aripiprazole, a poorly water soluble drug, loaded orodispersible films, and showed faster drug release kinetic compared to the solvent casting method[13]. Heo et al. developed a conductive hydrogel using a stereolithography-based 3D printer for neural tissue engineering[14]. The 3D-printed scaffold showed minimal toxicity to the neural cells and enhanced the neuronal differentiation under electrical stimulation. AM involves deposition of a wide range of materials layer-by-layer on the substrate to create the product with a 3D structure. Common methods of AM for pharmaceutical applications include FDM, powder bed fusion and drop-on-demand deposition. AM is a highly versatile and flexible technology that enables bespoke manufacturing of products on a small scale, which is particularly useful for fabricating personalised medicines. Moreover, AM is suitable for fabricating individualised doses of mediations with a narrow therapeutic index to reduce the regime complexity and optimise therapeutic outcomes[15]. The design of formulation, such as a tablet, starts from the design of a 3D model in 3D modelling software, followed by data processing in the slicer software to generate precise coordinates for the printing process. The shape and internal structures of the formulation are adjustable according to the patient's requirements.

SPRITAM® is the first commercial example of using AM to fabricate 3D-printed medications[16]. It is the first commercially available product using powder bed

technology, which fuses layers of powder vertically using a binding ink. The technology provided a novel method to produce orodispersible tablets and received FDA approval in 2015[17]. SPRITAM® is available in fixed strengths from 250 mg up to 1000 mg and no personalised dose is available yet given that the technology has the potential to do so. In 2021, FDA approved a 3D-printed tablet for treating rheumatoid arthritis[18]. The tablet was printed using melt extrusion deposition, which deposits a molten mixture of the API, polymer, and other excipients on the substrate to form tablets. The printing technology also enables precise control of the internal geometries of the tablet and shape to modify the drug release kinetics.

Other technologies, including FDM and drop-on-demand deposition, were investigated extensively in scientific research and detailed reviews are reported elsewhere[5,18–20]. Each printing technology offers its own set of advantages and disadvantages, and the decision to use which technology depends on the final formulation. FDM is a straightforward and cost-effective technique for producing pharmaceutical formulations, such as tablets[21]. A wide range of materials, such as thermoplastics and pharmaceutical polymers, can be used to create the filament for FDM printing. A gear system drives the drug-loaded filament through the heated nozzle to fabricate the solid dosage form. The method is suitable for printing medications with poor aqueous solubility[22]. However, the processing method can potentially degrade thermolabile APIs during the printing process. Drop-on-demand deposition, primarily inkjet-based printing, operates by depositing liquid droplets to construct the 3D object. The ink contains a solution of polymers, solvents, and APIs. A heat source is frequently employed to expedite the solidification of the deposited ink on the surface. The printing can be executed in a single layer or multiple layers, depending on the required formulation. Inkjet-based printing has been used in the fabrication of personalized orodispersible films by depositing drug-loaded ink onto edible substrates[23]. Printing tablets is also feasible by jetting binder ink onto the powder bed to fuse the powder, constructing solid oral dosage form[12]. While inkjet-based printing uses very small nozzles for high-resolution printing, it also restricts the range of physical properties of the ink formulation to ensure proper deposition.

No single printing technology can serve all purposes to print pharmaceutical formulations. Of all the additive printing technologies available, this thesis will focus on two different printing technologies for two separate drug delivery systems:

- Using the microdispensing (MD) technology to enable single-step fabrication of personalised orodispersible films using highly viscous ink without edible substrate, which is not achievable by inkjet printing.
- The nanoelectrospray system is designed to selectively coat the hydrogel contact lenses to deliver ophthalmic medications, overcoming the challenge of masking the contact lenses during coating to preserve the vision zone.

1.5. Orodispersible films as a drug delivery system

Orodispersible films (ODFs) have gained popularity in the past decade as an alternative solid dosage form to deliver oral medications[24]. ODFs consist of one or multiple layers that provide additional functionalities, such as adding taste masking layers to enclose the drug-loaded layer. ODFs are a unique oral formulation that dissolves rapidly in the mouth without the need of water. This unique advantage is particularly beneficial to several patient groups, including those with Parkinson's disease whose oesophageal muscles deteriorate to a point where swallowing will be difficult, and psychiatric patients who often struggle with medications compliance[25]. On the other hand, swallowing difficulties are also common in paediatric patients[17], especially infants whose swallowing reflex is not fully developed, posing a challenge to administering oral formulation[26]. ODFs have the characteristic of fast disintegration in the mouth or under the tongue without the need for swallowing, facilitating the absorption of APIs to the systemic circulation and resulting in faster onset of action[27].

ODFs have gained popularity in both over-the-counter and prescription medication markets. Pfizer's Listerine® Pocket film is a well-known example of an ODF that does not contain any APIs and is used as a mouth freshener. Other over-the-counter examples include Gas-X, Pedia-Lax and Triaminic[28]. The first prescription drug, ondansetron (Rapidfilm®), in the form of ODF, was approved in the EU in 2010[27]. Several prescription-only medications have been marketed subsequently, such as

risperidone and fentanyl. While many ODFs are manufactured on a large scale with fixed doses to comply with the current regulatory framework, there is a growing interest in producing personalised ODFs to meet individual patients' clinical needs. The growing interest of the small-scale production of personalised ODFs at the point-of-care is evidenced by the increasing number of publications on this topic in recent years. There was only 1 publication on personalised orodispersible films (ODFs) in 2013, but this figure grew over the years, reaching an average of 11 publications per year over the last 5 years, based on the data available on PubMed (Appendix Figure A.1.).

1.6. Methods to manufacture ODFs

There are several methods available for the manufacturing of ODFs, depending on the physical and chemical properties of the APIs as well as the choice of polymers.

1.6.1 Solvent casting

Solvent casting is the most common method with a simple equipment setup for preparing ODFs[29]. The APIs, film-forming polymer and excipients are dissolved in a suitable solvent system, such as water, ethanol, and acetone, to produce the casting solution. The solvent system has to be compatible with the API and the film forming polymer to create a homogenous casting solution. As water is the most commonly used solvent for solvent casting, cellulose-based polymers such as hydroxypropyl methylcellulose (HPMC)[30] and hydroxypropyl cellulose (HPC)[31] and pullulan are most often used[32]. The casting solution is then poured onto a substrate and spread evenly using a film applicator or a doctor blade to produce the master film. The resulting film is dried under elevated temperature or ambient conditions before being cut into the desired dimensions. Tailoring dosage is achievable by cutting the master film into the target dimensions before packing the films. While the solvent casting method is commonly used for lab-scale production and is suitable for heat-sensitive APIs, it has some significant disadvantages. The use of significant amount of solvents can pose potential hazards to the health of the operators and lengthy processes of solvent evaporation can be time-consuming. In addition, the casting method is not applicable for APIs that are sensitive to hydrolysis. Therefore, alternative methods

such as hot-melt extrusion and electrospinning have been developed to overcome some of the limitations to produce ODFs.

1.6.2 Hot-melt extrusion

Alternatively, hot-melt extrusion is a solvent-free method to prepare ODFs. The polymers, APIs, and other ingredients, such as plasticisers, are mixed inside an extruder with heating to form a homogenous mixture before being extruded through a die to create thin films[33]. The resulting films are cooled and trimmed into the required dimensions. Hot-melt extrusion is particularly useful for drug candidates with low aqueous solubility as it improves their solubility by producing a solid dispersion as a film. Besides, no solvent is involved in the mixing process, making it a safer option compared to solvent casting. Scaling up the production of ODFs is relatively easy for hot-melt extrusion and the manufacturing process is continuous to streamline the production of ODFs. However, hot-melt extrusion is undesirable for thermolabile APIs due to the elevated temperature used in the mixing step. Additionally, the film forming polymers for hot-melt extrusion are also restricted to those that are stable at high temperature and have thermoplastic characteristics[34]. For example, polyethylene oxide, maltodextrin and modified starch (hydroxypropyl starch) were used for preparing ODF by hot-melt extrusion[34,35]. Polymers that have high melting temperatures or glass transition are less preferable for hot-melt extrusion as the high process temperature can lead to degradation of the API. Plasticisers are often added to the formulation to improve the processability by reducing the glass transition temperature.

1.6.3 Electrospinning

Electrospinning is a method to produce ODFs using electrical force. In this process, the precursor solution containing polymers and API(s) is subjected to the applied voltage and forms continuous fibres at the apex of the nozzle. The fibres are then collected onto a substrate, and solvent evaporation takes place during the process, creating a non-woven mat. The resulting thin film produced by electrospinning has a highly porous internal structure that disintegrates almost instantly upon contact with water[36]. This feature also facilitates the dissolution of poorly water-soluble APIs[37].

28

The choice of solvent, favouring aqueous-organic or pure organic systems, is crucial to facilitate solvent evaporation during fabrication. This narrows down the choice of polymers which has good solubility in both aqueous and organic solvents. Additionally, polymers with high molecular weight are preferrable as they provide sufficient viscosity to the electrospinning solution and chain entanglements for stable fibres formation[38].

1.6.4 Additive printing for personalised ODFs

To fabricate personalised ODFs, AM technologies have been explored as novel methods to produce ODFs, such as inkjet printing[39–41], semisolid extrusion 3D printing[42], and fused deposition modelling 3D printing[43]. These methods provide flexibility in making ODFs with personalised drug doses to accommodate different patient groups and small-batch manufacturing at or close to the point-of-care, such as hospital pharmacies[44–46].

Among these novel methods mentioned above, inkjet printing is one of the additive printing technologies researched extensively to produce personalised ODFs[47]. Continuous and drop-on-demand are the two common types of inkjet printing technology available commercially. Drop-on-demand inkjet printing technology can deposit droplets with picolitre volume on the substrate with high precision and is the most discussed inkjet printing method in the literature for fabricating ODFs. Two types of inkjet printers are commonly available in the drop-on-demand category: thermal and piezoelectric inkjet printing systems[48,49]. The thermal system relies on heat to generate a bubble in the dispensing chamber to eject the ink out of the nozzle. Instead, the piezoelectric system has no heat involved and the piezoelectric material deforms in response to the applied voltage, indicating the piezoelectric inkjet system can handle a wider range of materials than thermal inkjet printer. The piezoelectric material is usually coupled to a diaphragm to expel the ink via the nozzle to eject droplets[50].

In most literature, a commercial inkjet printer was used with a modified ink cartridge to dispense droplets containing drugs[51–53]. Two methods were commonly reported in the literature to produce ODFs by inkjet printing. The mainstream method is to

dispense drug-loaded ink on-demand on edible supporting substrates, such as HPMC-based films and starch films[23]. The ink contains the API with viscosity modifiers to facilitate a stable deposition of droplets onto the supporting substrate which is usually prepared by solvent casting[54]. The solvent of the ink evaporates with time, leaving the drug molecules on the surface of the edible substrate. The printing is often repeated layer-by-layer to deposit enough APIs on the edible substrate. A less common approach is to print the ink-containing polymers and drugs onto the substrate directly to form ODFs[41,55]. The ink usually contains a film-forming polymer and APIs in a low concentration to maintain the viscosity within the printable range. Organic solvents or surfactants are often necessary to reduce the surface tension of the ink. For example, Cader et al. printed an ink-containing polyvinylpyrrolidone, polysorbate 20, glycerol, thiamine hydrochloride and water on a polyethylene terephthalate sheet with appropriate droplet spacing to fuse all the droplets, resulting in pore-less ODFs[55].

Inkjet printing enables printing patterns with high resolutions. Quality assurance and tracking of medication can be achieved by printing APIs with unique patterns on HPMC films, such as quick response (QR) codes containing patient information[56]. The QR code was printed with drug-loaded ink on the edible substrate and it contained information on patient details, medication, dosage, and batch details to ensure that the correct medication was administered to the patient (Figure 1.3).
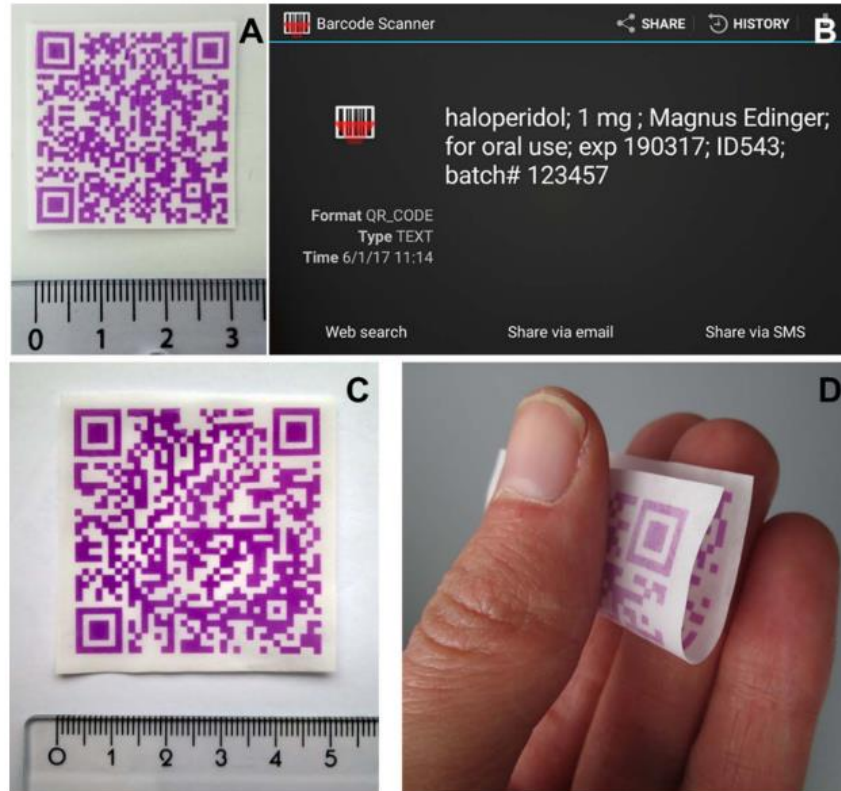
Figure 1.3. *Using modified inkjet printer to fabricate drug-loaded ODF with a QR code. (Figure is adapted from*[56] *with permission.)*

However, inkjet printing faces several significant limitations when it comes to fabricating personalised ODFs. Firstly, the physical properties of the ink are highly restricted for smooth printing. The viscosity of the ink has to be below 20 mPa.s and the surface tension should be in the range of 20-50 mN/m to avoid nozzle blockage[57]. Secondly, the drug loading of inks is limited, due to restricted viscosity, leading to high solvent content and extended drying times. A high drug loading of the ink increases the risk of drug crystallisation at the nozzle, affecting the printing precision. Multi-pass printing is usually required for high-dose formulations to deposit sufficient APIs on the ODFs. However, multi-pass printing results in a higher volume of solvent being used and requires a longer production time associated with longer printing time and solvent evaporation. Moreover, the interactions between the drug ink and the edible supporting substrate could increase the complexity of the ODFs printing and potentially affect the physical appearance of the final film. Genina et al. studied the printing performance of rasagiline on different substrates by inkjet printing and

concluded that the selection of substrates could significantly impact the uniformity of printed dosage[40].

1.7 Using MD system as an alternative method to manufacture solid dosage forms

In order to overcome some of the challenges of inkjet printing to fabricate ODFs, a liquid deposition method with high precision and the capability to dispense viscous ink is needed. In Chapter 3, a piezoelectric MD system was investigated to determine whether it can overcome some of the challenges faced by inkjet printing in ODFs fabrication with personalised dose adjustment capability. MD enables precise dispensing of a range of low and high viscosity (up to 2,000,000 mPa.s) materials to produce droplets, beads, and lines at high speed[58]. There are two main types of MD printhead: the piezoelectric-driven printhead and solenoid actuated printhead[59]. The piezoelectric actuated printhead contains a piezoelectric tappet rod in the dispensing chamber to control liquid flow by moving upwards and downwards in response to electrical signals. The solenoid-actuated printhead relies on the magnetic field change to control the opening of the dispensing valve for liquid dispensing. Both systems require pneumatic control to propel the liquid out of the orifice to form droplets and excel at different fabrication tasks[59]. The main advantage of using MD for ODFs fabrication is the ability to accurately dispense a low volume of viscous liquid without an edible supporting substrate. Although, to the best of our knowledge MD has yet to be reported for a one-step ODFs fabrication, it was explored to fabricate tailored dose medications. Bonhoeffer et al. proposed three new concepts to manufacture pharmaceutical formulations using a piezoelectric MD system (Figure 1.4)[60]. Naproxen nanosuspension was dispensed directly by a MD system onto excipients-loaded capsules, placebo tablets and edible polymer films rolled up into a capsule. Results showed that out of the three carriers, the capsule could load 30 mg of naproxen which is the maximum strength used in the experiment. Higher drug loading is achievable by using capsules with larger volumes or increasing drug concentration to reach the therapeutic dose[60]. The concept demonstrated the potential use of MD technology in the manufacturing line of pharmaceutical formulations. Apart from the above work, there is limited literature regarding the pharmaceutical application of MD technology.
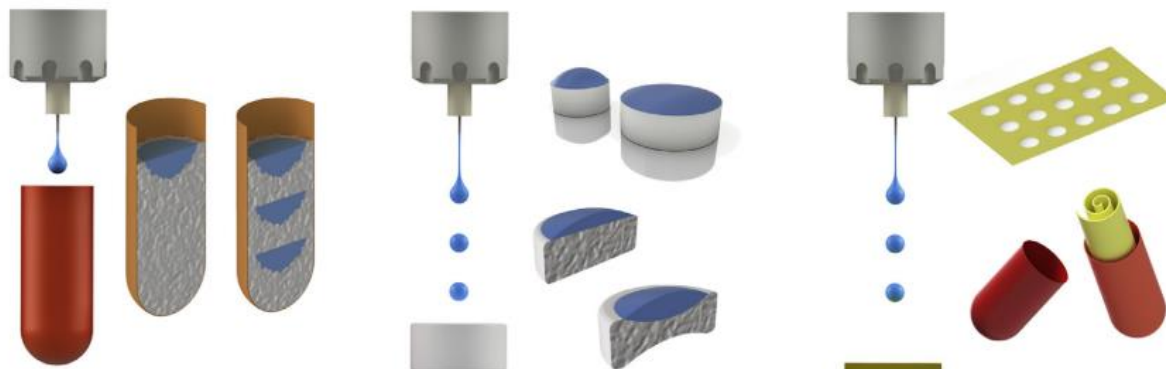
Figure 1.4. *The novel approaches to fabricate personalised oral solid dosage form suggested by*[60] *with permission.) A: Depositing naproxen nanosuspension directly into capsules containing excipients only; B: Depositing the drug ink on the surface of placebo tablets; C: Depositing the drug ink on the surface of ODFs before rolling and storing the drug-loaded film in the capsule.*

1.8 Additive printing for ophthalmic drug delivery

Eye drop remains the dominant formulation for delivering ophthalmic drugs globally. However, the unique ocular physiology and anatomy present several challenges for delivering drugs effectively via this route.

One of the major challenges is the rapid turnover rate of tears in the eye, which can wash away drug molecules and reduce the residence time of the drug on the cornea. The tear turnover rate is rapid (about 1 ml/min) to maintain moisture on the cornea and as a defence mechanism to wash away foreign objects on the cornea[61]. The tear fluid has a rebalancing mechanism to maintain an adequate amount of tear fluid. The tear volume is typically 7 µl in the posterior segment of the eye[62]. Upon instillation of eye drop onto the cornea, the total volume of liquid can surge up to 30 µl. Furthermore, the blink reflex drains the excess liquid, significantly reducing the resident time of drug molecules on the cornea. A portion of the drug can be absorbed systemically via the highly vascularised conjunctiva, leading to lower bioavailability and potential side effects. Therefore, the bioavailability of eye drops could be as low

as 1 - 5%, depending on the ophthalmic drug[63]. The low bioavailability also means a significant amount lot of APIs are wasted, which is not favourable for expensive APIs. In addition, non-compliance is a significant issue for patients as they may find it challenging to instil eye drops correctly[64]. It was found that the eye drop often lands on the eyelid and cheek. This can lead to missed drops and reduced efficacy of the treatment. While eye drop applicators are available to improve aiming the drop at the eye, they do not solve the problem of missed drops due to the blink reflex. This problem remained largely unsolved and patient non-compliance remains a challenge.

Alternative ocular drug delivery systems have been reported in the literature to improve bioavailability by using novel drug delivery systems. For example, ocular inserts, punctual plugs, in-situ forming gel and drug-eluting contact lenses (DECLs)[62]. Among these systems, DECLs have gained substantial interest in recent years due to their ability to act as a drug reservoir and prolong the resident time of APIs on the cornea, leading to improved bioavailability. Using DECLs can reduce the rate of drugs washed away by the tear fluid, which improves bioavailability. The main benefit of using DECLs was shown by Gause et al. in that the bioavailability of DECLs can be as high as 50%, compared to eye drops[63].

The idea of DECLs originated in the 1960s and has flourished in the past decade[65]. In 2021, Johnson & Johnson Vision launched the first commercial DECLs containing 19 μg of ketotifen fumarate for preventing ocular itchiness associated with allergies during contact lens wear[66]. The method to prepare the DECLs was the simple soaking method. The poly(2-hydroxyethyl methacrylate) (HEMA) contact lenses are soaked into the drug-loaded saline solution with a pre-defined drug concentration[67]. However, loading ketotifen fumarate to the contact lens relies on electrostatic interaction between drug molecules and the lens material. At pH 7.4, ketotifen is positively charged and the methyl acrylic group of the contact lens is negatively charged. This is highly drug-specific, making it not applicable to other ocular drugs that do not carry charges at pH 7.4. Nevertheless, the soaking method is relatively simple to prepare DECLs and is easy to scale up the production.

1.9 Methods to fabricate DECLs

A wide range of methods has been reported in the literature to produce DECLs using various ophthalmic drugs, including the soaking method, encapsulation of drug-loaded films in the contact lens, nanoparticles approach, supercritical fluid, molecular imprinting, and direct coating[68–71]. However, with most of these methods, the physical properties, such as optical transmittance and oxygen permeability, of the treated contact lens are often adversely affected[72,73].

1.9.1 Soaking method

The soaking method is the first and the most common method to prepare DECLs by immersing the contact lens into the drug solution. Johnson and Johnson vision launches the first commercially available DECLs using the soaking method to include ketotifen fumarate[74]. The drug molecules are loaded into the contact lens matrix by passive diffusion (Figure 1.5.). While the soaking method is simple and cost-effective, it has several limitations that need to be addressed.

One of the major limitations of the soaking method is the uncontrolled drug release rate. The drug uptake and release are highly dependent on the physicochemical properties of the contact lens material and the APIs. Considerable research has been done to study the relationship between lens materials and the physicochemical properties of the drug. It was found that the drug uptake is material-dependent, and that hydrophobic drugs are more favourable for silicon lenses, while hydrophilic drugs are better suited for lenses made of materials like poly(HEMA)[75]. Moreover, the soaking method also limits low drug loading capacity. Most of the literature reported using small molecules for the soaking method and reported that large molecules such as hyaluronic acid[76], are difficult to be loaded effectively into contact lenses by the soaking method[77].

In addition to the uncontrolled drug release rate, the soaking method also results in an immediate burst release of the drug upon immersion into the release media. To overcome the issue, an additional coating of vitamin E was used as a diffusion barrier

on the contact lenses to prolong the release of several ocular drugs[78–80]. Although the *in vitro* release results were promising, the method compromised the physical properties, such as the ion permeability, when high loading of vitamin E was used[81]. Alternatively, soaking the contact lenses in a nanosuspension was attempted to prepare DECLs[68]. Maulvi et al. prepare timolol-loaded DECLs by soaking the poly(HEMA) lenses in a timolol-loaded gold nanoparticle suspension. The result revealed that soaking the contact lenses in the timolol-loaded gold nanoparticle suspension enhance the drug uptake compared to soaking in timolol solution alone. However, such approach does not extend the *in vitro* release of timolol.
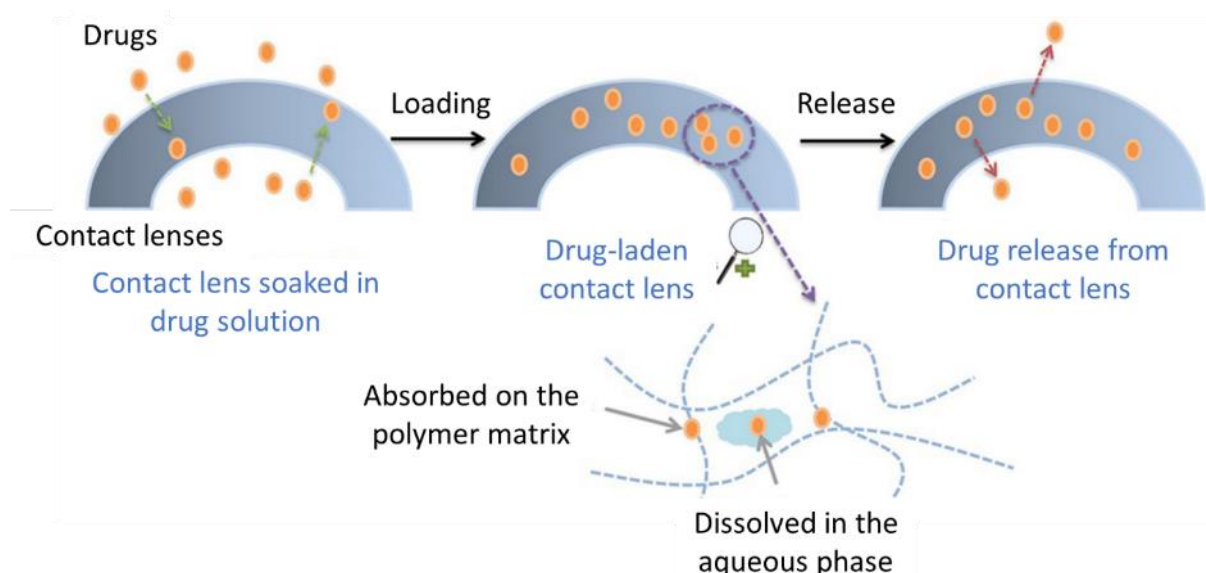
Figure 1.5. *Uptake and release of APIs from DECLs using the soaking method. (Figure is adapted from*[82] *with permission.)*

1.9.2 Molecular imprinting

Incorporation of functional molecules or drug-loaded nanoparticles during the polymerisation process of contact lenses offers a promising approach for preparing DECLs. This method allows for the creation of specific sites for drug loading within the polymer matrix of the contact lens using functional monomers, drug template and crosslinkers (Figure 1.6). This creates pockets that have strong intermolecular interactions with drug molecules to slow down their dissociation[83,84]. The drug

templates are extracted and replaced by the target APIs using the soaking method. The strong intermolecular interactions between the APIs and cavities can extend the drug release to weeks. However, the interaction between the contact lens monomer and the functional groups of APIs can vary significantly, implying optimisation of the functional monomers, drug template and crosslinkers is necessary for each API. This method is not suitable for loading more than one APIs since it will have impact on the physical properties of the contact lens, when multiple crosslinkers and monomers are used[72].
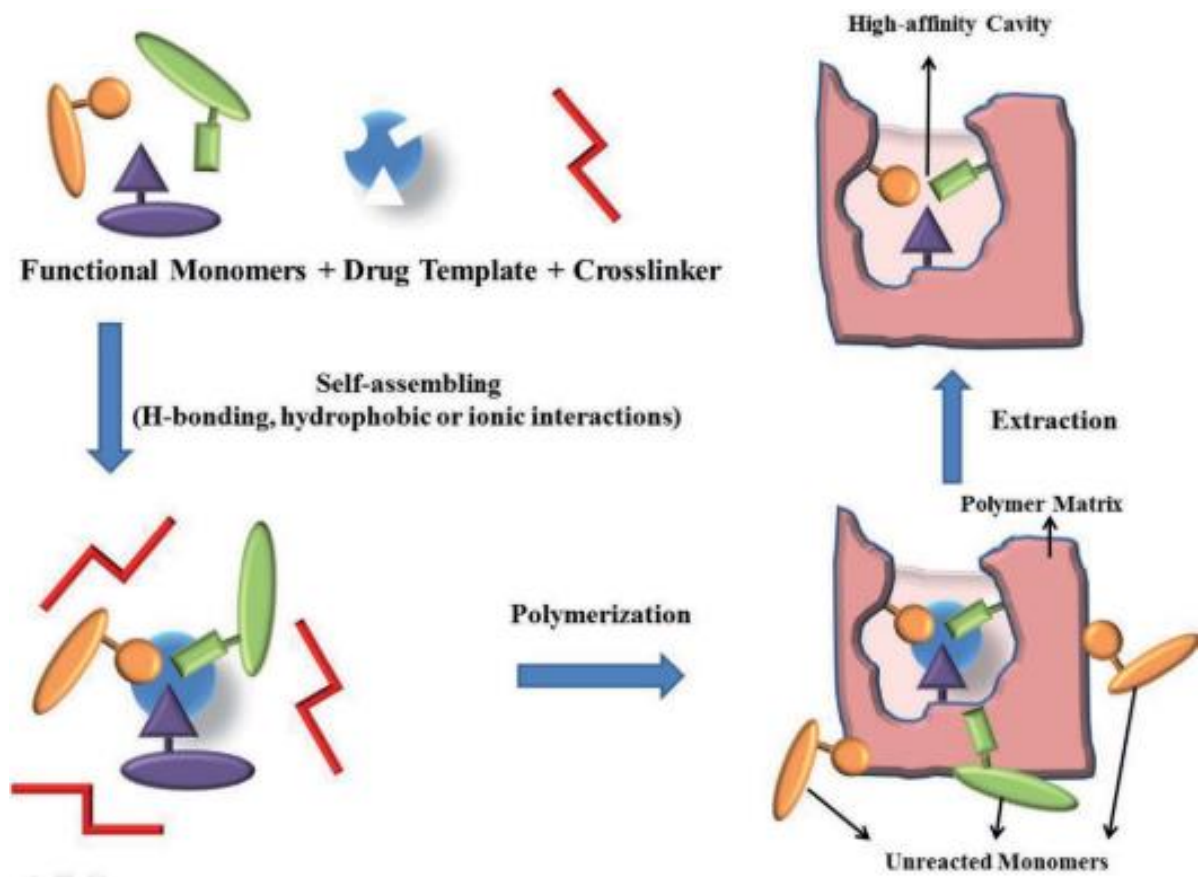
Figure 1.6. *Illustration of the molecular-imprinting method to create favourable binding site for the target APIs. (Figure is adapted from*[85] *with permission.)*

1.9.3 Nanoparticles-laden

The nanoparticles-laden method is similar to molecular imprinting in that the APIs are dispersed into the contact lens materials during the polymerisation step. The drug-loaded nanoparticles can be incorporated into the contact lenses matrix via polymerisation with the contact lenses formulation or the soaking method. This method

has shown encouraging results in the sustained release of certain ophthalmic drugs[86,87]. However, drug leaching was observed during the monomer extraction step and the terminal sterilization step. The presence of nanoparticles in the contact lens matrix can impact critical properties such as swelling, optical transmittance, and mechanical properties[88].

1.9.4 Encapsulation of polymeric films

Encapsulation of polymer film in contact lenses is another method which shares a similar principle to nanoparticle-laden contact lenses. This approach involves preparing a drug-loaded polymer film by the solvent casting method, followed by cutting the film into a doughnut shape. The polymerisation step of monomer is divided into two steps which the polymer film is placed onto the contact lens after the first polymerisation, followed by a second polymerisation of monomers to enclose the polymer film in the contact lens (Figure 1.7). Poly(lactic-co-glycolic acid) (PLGA) and Eudragit S100/ethyl cellulose are examples of polymers that have been used to prepare this type of DECLs[89–91]. Moreover, loading multiple drugs in the contact lens matrix is also possible by including different drug-loaded polymer films[90]. However, there are several challenges associated with this approach. The drug-loaded polymer film can affect the physical properties of the contact lens, such as its mechanical strength and oxygen permeability. The optical transmittance of the contact lens depends on the coverage of the polymer film. The author claimed that the contact lens in Figure 1.8 has a clear aperture, but the diameter of it was not defined.
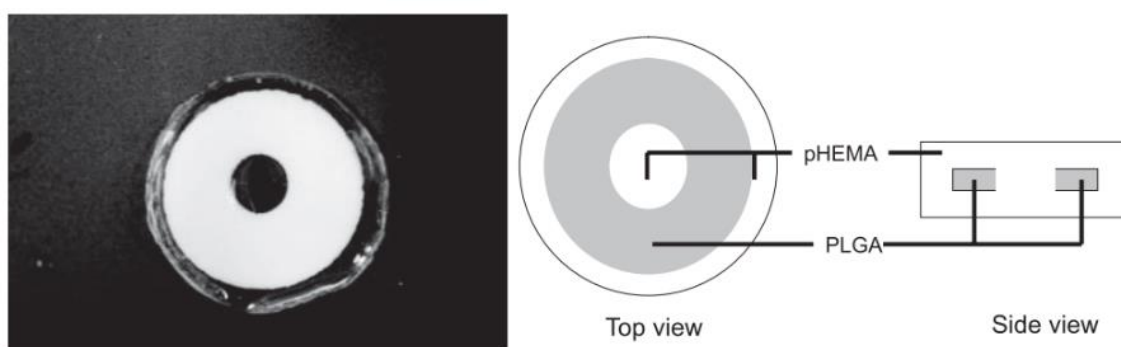
Figure 1.7. *Encapsulation of ciprofloxacin-loaded PLGA film in poly(2-hydroxyethyl methacrylate) (pHEMA) contact lenses. (Figure adapted from*[89] *with permission.)*

1.9.5 Additive coating drug-loaded polymer films on contact lens by electrospinning

Direct coating of drugs and polymer onto contact lenses was demonstrated to be an alternative approach to preparing DECLs. The formulation of the precursor solution contains the drug and polymers and or other excipients to be coated topically onto the interior surface of contact lenses using electrospinning. One advantage of this approach is its versatility, as it allows the use of a wide range of polymers and commercially available contact lenses off the shelf. Mehta et al. demonstrated the use of electrospun fibres containing a mixture of polyvinylpyrrolidone, poly (N-isopropyl acrylamide), four permeation enhancers and timolol to coat the interior surface of silicon contact lenses (Figure 1.8)[70]. However, the unselective coverage of the polymer coating on the contact lenses requires a mask to preserve the vision zone[70]. Moreover, the large coverage of the polymer coating can affect the critical properties of the contact lens, such as its mechanical strength and oxygen permeability.
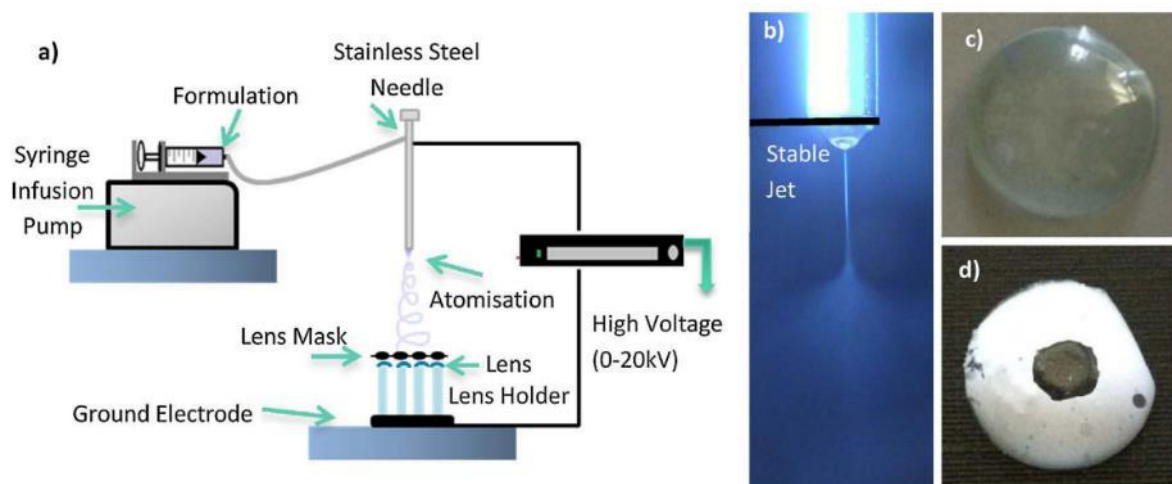
Figure 1.8. A: Illustration of the non-elective electrospinning coating method to prepare DECLs; B: digital image of the nozzle for electrospinning; C&D: uncoated and coated DECLs, respectively. (Figure is adapted from[70] with permission.)

1.10 Nanoelectrospray – an on-demand deposition technique to fabricate DECLs

To precisely deposit the polymer and drug coating on commercially available contact lenses to minimise the interference of the intrinsic properties of the contact lenses, a novel method using nanoelectrospray (nES) was investigated. The nES can deposit a small amount of material with a flow rate down to picolitre per minute[92]. It is an on-demand spraying technique that can achieve patterned and controllable deposition. The materials and the mode of depositions are highly flexible, which gives the potential of the technology to be used for the production of individualised or personalised medical products. The miniaturized size of nES allows deposition of materials on confined and selective areas. Unlike conventional electrospray and electrospinning, nES can achieve confined spraying areas on the contact lenses without masking the vision zone, implying less waste of APIs and polymers generated. Depending on the processing parameters and material properties, the deposited layer can either be a smooth, continuous layer of materials without pinholes or a textured layer composed of semi-fused nanoparticles. Multiple coating layers can be deposited by nES layer-by-layer to build up the required thickness.

nES is a type of electrospray that shares the same working principle, known as electrohydrodynamic atomisation (EHDA). EHDA is a one-step technique to produce nano-carriers, namely nanoparticles and nanofibers, using electrostatic force to overcome the surface tension of the precursor liquid. EHDA has been studied extensively to explore its pharmaceutical applications and develop new drug delivery systems[93,94]. EHDA is commonly used to fabricate nanoparticles and nanofibers with high particle size uniformity, modifiable kinetic to control drug release and improved dissolution rate[60]. Using EHDA to produce thin coatings on surfaces is relatively less common, but it is possible with the help of motorised multi-directional substrates. Besides, ambient working condition enables EHDA to process biochemical molecules such as DNA, proteins, and cells[94].

The experimental configuration of traditional electrospraying comprised four main components, including a pumping system to provide a controllable flow rate of the

liquid sample, a metal nozzle connected to the high voltage supply, a high voltage supply to provide sufficient electrostatic force to overcome surface tension; and a grounded substrate to collect the resulting products. A range of nozzles with different designs has been manufactured to accommodate pharmaceutical purposes, named co-axial and tri-axial nozzle, to produce core-shell particles or fibres[95,96]. Direct current is commonly used and reported in the literature for EHDA, but the use of alternate current has been explored[97–99]. The grounded collector can be a drum, a flat surface, or a solution to collect the resulting product, depending on the required pattern or geometry of the end product. For nES, the flow rate of the precursor liquid is entirely controlled by the applied voltage, omitting the need for a pumping system. As mentioned earlier, nES is an on-demand spraying technique, whereas traditional electrospray is often a continuous process. The detail of the experimental configuration is reported in Chapter 2.

1.11 Principle of nES

The nES process involves applying an electric field to the working fluid, typically held in a capillary tube, to overcome the surface tension and initiate the ejection of a charged liquid jet, which can subsequently break up into a plume of charged droplets (Figure 1.9). The nES process shares the same working principle as electrospray and electrospinning, but in nES, the sprayed liquid flow rate is dictated solely by the applied electric field, and in the absence of applied voltage, no flow or liquid ejection from the nozzle occurs[100,101]. The applied voltage has to pass the threshold to initiate the spray. Further voltage increase positively correlates with the flow rate, but it also affects the spraying mode. Similar to conventional electrospray, nES can operate in several modes, including the most studied stable cone-jet mode (which occurs over a limited range of field strength and flow rate) and may also exhibit quasi-steady pulsating spray modes[102]. An oscilloscope can be used to monitor the spraying mode of nES and to understand the reproducibility of the spray. The key to nES printing, the precise control of nES in a drop-on-demand fashion has also been demonstrated[103], where minute volumes, as low as femtolitres, were reproducibly isolated and deposited onto a substrate.
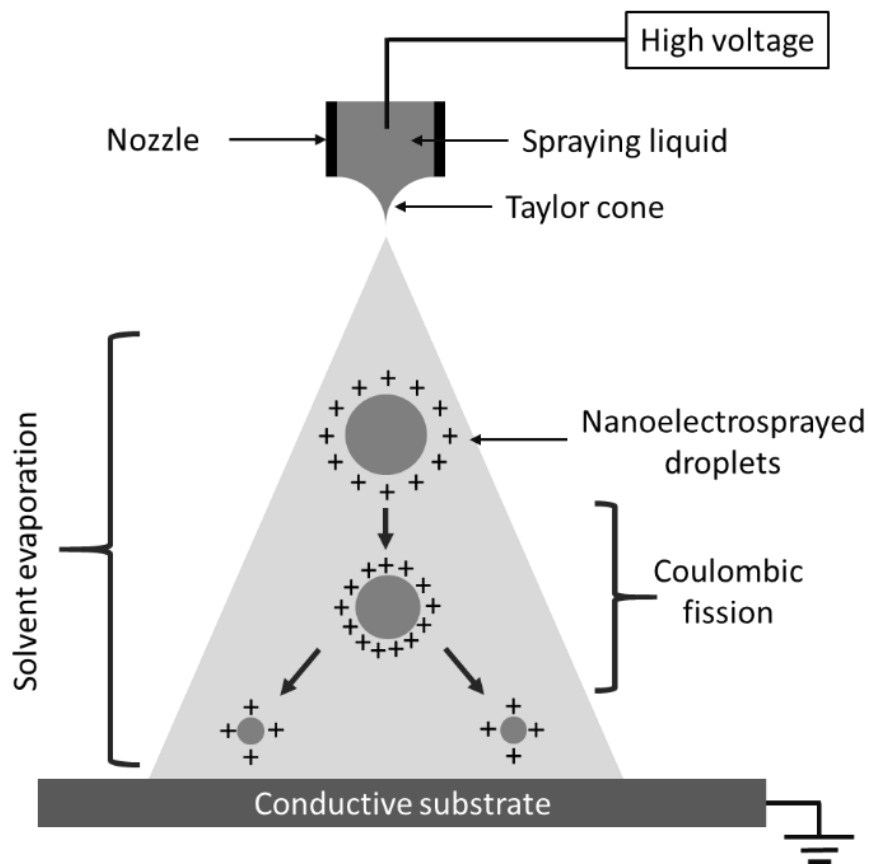
Figure 1.9. The illustration of the nES process. The flow rate depends on the applied voltage and no syringe pump is required in the experimental configuration. (Figure is not to scale)

One feature of the nES is the capability to deposit materials on-demand. The initiation of nES can be controlled by switching the applied voltages using a high frequency switch. Figure 1.10 illustrates the spray behaviour related to the switch of voltage. The V_1 voltage is the lower voltage which is below the onset voltage of nES. The spray only initiates at a voltage higher than the onset voltage (V_2). By switching the applied voltage rapidly between a lower level (V_1) where no liquid ejection occurs to a higher value (V_2) above the voltage required for nES onset, the number of pulsation events occurring could be controlled by the dwell time at the higher potential.

These benefits have led to the application of nES printing in many fields including the fabrication of conductive interconnects[104], touch-screen sensors[105], tissue engineering scaffolds[106,107],light-emitting devices[108] and possibly surface modification for soft hydrogel[109].
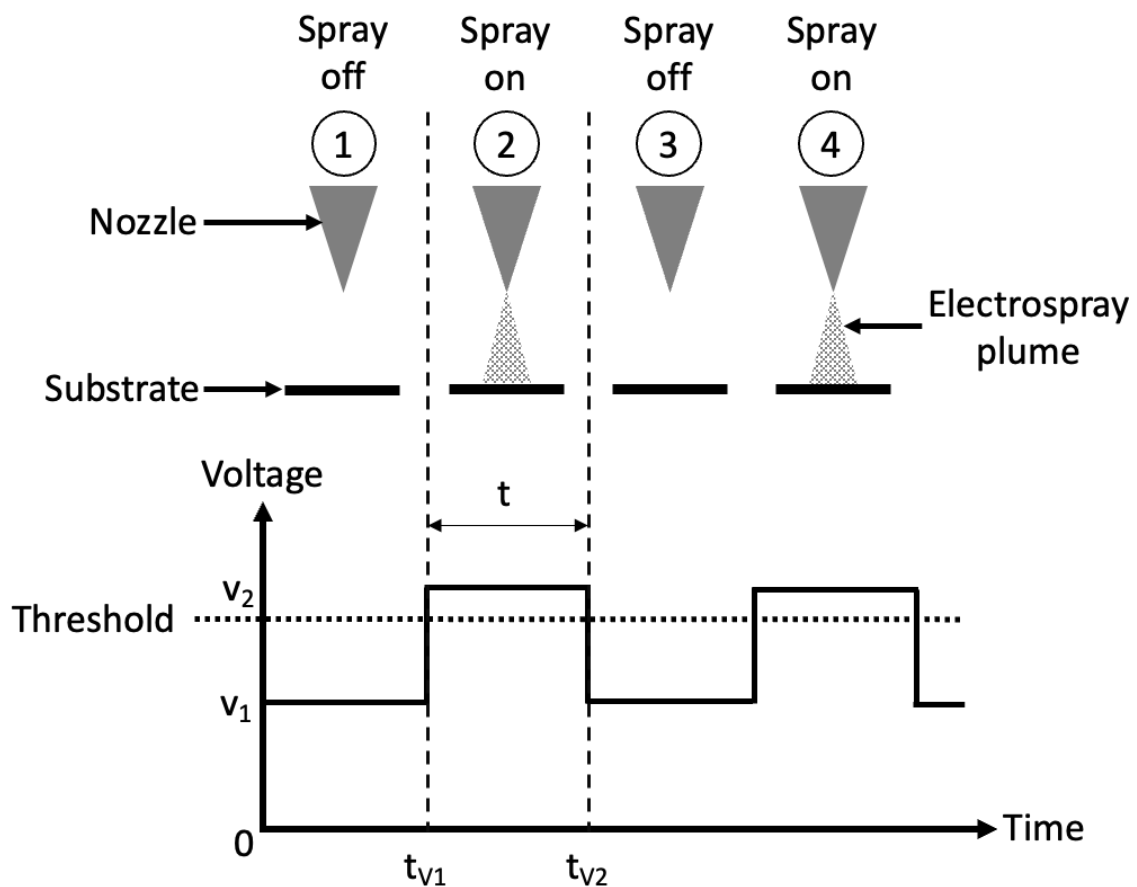
Figure 1.10. *An illustration of the switching of voltages to control the spray of nES.*

A wide range of synthetic and natural polymers can be processed by nES, with examples including poly(lactic-co-glycolic acid), ethylene-vinyl acetate, polycaprolactone, zein, chitosan and hyaluronic acid. The processability of a polymer solution for nES is highly dependent on the electrical conductivity and viscosity of the precursor solution[110]. The conductivity depends on the solvent system and intrinsic property of the polymer[111]. The viscosity of a polymer solution is subject to the polymer concentration and molecular weight of the polymer, which also influences the morphology of the coating[112]. The molecular weight cut-off of a polymer is considered individually to generate coatings with desired morphology[113].

The nES utilises a miniature spraying method that allows layer-by-layer drug deposition with flexible dosing and placement precision for rapid production of DECLs

using commercially available CLs. The nES system enables the on-demand deposition of a thin layer of polymeric coating onto the peripheral area of the contact lens to preserve the vision zone, aiming to mitigate its influence on the intrinsic physical properties of the contact lens. These features mean that nES is a less wasteful method since all the sprayed materials are transferred onto the contact lens and have the potential to deposit tailored doses of medications. nES can coat various drugs on different types of commercially available CLs to prepare DECLs for treating ocular diseases. Additionally, the technology could be readily integrated into the manufacturing lines for contact lenses.

1.12 Thesis objectives

The works in this thesis aim to explore the potential of MD and the nES systems to fabricate personalised medicines for oral and ophthalmic drug delivery, respectively. The key objectives of the experimental chapters are listed below.

Chapter 3:

- To characterise the MD system to prioritise the dispensing parameters for volume adjustment.
- To examine the dosing accuracy of printing personalised ODFs and the influence of printing on the mechanical properties and disintegration behaviour of printed ODFs.

Chapter 4:

- To characterise the nES system built in-house to understand the influence of the spraying parameters on coating thickness, width, and morphology.
- To assess the spraying location on soft hydrogel contact lenses for maximum optical transmittance.
- To compare the experimental spraying volume and the theoretical value derived from the established scaling law.

Chapter 5:

- To develop DECLs using the nES system and assess the *in vitro* release using three model drugs with different hydrophobicities.
- To assess the influence of steam sterilisation on the DECLs fabricated by nES.

Chapter 2 Materials and methods

2.1 Introduction

In this chapter, the materials used in all studies and the general methodologies are described. Some experimental methods are excluded in this chapter and specified in the relevant chapter. The methods to fabricate the personalised orodispersible films and drug-eluting contact lenses are described in this chapter.

2.1.1 Model drugs

2.1.1.1 Paracetamol (PAR)

Paracetamol is an analgesic and antipyretic commonly available to be purchased over the counter from pharmacies globally. It is commonly available in tablet form and is also available in liquid form for patients who struggle to swallow solid dosage forms, for example, paediatric and geriatric patients. The usual dose of PAR is 0.5 – 1 g four times daily for adults with a maximum dose of 4 g in 24 hours[114]. The dose for paediatric patients is usually based on their body weight and therefore, formulation with flexible dosing would be highly suitable for them.
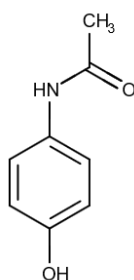
Figure 2.1. *Chemical structure of paracetamol.*

2.1.1.2 Ketotifen fumarate (KF)

Ketotifen fumarate is a second-generation antihistamine drug for treating itchiness associated with allergic conditions. It is formulated as an eye drop and requires a twice daily application to alleviate the symptoms[115]. The tablet form of KF is also available, but it is less commonly used to treat itchiness associated with allergic reactions. KF comes in one strength of 250 μg/ml and the effective dose delivered topically to the

eyeball is 12.5 µg per day when the 5% bioavailability is considered. Johnson and Johnson vision marketed the first drug-eluting contact lens (DECL) ACUVUE® Theravision™ in 2022. The DECL contains 19 µg of KF to prevent ocular allergic itch while wearing contact lenses[74].
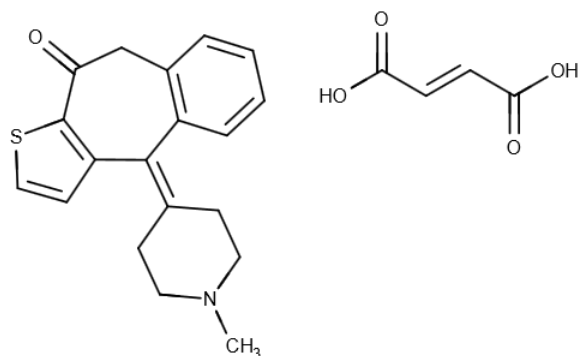
Figure 2.2. *Chemical structure of ketotifen fumarate.*

2.1.1.3 Bimatoprost (BIM)

Bimatoprost is a prostaglandin analogue that is indicated to treat open-angle glaucoma by reducing intraocular pressure[116]. BIM is mainly formulated as an eye drop, but also available as an implant for patients with stable ocular pressure[117]. BIM eye drop is available in two strength, 100 µg/ml and 300 µg/ml, and is administrated once daily, preferably at night[118]. Considering the 5% bioavailability, the amount of BIM delivered topically to the eye is 5 µg and 15 µg, respectively, for the abovementioned strengths.
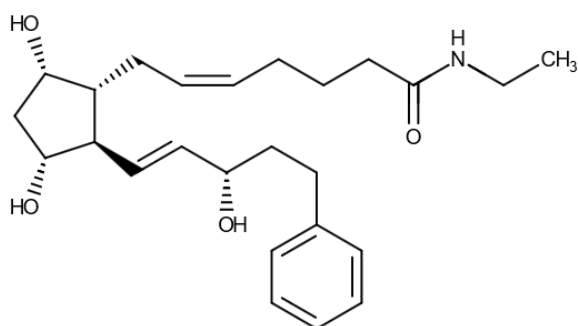
Figure 2.3. *Chemical structure of bimatoprost.*

2.1.1.4 Latanoprost (LN)

Latanoprost is a prostaglandin $F_2\alpha$ analogue indicated for ocular hypertension to treat open-angle glaucoma[119]. It is only available as an eye drop. Only one strength of LN eye drop is available as 50 µg/ml, and similar to BIM, LN is administrated once daily, preferably at night[120]. The amount of LN delivered to the eye will be 2.5 µg if the 5% bioavailability is taken into consideration.
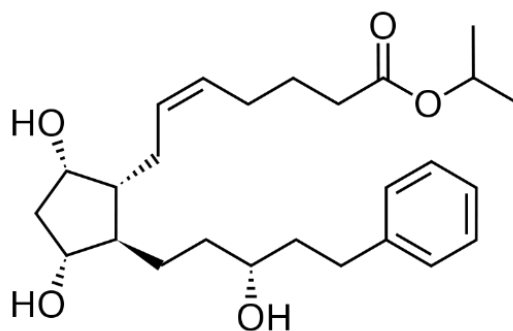
Figure 2.4. *Chemical structure of latanoprost.*

Table 2.1. *Physicochemical properties of model drugs*

	PAR[121]	KF[122]	BIM[123]	LN[124]
Molecular weight (g/mol)	151.2	425.5	415.6	432.6
Aqueous solubility at 25°C (mg/ml)#	14[125]	17.5[126]	0.04[127]	0.006[127]
Partition coefficient (Log P)	0.91	3.85*	3.2	3.98
Acid dissociation constant (pKa)	9.5	8.43	14.3	14.47

* Of the free base. # At 25 °C and pH 7.0.

2.1.2 Excipients

2.1.2.1 Hydroxypropyl Methylcellulose (HPMC)

HPMC is a common cellulose ether that forms swellable matrices in water and is classified as generally regarded as safe (GRAS) by FDA[128]. HPMC is a versatile material for pharmaceutical applications. It can be used for tablet coating, as a thickening agent in liquid formulations, and as a gelling agent to achieve controlled release of medications[129]. HPMC is available in a wide range of molecular weights for different applications and the molecular weight is highly correlated to its dynamic

viscosity. For example, the low molecular weight HPMC is suitable for coating applications. In contrast, the high molecular weight HPMC is used for the prolonged release of medications by forming a hydrogel to slow down the diffusion rate of APIs. The low molecular weight HPMC (Pharmacoat 606) was chosen to be the film-forming polymer in Chapter 3 to facilitate the disintegration of ODFs.

R is H, CH$_3$ or [CH$_3$CH(OH)CH$_2$]
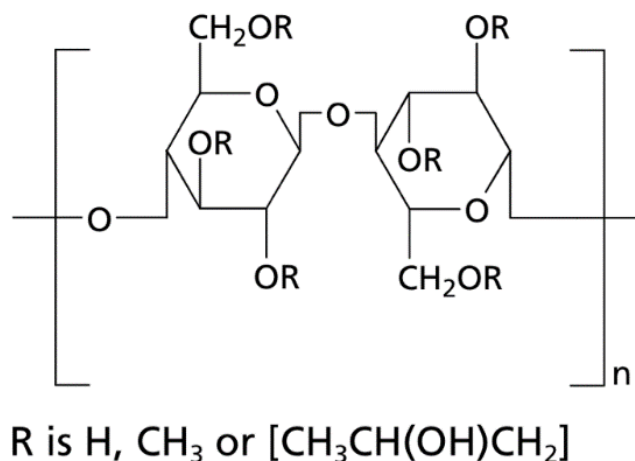
Figure 2.5. *Chemical structure of HPMC*[128].

2.1.2.2 Zein

Zein is a water-insoluble protein that serves as the major store protein in corn[130]. Commercial zein contains a mixture of α-, β-, γ- and δ-zein, which represent zein with different molecular weights and solubility. A-Zein has molecular weights between 22-27 kDa and is the dominant species accounting for 80% of zein powder[130]. Zein has low nutritional value to humans since it lacks basic and essential amino acids. Therefore, zein is often used for other applications, such as confectionery coating and stock feed. The applications of zein have extended across industries, ranging from food, cosmetic and pharmaceutical industries[131]. Zein film fabricated by electrospray has also been demonstrated[132]. Zein films prepared by electrospraying showed a homogenous surface without compromising the water barrier capacity compared to the casted zein films[132], showing electrospray can be an excellent alternative to preparing functional zein coating. The good biocompatibility and biodegradable property of zein provide a wide range of biomedical applications[133] and it is considered generally recognised as safe (GRAS) by the FDA in 1984[134].

Zein was chosen as the model polymer for the study in Chapter 4 since it is commonly used as a coating material with excellent film-forming properties. Zein can be dissolved in various solvents, including glacial acetic acid, urea, or alkaline solution (pH ≥ 11). It is also soluble in aqueous ethanol mixtures such as methanol, ethanol and isopropyl alcohol but insoluble in pure water and alcohol[130]. For electrospray, a solvent system with a high electric conductivity and high dielectric constant is preferable to achieve better ionisation efficiency[135]. A solvent system with high vapour pressure can promote evaporation of the electrosprayed droplets during its flight to the substrate[113]. Therefore, aqueous ethanol was used in this work. The binary solvent system has to have at least 50% v/v ethanol to solubilise zein to form a solution[130].

2.1.2.3 Poly Lactic-co-Glycolic Acid (PLGA)

PLGA is a synthetic copolymer of lactic acid and glycolic acid that is biodegradable and biocompatible. It is a FDA-approved material that is widely studied and used for biomedical applications, such as the production of polymeric nanoparticles, scaffolds for tissue engineering and the production of drug-eluting medical devices[136,137], thanks to its non-toxic and non-immunogenic properties. PLGA with different physicochemical properties, such as molecular weight, end group, and the ratio of lactic acid and glycolic acid are available commercially for specific biomedical purposes[136]. PLGA with high molecular weight has a slower degradation rate than those with lower molecular weight because more time is required to break down the long polymer chain[138]. Therefore, a PLGA with a relatively high molecular weight (76 – 114 kDa) was used in Chapter 5 for drug-eluting coating on commercially available contact lenses.
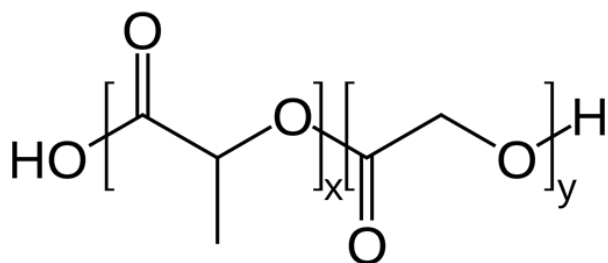
Figure 2.6. *Chemical structure of PLGA (x is the number of lactic acid units and y is the number of glycolic acid units.*

2.2 General physicochemical characterisation methods

2.2.1 Physical characterisation of the ODF inks and/or nES precursor spraying solutions

2.2.1.1 Density

The density of the solutions was measured by a DMA 4500M density meter (Anton Paar GmbH, Graz, Austria) equipped with an oscillating U-tube at 25 °C. The measurement was done in triplicate to calculate the average density.

2.2.1.2 Surface tension

The surface tension of the solutions was measured by a DMS-401 tensiometer (Kyowa, Niiza-City, Japan) using the pendant drop method. Ten measurements were carried out for each sample to calculate the average surface tension.

2.2.1.3 Conductivity

The conductivity of spraying precursors was measured by the Jenway 4510 conductivity meter (Stone, UK) equipped with a microvolume conductivity probe (027816, Jenway, Stone, UK) at 25 °C.

2.2.1.4 Rheological properties

Rheometers are widely used to measure the flow and deformation of a substance, specifically, the change of internal structure of the sample subjected to an external force. A rotational rheometer was used in the study to measure the dynamic viscosity of samples. A fluid can be classified as Newtonian or non-Newtonian fluid. The viscosity of a Newtonian fluid is independent of the shear rate, whereas the viscosity of non-Newtonian fluids changes accordingly to the applied shear[139]. Non-Newtonian fluid can be further categorised by pseudoplastic, dilatant and Bingham plastic. The specific behaviour of the polymer solutions used in each chapter is detailed in the corresponding results sections.

The dynamic viscosity of the solutions was measured by a Discovery HR-2 rheometer (TA Instruments, Delaware, USA) equipped with a 2°, 40 mm cone-and-plate geometry. The method was set as a flow ramp procedure from 0.1 to 100 s^{-1} at 25 °C for 60 s. The measurement was done in triplicate to calculate the average viscosity.

2.2.2 Thermogravimetric analysis

Thermogravimetric analysis (TGA) is often used to determine the weight change of a material to a range of temperatures. The thermogravimetric analyser contains a sensitive balance to measure the weight change of samples against temperature. The resulting data provides insight into determining the thermal stability of the tested materials. Therefore, TGA is often used to determine the degradation temperature of pharmaceutical materials. Measuring the moisture content of the sample is also possible by using the TGA. The TGA data is essential to set the maximum temperature of a method for the differential scanning calorimetry (DSC) to avoid the degradation of samples.

The degradation temperature of all samples (2.5 mg – 6 mg) was loaded to an open aluminium pan and measured by the TGA 5000 (TA Instruments, USA), heating from 25 °C to 400 °C at a heating rate of 10 °C/minute. The temperature at 95% weight change was adopted for the corresponding DSC methods.

Three samples (approximately 2.5 – 6 mg) of MD printed films with different printing cycles and cast film were measured for moisture content. The films were placed on platinum pans and heated from 25 °C to 300 °C at a rate of 10 °C/min under a continuous flow of nitrogen (50 ml/min). The weight change between 25 °C to 100 °C is considered the loss of moisture from the film and analysed using TRIOS software (TA Instruments, USA).

2.2.3 Differential scanning calorimetry

Differential scanning calorimetry (DSC) is a standard method to measure the heat flow to a sample and its associated thermal events, such as melting point, glass transition temperature and crystallisation temperature[140]. DSC can characterise materials including active pharmaceutical ingredients, polymers and inorganic materials to evaluate the crystal state, solubility of API in the polymer and purity[141]. There are two types of DSC available commercially, heat-flux, power differential and power-compensated DSC. The heat-flux DSC, which measures the supplied heat difference between the sample and reference, was used for all studies.

The DSC 2500 (TA Instruments, USA) was used to measure the crystallinity of PAR in the orodispersible films prepared by the printing and casting methods. All samples and raw materials were separately crimped in an aluminium pan. PAR and HPMC were subject to the standard heat-cool-heat cycle from 0 °C to 220 °C and 300 °C respectively, at 20 °C/min heating and cooling rate. The film samples were cut to fit the aluminium pan and heated to 220 °C at 20 °C/min. All measurements were conducted with nitrogen as the purge gas with a 50 ml/min flow rate. The analysis was performed by TRIOS software (TA Instruments, USA).

2.2.4 Attenuated total reflectance Fourier transform infrared (ATR-FTIR) spectroscopy

FTIR is a vibrational spectroscopy that is widely used in the pharmaceutical industry. It emits electromagnetic radiation between 400 cm^{-1} – 4000 cm^{-1} to the sample of which the chemical bonds of the sample stretch and/or bend by absorbing the electromagnetic wave[142]. The characteristic bonds absorb particular wavelengths and show peaks in the IR spectrum that can be used as a fingerprint of molecules, which helps identify impurities in the sample, chemical changes of molecules and drug-excipient interactions. The ATR attachment enables simple and non-destructive measurements without prior sample preparation.

The distribution of paracetamol at different areas of the MD printed film with eight printing cycles and the cast films and any potential drug-polymer interactions were studied using the FTIR spectrometer Vertex 70 (Bruker Optics Ltd, Coventry, UK) equipped with a golden Gate Attenuate Total Reflectance accessory (Space Ltd, Orpington, UK). Three random locations on each film were selected for measurement. The measurement was performed from the wavenumber range of 500 – 4000 cm^{-1} at a resolution of 2 cm^{-1} and 32 scans. The results were analysed using the OPUS software version 7.8 (Bruker Optics Ltd, Coventry, UK).

2.2.5 Ultraviolet-visible spectroscopy (UV-Vis)

UV-Vis spectroscopy is a technique to quantify the amount of light absorbed by a sample. A chromophore has to be present in the sample to be UV-active, meaning the sample would absorb light waves in the UV-Vis region. Using Beer-Lambert Law, the concentration of a material that absorbs light is calculated by the following equation[143].

$$A = \varepsilon c l$$

, where A is the absorbance, ε is the molar absorption coefficient, c is the molar concentration and l is the optical path length. Alternatively, the transmittance of a sample can be measured using a UV-Vis spectrophotometer by using the following equation.

$$T(\%) = 100\frac{I}{I_0}$$

, where T is the transmittance in %, I_0 is the intensity of incident light, and I is the light intensity after passing through the sample.

The amount of PAR in the cast and printed ODFs was quantified by UV-Vis spectrophotometer (Lambda 35, Perkin Elmer, UK) at the λ$_{max}$ of 243 nm. A calibration curve of PAR in PBS pH 7.4 was built by measuring the concentration ranging from 1.5 µg/ml to 15 µg/ml. The cast ODFs and MD printed ODFs were dissolved individually in 5 ml of PBS pH 7.4 and diluted accordingly to be quantified by the UV-Vis spectroscopy. The average value was calculated by five samples from printed ODFs and cast ODFs.

2.2.6 Optical transmittance of nES-coated contact lenses

The method to measure transmission of light through contact lenses was adopted from the literature[144]. Briefly, the lenses were measured at a 1 nm interval from 200 – 800 nm using a UV-Vis spectrophotometer (Lambda 35, Perkin Elmer, UK). The light beam has a dimension of 7.5 mm in height and 1 mm in width according to the instrument specifications. The contact lenses (N=3) were immersed into a quartz cuvette containing PBS pH 7.4 solution to maintain the hydration of contact lenses during measurement. The convex side of the contact lens was facing the incoming beam (Figure 2.7). The % transmittance of blank contact lenses was used as control. The lenses are expected to have at least 95% transmittance to provide clear vision[68].
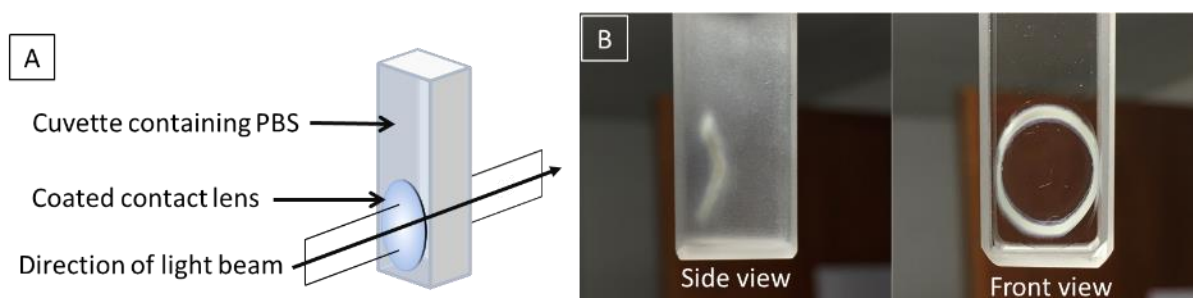
Figure 2.7. *A: An illustration of the setup for measurement of optical transmittance for nES-coated contact lenses. B: The position of coated contact in a quartz cuvette containing PBS pH 7.4 solution.*

2.2.7 High-performance liquid chromatography (HPLC)

HPLC separates a mixture of compounds in the sample by using the difference in polarity of the compounds in the sample. A typical HPLC system consists of the mobile phase, an injector, a column, a pump and a detector. A reverse phase column is usually used for drug assay in the pharmaceutical field. A range of detectors is available depending on the physical properties of the analyte. For example, UV detectors, refractive index detectors and fluorescence detectors[145]. In the study, the HPLC system (Jasco, Hachioji, Japan) consisted of a PU-1580 solvent delivery system linked to an UV-1570M UV detector and an AS-2055 Plus auto-injector. Chromatography was carried out using a reversed-phase HC-C18(2) column (250 x

4.6 mm, 5 μm) (Agilent, Santa Clara, USA) with a C18 guard column (12.5 x 4.6 cm, 5 μm) (Agilent, Santa Clara, USA).

2.2.8 Scanning electron microscopy (SEM) and cryo-SEM

SEM is a common imaging method to observe micro- and nanostructure. The imaging method provides qualitative information on the surface topology with a magnification range from 10x to 100,000x[146]. Sputter coating of a metal, usually gold, is required prior to SEM imaging, to scatter the incident electron beam from the sample to the detector. The surface morphology of orodispersible films and nES coating on contact lenses was imaged using the Gemini 300 scanning electron microscopy (SEM) (Zeiss, Cambridge, UK). For the orodispersible films, film samples were cut and attached to a sample holder with carbon adhesive tape and sputter-coated with gold for 30 seconds and 2.2 kV at 55 mm and 5x10-2 mbar (Quorum Technologies, Lewes, UK). Images of cross-sections and surfaces of printed and cast films were captured using SEM. The nES-coated lenses were imaged using the above SEM equipped with the PP3010T cryo-chamber (Quantum Design AG, Marly, Switzerland). The nES coated lenses were stored in a container with a lint-free wipe moistened with PBS before imagining. The lens was cut to one-fourth of the whole lens, which was frozen rapidly by nitrogen slush. The frozen sample was transferred to the cryo-chamber for the sublimation of surface ice and sputter coating with platinum under vacuum before being sent to the SEM cold stage for image acquisition.

2.3 Configuration of the microdispensing (MD) printing system

The MD system mentioned in Chapter 3 was built in-house to fabricate personalised ODFs. The system consists of an air compressor, the control unit for dispensing, a valve-based printhead, a pressurised reservoir to carry the drug-loaded ink and the substrate to carry the deposited liquid (Figure 2.8). The components of the MD system built in-house and the procedure to print ODFs are detailed in Chapter 3.
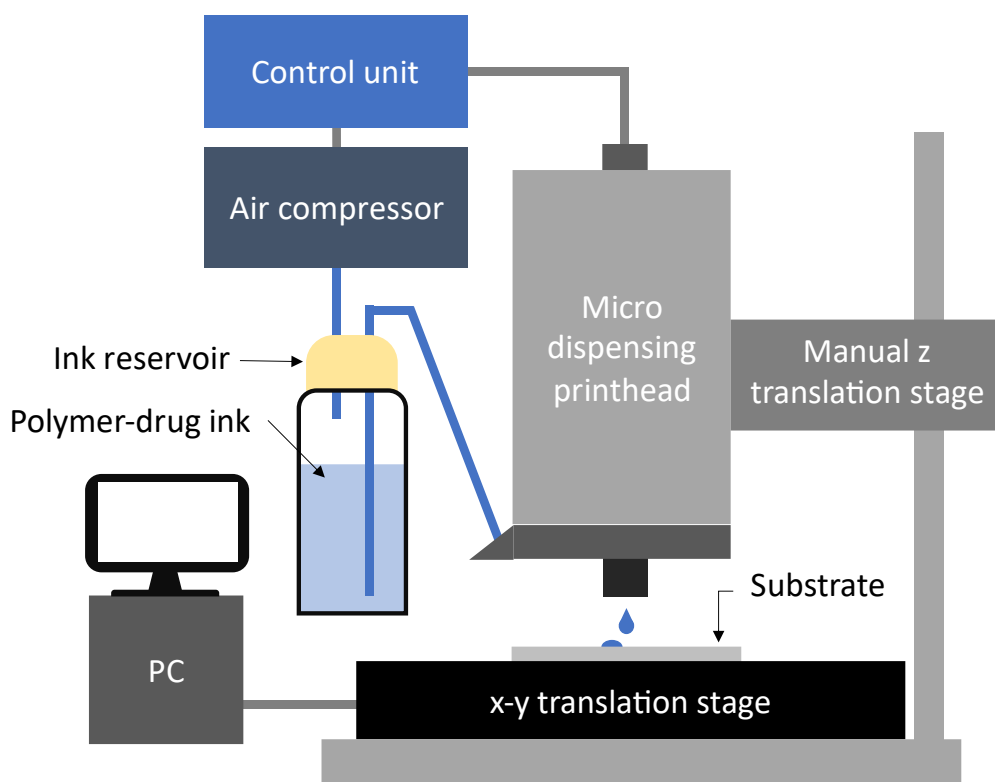
Figure 2.8 *Illustration of the MD system built in-house to print personalised ODFs on-demand (components are not to scale).*

The MD system is flexible and provides a range of dispensing parameters to be adjusted as listed in Table 2.2. The characterisation of the MD system using placebo inks and the physical characterisation of printed ODFs are discussed in Chapter 3.

Table 2.2 *List of all dispensing parameters that are adjustable from the MD system.*

Dispensing parameters	Operation range
Pressure (kPa)	0 – 350
Rising time (ms)	0.5 – 999.9
Opening time (ms)	0 – 3000
Falling time (ms)	0.3 – 999.9
Delay time (ms)	1 – 1000
Opening height (%)	2 – 100
Number of pulse(s)	1 – 32000
Nozzle diameter (µm)	60, 100, 200

2.4 Configuration of the nanoelectrospray (nES) printing system

The custom-made nES printer (PCE Automation, Beccles, UK) shown in Figure 2.9. was built to automate the nES process to fabricate circular films or dots on surfaces. Within the system, a ceramic nozzle with a 50 μm internal diameter (MicroDot tip 7364054, Nordson EFD, Dunstable, UK) was connected to a 2.5 ml Luer lock syringe (Terumo, Japan), which is fixed to the motorised z-translation stage (EGSC-BS-KF-32-100-8P, Festo, Esslingen am Neckar, Germany) and travels vertically. Pneumatic pressure supplied to the syringe can be regulated by the in-line pressure gauge, which enables nES printing of highly viscous liquid. A digital camera with a high magnification lens (MVL6X12Z, Thorlabs LTD, Lancaster, UK) was used to monitor the spraying process. The fluorine-doped tin oxide glass slide was secured and grounded on the 2-dimension motorised x-y translation stage (5155-1000A, Festo, Esslingen am Neckar, Germany), which moves simultaneously to generate circular movements. The substrate is interchangeable with other substrate materials, such as metal or insulators if required. All the movement in x, y and z directions and spraying parameters are controllable from the built-in control panel of the machine. There are a few components connected to the nES system externally that are not shown in the top image of Figure 2.9 and explained as follow. As illustrated in the schematic diagram in Figure 2.9, the high voltage power supplies (HCP 14-6500, F.u.G. Elektronik GmbH, Schechen, Germany) were connected to the high voltage switch (PVX-4140, Direct Energy, Inc., Colorado, USA), which is linked to the nES printer and responsible for switching voltage to get into pulsation mode. The function generator (TG 1000, Aim-Tti, Huntingdon, UK) was used to control the frequency and amplitude of the square waves generated. A current amplifier, (DLPCA – 200, Laser Components, Chelmsford, UK) was used to amplify the voltage and connected to a digital storage oscilloscope (TBS1104, Tektronix, Beaverton, USA) to monitor the waveform of the spraying process. The measurement resistance of the amplifier was set to 10^6 Ω for all measurements. The nES system enables switching of the applied voltage to reduce the time required to charge the precursor solution beyond the spraying threshold (Figure 1.10). The nES system was set to a continuous spraying mode (disable the switching components) to maximise the delivery rate of polymer onto the substrate. The lower supplied voltage (V_1 in Figure 1.10) was set to zero in all experiments to reduce variables. Direct current was adopted in all experiments.
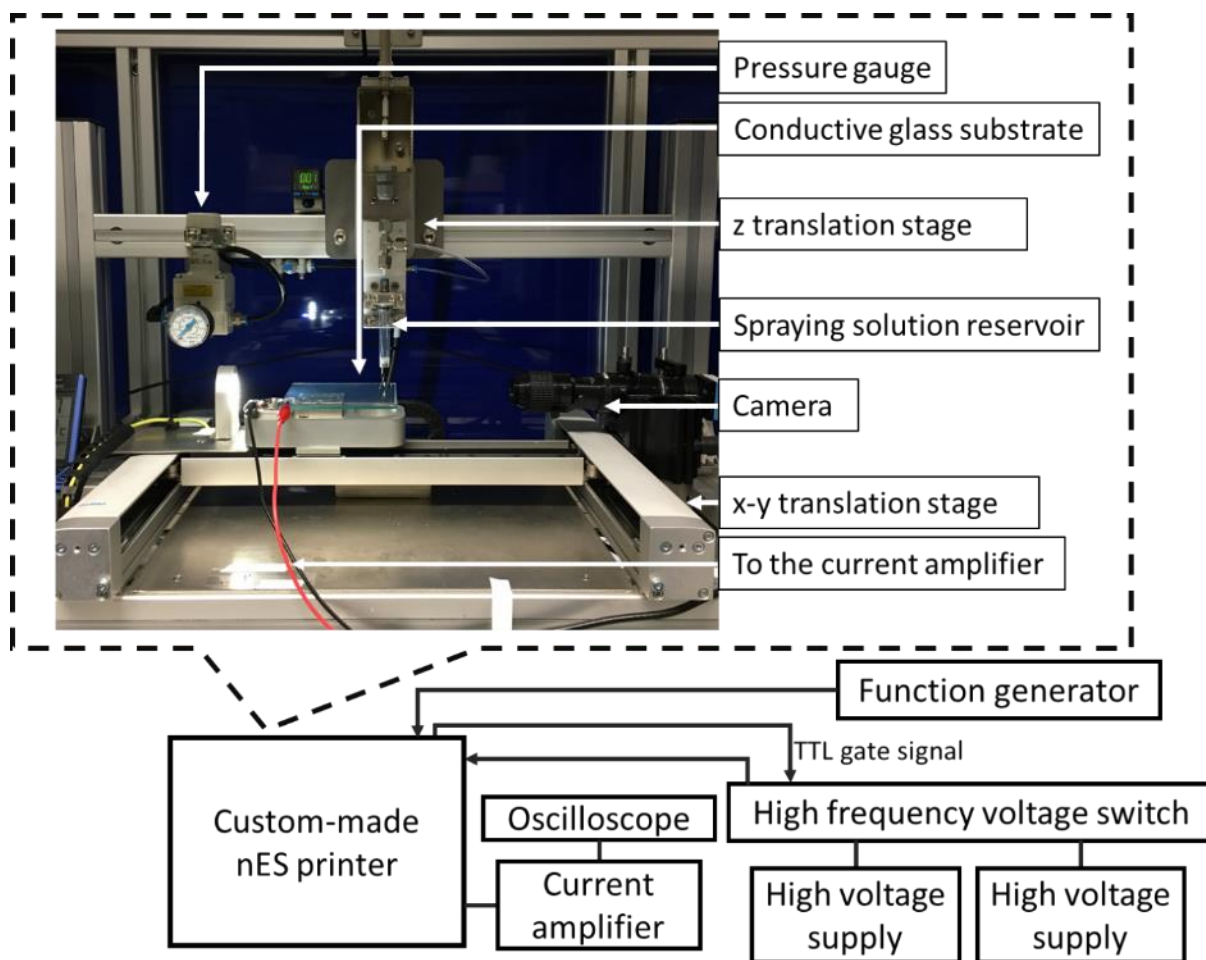
Figure 2.9. *Experimental setup of the custom-made nES system to deposit atomised polymer droplets on the substrates.*

2.5 Fabrication of drug-eluting contact lenses

The hydrogel contact lens was soft, and its shape often changed when it was placed on the conductive glass substrate, leading to poor reproducibility of the lens position. The contact lens specification was used to produce a lens holder by FDM 3D printing to resolve such an issue. The 3D model (Figure 2.10 B) of the lens holder was built in an open-source software named Blender (v2.9, Amsterdam, Netherlands), according to the dimension of the contact lenses. The 3D model also provides information to calculate the coating location (radius) and the nozzle substrate distance as seen in Figure 2.10 D.

The spraying solution and contact lens required preparation before the nES coating process. The spraying solution was prepared by dissolving the polymer into a suitable solvent system under vortex until complete dissolution. The resulting solution was filtered via a syringe filter to remove any particulates in the solution, preventing blockage of the spraying nozzle. As for the contact lens, it was removed from the packaging and equilibrated in PBS pH 7.4 for 30 minutes. Excess liquid on the lens was removed by a lint-free dry wipe before transferring the contact lens to the lens holder.

To maintain the hydration of contact lenses, 10 µl of PBS pH 7.4 was pipetted onto the silver region of the 3D-printed lens holder before positioning the semi-dry contact lens on it (Figure 2.10 C). The polymer-drug solution was sprayed at the peripheral region (Figure 2.10 A) of contact lenses (N=3) with the predetermined parameters. Once the lenses were nanoelectrosprayed, they were stored in a container with lint-free cloth moistened with PBS 7.4 to maintain hydration before other measurements.
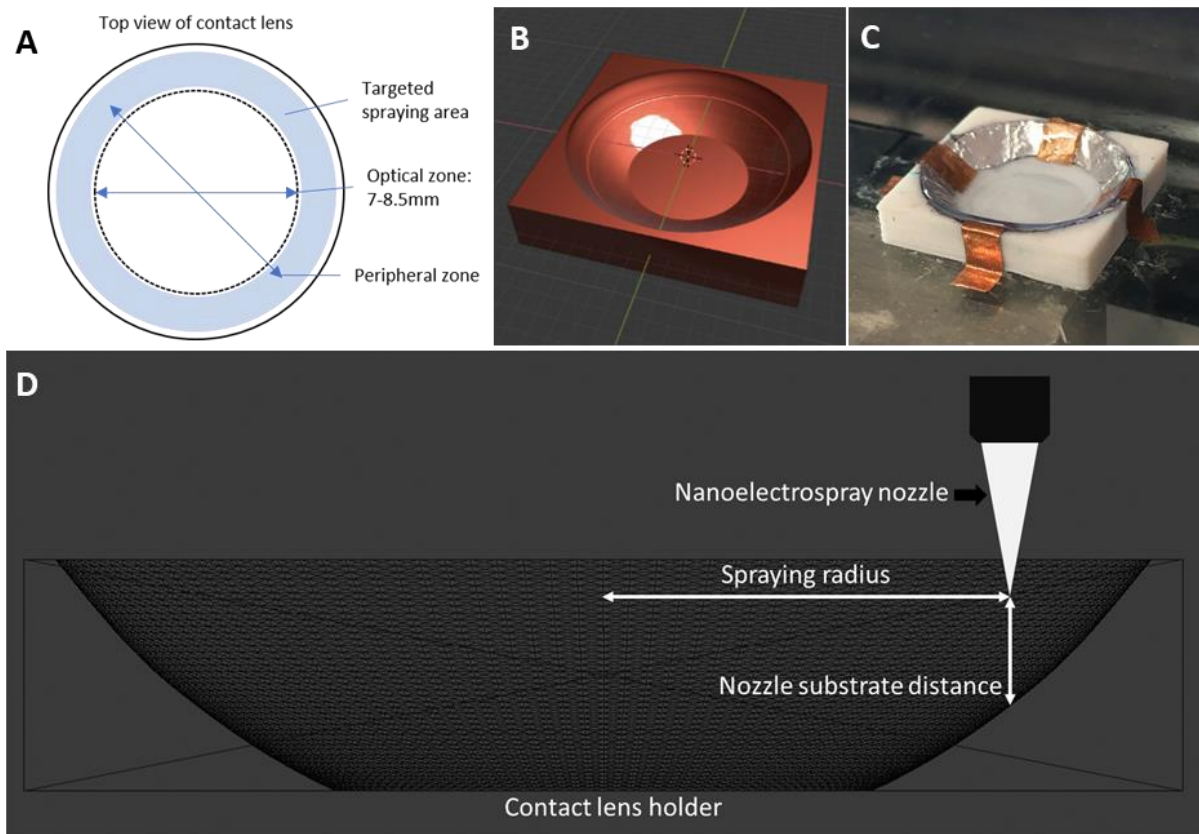
Figure 2.10. *The targeted deposition of a polymer-drug layer on contact lens by nano-electrospraying (A), the 3D model of the lens holder (B), the 3D-printed lens holder with a blank contact lens (C) and illustration of the 3D-printed lens holder with reference to different spraying parameters (D).*

Chapter 3 Drop-on-demand printing of personalised orodispersible films fabricated by precision micro-dispensing

3.1 Introduction

Personalised orodispersible films (ODFs) manufactured at the point-of-care offer the possibility of adapting the dosing requirements for individual patients. Inkjet printing has been extensively explored as a tool for producing personalised ODFs[50,56,147]. However, it is limited to dispensing liquids with low viscosity and the interaction between the ink and edible substrate complicates the fabrication process[40].

In this study, the feasibility of using a micro-dispensing (MD) jet system built in-house to fabricate substrate-free ODFs on demand was evaluated. The aim was to demonstrate the fabrication of personalised ODFs using a MD system, evaluate the accuracy of printing, and understand the droplet fusion and film-forming properties, as well as their impact on the disintegration behaviour of the printed ODFs. The model ink contains HPMC as the model polymer and paracetamol as the model drug. HPMC, with the particular grade of Pharmacoat 606, is selected because of its excellent film-forming, rapid hydration, and disintegration properties. Paracetamol is used as the model drug to demonstrate the dose adjustment capability of ODFs prepared by MD printing according to the patient's clinical needs. A repeatable printing sequence was designed to produce ODFs with various doses using the model ink (an ink with a fixed model drug concentration), and different numbers of printing cycles for dose adjustment. Cast films of the same formulation were used as the control sample to benchmark the mechanical properties, disintegration time, and dosing accuracy of MD-printed ODFs. Both the cast and printed film showed smooth surface morphology without any air bubbles. No significant difference was found in the disintegration time of the MD-printed films compared to the cast films. High precision in dosing by MD printing was achieved. The dose of paracetamol had a linear correlation with the dimension of the printed films (R^2 = 0.995). The results provide clear evidence of the potential of MD printing to fabricate ODFs and the knowledge foundation of advancing

MD printing to a point-of-care small-batch manufacturing technology of personalised ODFs.

3.2 Materials and methods

Unless considered in this chapter, the materials and methods are specified in Chapter 2.

3.2.1 Materials

Hydroxypropyl methylcellulose (HPMC) (commercial name as Pharmacoat 606) was kindly donated by Shin-Etsu (Niigata, Japan) and used as the film-forming polymer to fabricate the ODFs. Paracetamol and phosphate buffer saline (PBS) tablet pH 7.4 were purchased from Sigma-Aldrich (Gillingham, UK). Milli-Q (Millipore, Merck, USA) ultra-pure water was used as the solvent of the ink. The model of the micro-dispensing (MD) system used in this study is a Nanojet Piezo Valve NJ-K-4020 with an inner nozzle diameter of 200 µm (Microdrop Technologies GmbH, Norderstedt, Germany). Polyethylene terephthalate (PET) plastic film (KF26066) was purchased from Q-connect (Sheffield, UK) and used as the substrate for printing and casting ODFs. Listerine PocketPaks® breath strips (a pullulan-based oral film) were purchased from Johnson & Johnson (New Brunswick, USA). All materials were used without further processing.

3.2.2 Preparation of placebo and polymer-drug inks

Three concentrations of HPMC solutions (5%, 10% and 15% w/v) were prepared as the placebo ink to characterise the MD system. The polymer was dissolved in water with stirring at 50 °C using a magnetic stirring hot plate until all powder dissolved and allowed to degas overnight at ambient conditions. The polymer-drug ink (HPMC 15% w/v, paracetamol 1.4% w/v) was prepared by dissolving all the dry ingredients into the water and following the same procedure as the placebo ink. Only the HPMC 15% w/v proceeds to printing drug-loaded ODFs since it has similar dynamic viscosity to the suggested viscosity (1000 mPa.s) for casting ODFs[30]. All resulting solutions were

filtered by a glass fibre syringe filter with a 5 µm pore size (OU-12915-33, Cole-Parmer GmbH, Wertheim, Germany) and allowed to settle down before printing.

3.2.3 Microdispensing (MD) printing system setup

The components of the MD system built in-house are shown in Figure 3.1. The system consists of a piezoelectric MD printhead with an inner nozzle diameter of 200 µm and is attached to a manual z-translation stage (PT1B, Thorlabs, USA), a Sil-Air 30D air compressor (Sil-Air, Emilia Romagna, Italy) to pressurise the ink reservoir, a computer to control the movement of the motorised x-y translation stage (MTS-25, Thorlabs, USA) and to design the printing sequence, a control unit to adjust the dispensing parameters and to control the supplied pressure to the liquid reservoir and a liquid reservoir connected to the MD printhead.
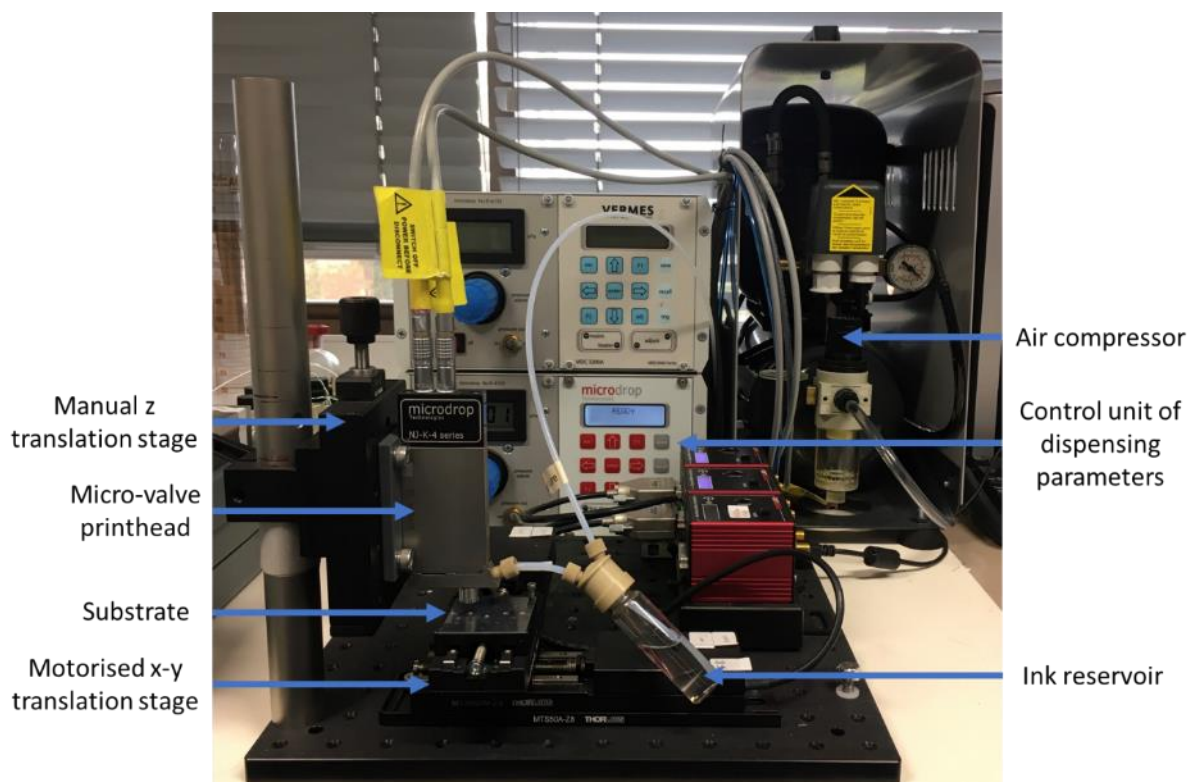
Figure 3.1. *The MD system built in-house to print personalised ODFs on-demand.*

Figure 3.2 illustrates the dispensing mechanism of the piezoelectric MD printhead and its corresponding dispensing parameters. The microdispensing system contains a piezo-actuated valve, which remains closed in the non-operational state to avoid leakage of the ink (step 1 in Figure 3.2). The tappet rod moves upward with the rising time to allow the liquid stream to flow out of the orifice (step 2 in Figure 3.2). The rising time (0.5 – 999.9 ms) defines the required time for the tappet travels upward. The relative displacement of the tappet rod away from the nozzle represents the opening height, where 100 % is fully lifted, and 2 % is the minimum value. The actual displacement of the tappet rod was not measurable and presented as % as mentioned earlier. The opening time (0 – 3000 ms) indicates the time when the tappet rod remains at a particular position to allow free flow of liquid out of the nozzle (step 3 in Figure 3.2). The tappet rod then moves downwards to eject the liquid out of the nozzle (step 4 in Figure 3.2). The time required to move the tappet rod back to its original position defines the falling time (0.3 – 999.9 ms). Once the dispensing cycle is completed, the valve remains closed for a specific time before the next dispensing cycle (delay time, from 1-1000 ms).
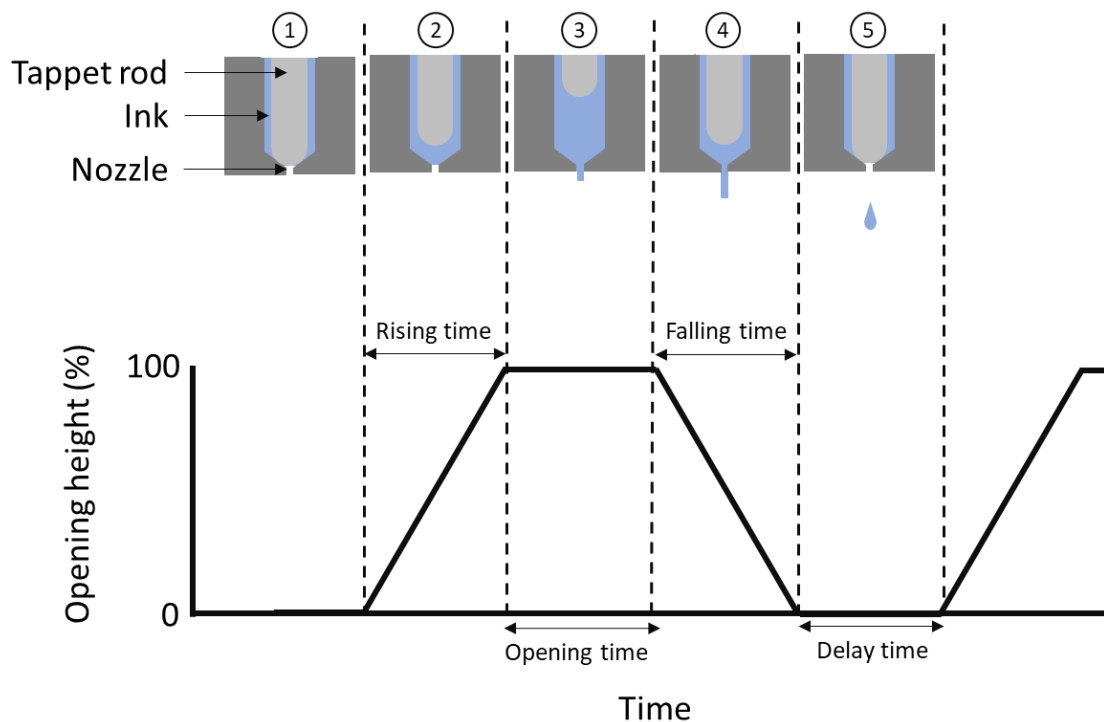
Figure 3.2. *A complete dispensing cycle and the corresponding dispensing parameters.*

3.2.4 Effects of MD printing parameters on the accuracy of dosing volume

Placebo HPMC inks were used to investigate the critical dispensing parameters of the MD system that can affect the accuracy of the dispensed volume. The importance of this investigation lies in the direct link between the accuracy of the dispensing volume and the accuracy of the drug dispensed into the ODFs. The one-factor-at-a-time approach was adopted. The rising time (0.5 ms) and falling time (0.3 ms) were set to the minimum value for ease of characterisation. The gravimetric method was used to measure the change in dispensing volume against different dispensing parameters[148]. Dispensing volumes were measured when one of the four key dispensing parameters was varied while the others were held constant. The investigated parameters include supplied pressure, opening height, opening time and delay time. Within each experiment set, ten drops of the placebo ink were dispensed into a pre-weight glass vial containing dodecane as a barrier liquid (to prevent evaporation of the ink). The weight difference of the vial before and after dispensing was measured. The dispensing volume was calculated using the density equation, $v = m/\rho$, where ρ is the density, m is the mass and v is the volume. For each set of parameter changes, three independent sets of ten drops of dispensing were performed and measured to examine the reproducibility of the tests. A light microscope FDSC196 (Linkam Scientific, Tadworth, UK) was also used to observe the change of droplet morphology with different dispensing parameters.

3.2.5 Fabrication of drug-loaded ODFs

3.2.5.1 Cast ODFs

The cast ODF was prepared by casting 10 ml of the polymer-drug ink stated above onto the PET substrate by an adjustable film applicator 1117 / 100 mm (Sheen Instruments, Herefordshire, UK) set at a 550 µm gap height. The cast ODF was dried in an oven set at 30 °C for approximately 2 hours. The resulting film was cut into square films with 18 mm x 18 mm dimensions using a craft puncher before being stored in a desiccator for further measurements.

3.2.5.2 Printed ODFs

The printing of ODFs started with the characterisation of droplet dimensions and morphology, followed by designing the printing sequence. The printing parameters, such as the nozzle substrate distance, pressure, opening height and opening time, were characterised. Once the droplet has achieved an acceptable quality (no air bubbles, no distorted shape), the printing sequence was designed as shown in Figure 3.3. When the printing started, the translation stage moved in the y-direction from the pre-set coordinate towards the zero point, followed by the movement to the x-direction. The translation stage moved back to the original y-coordinate when the movement along the x-axis was completed. The ODFs were formed by depositing a specific number of droplets as a printing cycle onto the PET substrate using the optimised dispensing parameters stated in Table 3.1. It is worth noting that the frequency of droplet dispensing is not specified here. It is controlled by combining a range of operational parameters, including the raising, the falling, the opening and the delay time. These are discussed in the result section in Chapter 3. The drug loading of ODFs was increased by repeating the printing cycles (1, 2, 4, 6 and 8) to expand the print area along the x-direction. The printed ODFs were subsequently dried in a 30 °C oven for 2 hours before being stored in a desiccator for measurements.
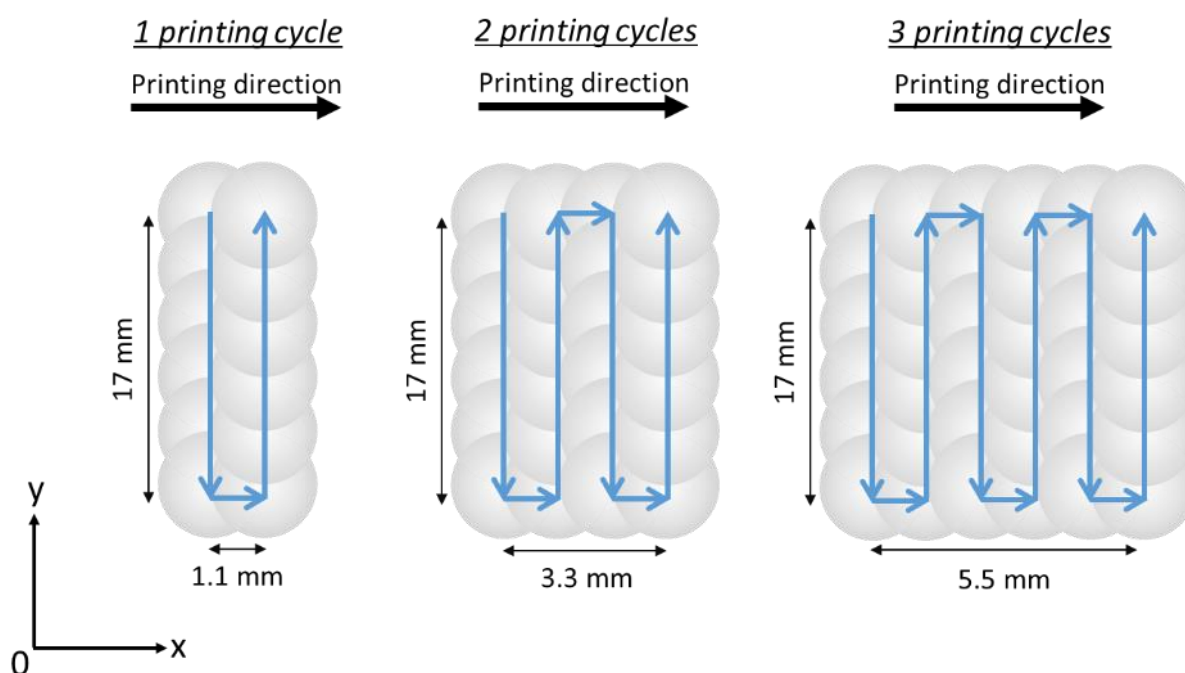
Figure 3.3. Examples of printing cycles to fabricate ODFs with different drug loading.

Table 3.1. *Optimised printing parameters for printing drug-loaded ODFs by the MD system.*

Pressure (kPa)	295
Opening height (%)	45
Opening time (ms)	14
Rising time (ms)	0.5
Falling time (ms)	0.3
Nozzle substrate distance (mm)	3
Delay time (ms)	350

3.2.6 Physical characterisation of cast and printed ODFs

3.2.6.1 Thickness:

The thickness of 18 mm x 18 mm cast ODFs, printed ODFs with eight printing cycles and Listerine PocketPaks® films were measured by an electronic thickness gauge ET-3 (Rehder-dev, Greenville, USA). The measurement was performed at four corners and the centre of the film. Five samples of each type of film were measured and the average thickness was calculated.

3.2.6.2 Weight:

The weight of printed ODFs with different printing cycles and cast ODFs were measured by the analytical balance XS205DU (Mettler Toledo, Leicester, UK) after the film was stored in the desiccator for 24 hours. The average weight was calculated by five samples from each type of film.

3.2.7 Mechanical properties of ODFs

Four samples of the 18 mm x 18 mm MD-printed ODFs and cast ODFs were subjected to mechanical testing using a Texture Analyser TA-Xtplus (Stable Micro Systems, Godalming, UK) to determine the tensile strength and elongation at break. Listerine PocketPaks® films were used as the guide for film handling by comparison with the cast and printed films. The films were fixed between two clamps with a 1 cm gap using tensile grips A/TG (Stable Micro Systems, Godalming, UK). The clamps moved away

from each other with 50 mm/min velocity until the film was torn. Tensile strength (N/mm^2) is defined as the maximum force required to break the film and is calculated by Eqt. (3.1).

$$Tensile\ strength = \frac{force\ at\ break}{cross-sectional\ area\ of\ films} \quad \text{...Eqt. (3.1)}$$

Elongation at break (%) is defined as the ratio of length increased after fracture to the original length of the film as shown in Eqt. (3.2).

$$Elongation\ at\ break = \frac{increased\ lenght\ at\ break}{original\ length} \times 100 \quad \text{...Eqt. (3.2)}$$

3.2.8 Disintegration test of ODFs

A modified petri dish method was adopted to evaluate the disintegration time of MD-printed and cast ODFs[149]. A watch glass with a 10 cm diameter containing 2 ml PBS pH 7.4 was equilibrated in a shaking incubator (KS 3000 I control, IKA, Germany) set at 60 rpm and 37 ± 0.5 °C. The films were laid on PBS and recorded when the film started to disintegrate[150]. The measurement was done in triplicate for all types of films.

3.2.9 Statistical analysis

The basic calculation was performed by Microsoft Excel® (Microsoft Office 365). The data analysis was performed using SPSS statistical program (SPSS 25, IBM, New York, USA). Analysis of variance (ANOVA) and the Tukey test were used to compare the thickness of ODFs at different locations. A statistical significance is considered when the p-value is lower than 0.05.

3.3 Results and discussion

3.3.1 Ink characterisation

The main advantage of MD in comparison to inkjet printing is the capability to dispense viscous ink. The viscosity of the ink has a direct impact on droplet spreading on the substrate and drug distribution. A highly viscous solution can reduce its spreading on the PET substrate and thus achieve a higher quantity of drug per area. The high ink

viscosity also enables single pass printing to fabricate ODFs with sufficient thickness and drug loading, improving the production efficiency and the range of medications that can be printed as ODF potentially. This is a major challenge for direct inkjet printing of ODFs. The measured dynamic viscosity of 15% w/v HPMC placebo ink was 813.92 ± 1.72 mPa.s. The dynamic viscosity of the polymer-drug (15% w/v HPMC and 1.4% w/v paracetamol) ink was 818.32 ± 4.45 mPa.s as shown in Table 3.2. The polymer-drug ink behaved as a Newtonian fluid since the shear stress and shear rate showed a linear relationship.

Table 3.2. *Physical properties of placebo and polymer-drug inks.*

Formula	Viscosity (mPa.s)	Density (g/ml)
HPMC 5% w/v	32.58 ± 1.65	1.01 ± 0.01
HPMC 10% w/v	202.18 ± 2.62	1.02 ± 0.01
HPMC 15% w/v	813.92 ± 1.72	1.03 ± 0.01
HPMC 15% w/v + paracetamol 1.4% w/v	818.32 ± 4.45	1.03 ± 0.01

3.3.2 Effects of MD printing parameters on the accuracy of dosing volume

The placebo HPMC inks were used to determine the effect of dispensing parameters on dispensing volume. The dispensing volume is influenced by the opening time (ms), applied pressure (kPa), and opening height (%), as illustrated in Figure 3.4. The applied pressure must be sufficiently high to ensure the liquid has enough velocity to leave the nozzle and travel to the substrate. Low applied pressure leads to dispensing failure because of the accumulation of ink at the nozzle. High applied pressure increases the dispensing volume, but the effect on dispensing volume is less than the effect of the opening time. As seen in Figure 3.4 A, for all concentrations of HPMC ink, the volume of the placebo ink dispensed is linearly proportional to the applied pressure. There is no linear correlation between dispensing volume and opening height as seen in Figure 3.4 B Air bubbles were observed in the droplets when the opening height was set to 100%, as shown in Figure 3.5. This issue was addressed by reducing the opening height to below 45%. However, this adjustment resulted in a significant reduction in the volume dispensed. Therefore, the opening height was set at 45% for printing the drug-load ODFs. The opening time is the most critical parameter

to control the dispensing volume among the tested dispensing parameters. Figure 3.4 C shows that the opening time is highly linearly correlated with the dispensing volume for all three placebo inks tested. More importantly, compared to Figure 3.4 A, the sensitivity of the opening time to adjust the dispensing volume is much greater than the pressure. By changing the opening time from 10 ms to 200 ms, the dispensed volume of 5% HPMC ink can be changed from less than 20 µl to nearly 600 µl. The test range of delay time has a minimal impact on the dispensing volume as shown in Figure 3.4 D. To optimize the dispensing parameters for new ink, the pressure should be adjusted first to provide enough energy to the ink leaving the nozzle. The droplet morphology should be monitored for a range of opening heights until defect-free droplets form. The opening time is adjusted subsequently to dispense the required volume. Finally, the delay time is changed to achieve the targeted droplet pitch.
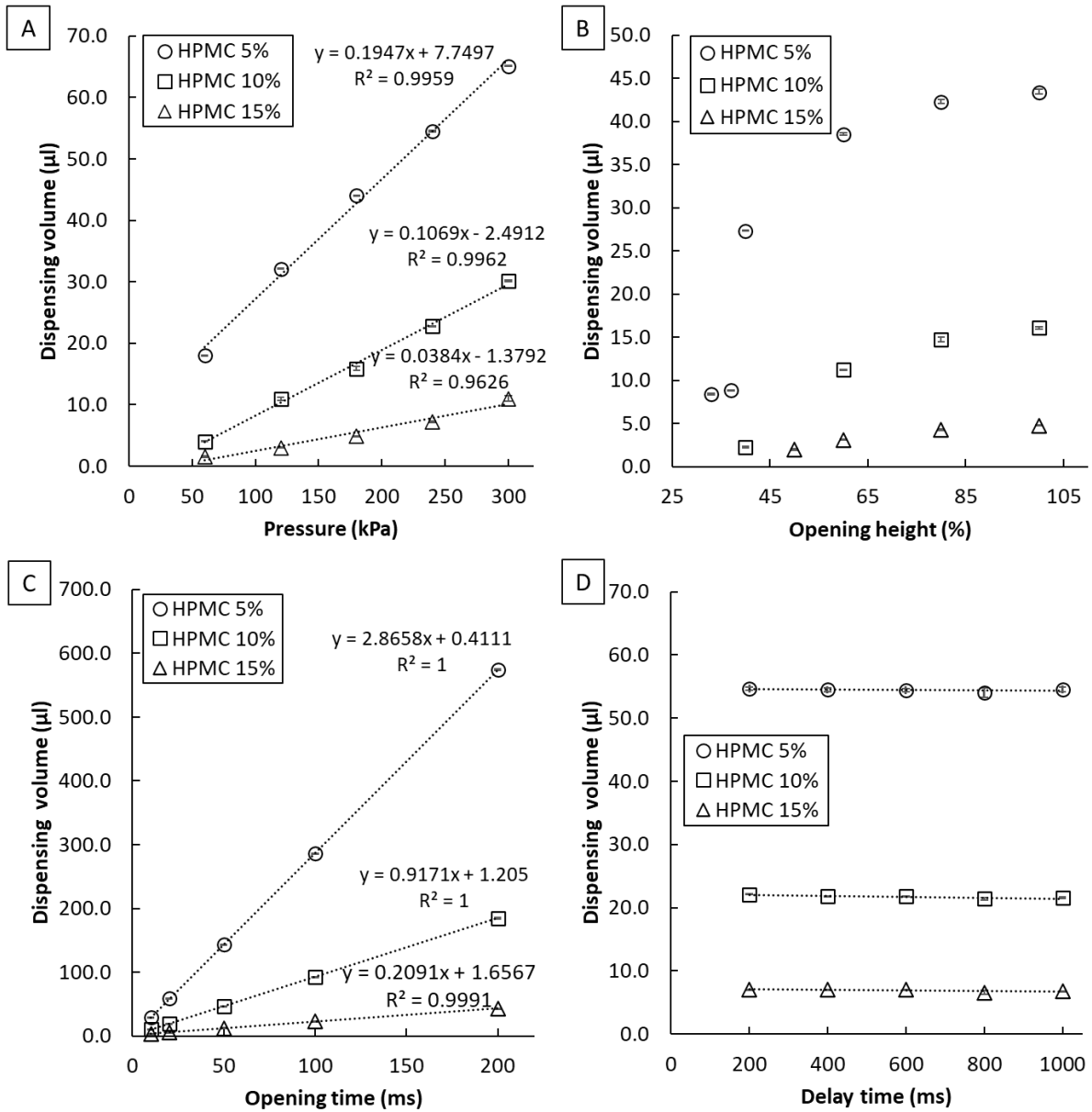
Figure 3.4. *The correlations between the dispensing volume of the placebo HPMC ink and (A) pressure; (B) opening height; (C) opening time and (D) delay time. (For each graph, only the defined parameter was changed. The rest of the dispensing parameters remained constant.)*

| Opening height 45% | Opening height 75% | Opening height 100% |

Air bubble-free

600 μm | 600 μm | 600 μm
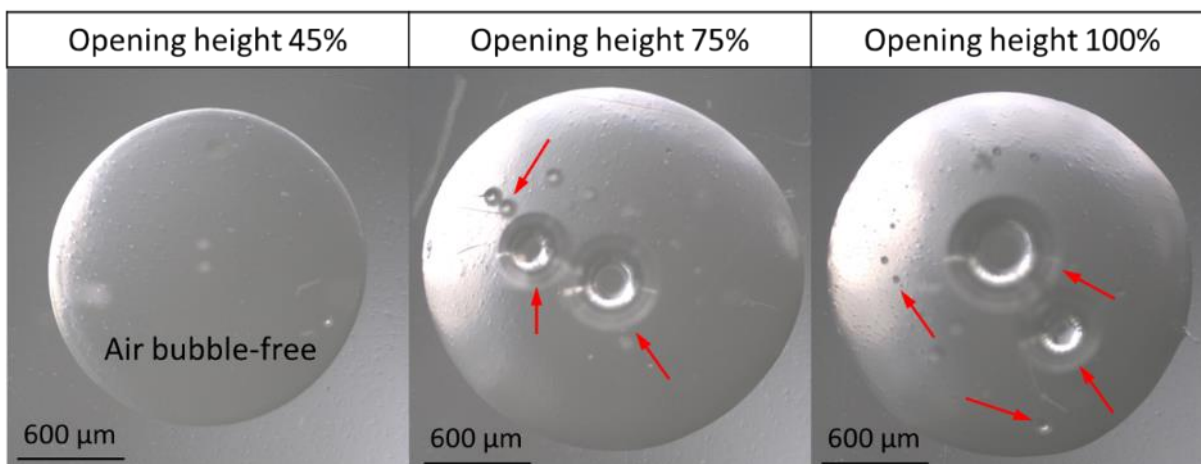
Figure 3.5.*Example microscopic images of the droplet of the placebo HPMC ink containing air bubbles (highlighted by red arrows) dispensed at different opening heights.*

3.3.3 MD printing parameter optimisation for drug-loaded ODF fabrication

Following the investigation into the effects of individual printing parameters on the dispensing volume, the printing parameter optimisation using the polymer-drug ink (HPMC 15% w/v, paracetamol 1.4% w/v) was performed. The nozzle-substrate distance was set as low as possible to expand the operational range for other dispensing parameters[148]. The rising time and falling time were set to the minimum value for ease of optimisation. The pressure was adjusted to ensure the droplet had sufficient velocity to leave the nozzle without splashing when it landed on the substrate. The opening height was then adjusted to produce droplets free of bubbles to ensure bubble- and defect-free films. Once these were optimised, the opening time was optimised to allow the dispensing of droplets with diameters of 1.65 mm on the PET substrate so that the overlapping of droplets forms a straight line of 18 mm in length. Finally, the delay time was adjusted according to the movement speed of the x-y translation stage (2.4 mm/s) to control the degree of overlapping of droplets. The optimised printing parameters adopted to print ODFs are shown in Table 3.1.

3.3.4 Thickness and surface morphology of drug-loaded ODFs

Figure 3.6 A demonstrates the locations of measurements for the thickness of ODFs. The thickness of 18 mm x 18 mm drug-loaded ODFs prepared by solvent casting, MD

printing (with eight printing cycles) and Listerine PocketPak® films is shown in Figure 3.6 B. The average (taking into consideration of corners and centres of the films) thickness of cast films and MD-printed films were 60.12 ± 1.67 µm and 51.24 ± 8.8 µm, respectively. The thickness of Listerine PocketPak® films is 45.64 ± 1.04 µm. In terms of the evenness of the thickness across the films, the cast films and Listerine PocketPak® films showed even thickness throughout the film (p = 0.932 > 0.05 and p = 0.508 > 0.05, respectively); whereas the MD-printed films showed uniform thickness at the corners (p = 1 > 0.05) with an elevated centre (p = 0.0001 < 0.05) (Figure 3.6 B). The marketed product, Listerine PocketPak® films, is used as the benchmark to assess the film quality since it shows high consistency in the thickness of the entire film. The results of this film obtained in this study agree with other reported results[151]. The high evenness of the film thickness of the cast film is because the cast films tested were cut from the centre of a large parent film. The cast parent films had significantly thinner edges than the centres, thus only the central areas were used. For the MD-printed films, the thicknesses of the edges and centres are the accurate representation of the properties of the film directly after manufacturing.
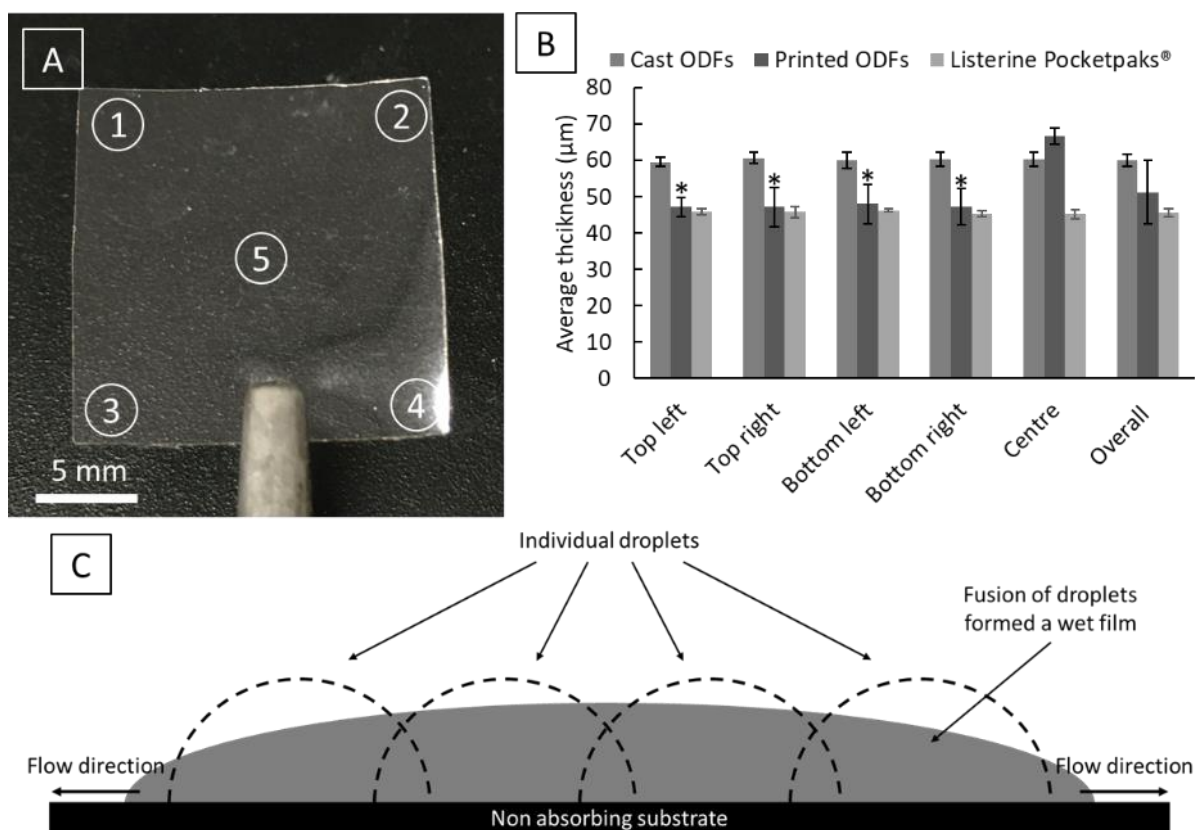
Figure 3.6. *(A) An example of drug-loaded ODF prepared by MD printing to show the location of measurement; (B) the thickness of 18 mm x 18 mm cast, MD-printed drug-loaded ODFs (with eight cycles) and Listerine PocketPak® films at different locations. Asterisks refer to a statistically significant difference ($p = 0.0001 < 0.05$) with the thickness at the centre; (C) graphic illustration of the drying and ODF formation processes of the partially overlapped droplets deposited by MD.*

It was observed that the drying of the MD-printed drug-loaded ODFs originated from the edge of the film and emerged slowly towards the centre. The possible cause of the higher thickness of the centre of the MD-printed ODFs than the corners may be explained by the lateral spreading of the wet film, as illustrated in Figure 3.6 C. As defined by the print path design, there is a degree of overlap between individual droplets. After deposition, this leads to rapid coalescence or fusion of adjacent droplets to form the liquid 'pool' and cause opposing flow in the centre. However, at the edges, there is mainly lateral spreading of the droplets deposited at the outer edge leading to the formation of a thinner layer of liquid than the centre prior to solidification via drying. Using a non-wetting substrate is likely to suppress the lateral spreading. The large

parent film prepared by the casting method also exhibited lateral spreading, resulting in nonuniform thickness with thinner edges and a thicker centre. However, the cast films used as the controls were cut from the centre of the parent film using an 18 mm x 18 mm craft punch, thus with good consistency of the thickness of the corners and the centres.

3.3.5 Surface morphology of MD-printed drug-loaded films

The texture of drug-loaded ODFs can affect patient's acceptance to some extent. The film should show a homogenous surface or colour to demonstrate its quality[152]. As discussed earlier, ODFs prepared by inkjet printing often require the printing of drug-containing inks onto a pre-prepared edible substrate film. This poses the risk of substrate malformation because of the printing process[47]. It is often attributed to the high proportion of solvent used in inkjet printing ink to control viscosity. The solvent can solubilise the substrate film upon contact, leading to an uneven substrate surface after multi-pass printing. The MD uses a single pass printing approach to fabricate ODFs to reduce the risk of poor surface texture associated with overprints. The surface properties of cast and MD-printed drug-loaded ODFs are shown in Figure 3.7. The MD-printed ODFs demonstrated a smooth surface (Figure 3.7 A – D), indicating the overlapping of droplets was sufficient to allow the complete fusion of adjacent droplets to form a homogenous film. The cross-sectional images of printed ODFs show homogeneous distribution of materials. Similar surface morphology was also observed from the cast film (Figure 3.7 E – H). A layered appearance is observed in some of the cross-sectional images of the MD-printed ODFs, but not in others. Thus, we believe the appearance of the layering I– due to the artefacts caused during the cutting process of the films.
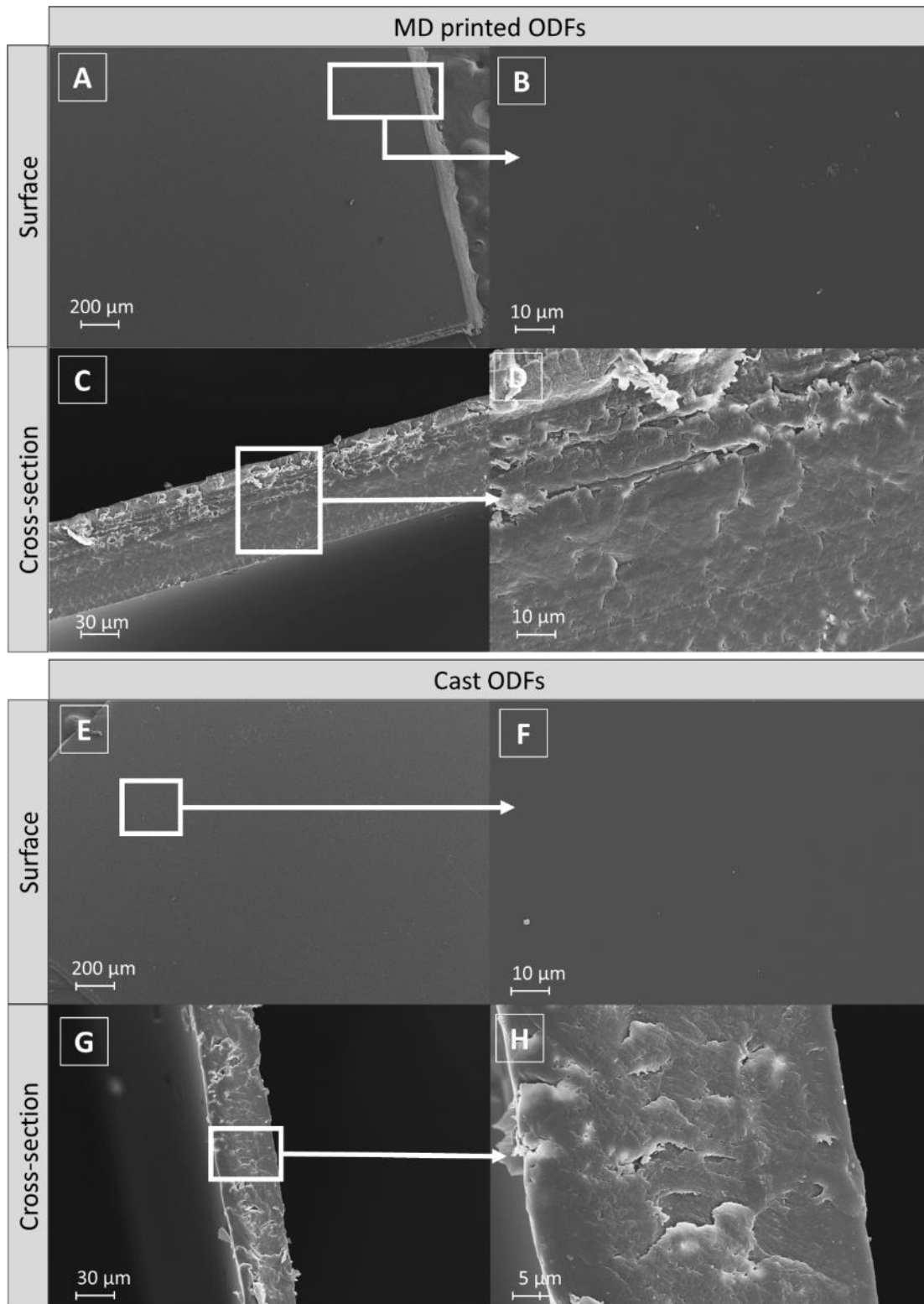
Figure 3.7. *Representative SEM images of the drug-loaded ODFs prepared by MD and the casting method. A & B: surface of the MD-printed ODF, C & D: cross-section of the MD-printed ODF ; E & F: surface of the cast ODF, G & H: cross-section of the cast ODF. The white boxes in the figure show the images of higher magnifications of the area of interest.*

3.3.6 Physicochemical characterisation of the drug-loaded ODFs

Table 3.3 shows the measured physicochemical properties of MD-printed and cast ODFs. The printed films were set to have a fixed length of 18 mm and the film width, and the overall film area was expanded by increasing the number of printing cycles. A range of printing cycles, between one to eight, were used to produce the films and investigate the correlation between the number of printing cycles and mechanical properties (section 3.3.7), film weight and drug content (section 3.3.8), and disintegration behaviour (section 3.3.9). A detailed discussion of these can be found in later sections. Eight printing cycles provide a film with a dimension of 18 mm x 18 mm which is comparable to the cast films, and thus used for further mechanical testing. The data demonstrated that the dimension and drug dose of the MD-printed films is freely adjustable by altering the number of printing cycles.

Table 3.3. *Physical characterisation, concentration and disintegration time of drug-loaded ODFs prepared by MD printing and casting (n=5).*

Printing cycle(s)	1	2	4	6	8	Cast
Print time(s)	16	32	65	98	131	-
Film dimension: Width (mm) x Length (mm)	2.7 x 18.0	4.6 x 18.0	9.4 x 18.0	13.6 x 18.0	18.0 x 18.0	18.0 x 18.0
Film weight ± SD (mg)	2.98 ± 0.34	5.88 ± 0.35	10.30 ± 0.34	14.46 ± 0.21	18.86 ± 0.08	23.34 ± 0.55
Paracetamol content ± SD (µg)	235.17 ± 24.25	453.22 ± 28.88	775.78 ± 53.19	1115.90 ± 16.46	1372.20 ± 16.27	1779.74 ± 46.56
Moisture content (%) ± SD	2.82 ± 0.79	2.46 ± 0.40	2.63 ± 0.23	3.16 ± 0.39	2.20 ± 0.74	2.93 ± 0.07
Disintegration time ± SD (s)	19.0 ± 4.0	28.7 ± 5.5	26.0 ± 5.3	30.7 ± 3.1	29.0 ± 3.6	30.0 ± 3.6

3.3.6.1 Moisture content in the ODFs

TGA was used to determine the moisture content of printed and cast films, as shown in Table 3.3. The MD-printed films show a range of moisture content from 3.16 to 2.2%, while there is 2.93% moisture in the cast films. No guidelines on the moisture content are currently available in the pharmacopoeia. Borges et al. suggested that the residual moisture content in the ODF should range from 3 – 6% based on measurements of commercially available ODFs[153]. ODFs with up to 10% moisture have been shown to be acceptable without any problems related to sticky or tacky films[154]. The moisture content of ODFs could impact the crystal state of the API and the mechanical properties of ODFs. The low moisture content that remained in the ODFs was likely due to the hydrophilic nature of HPMC. A small quantity of moisture also can act as a plasticiser and provide flexibility to the film. Since the ODFs prepared by MD are on-demand and expected to supply quantity from a few days to a month's worth of medications, the packaging is still required to protect the ODFs from moisture[152].

3.3.6.2 Thermal analysis of printed and cast ODFs

The physical state of the model drug in the drug-loaded ODFs was characterised using two analytical methods. The DSC results in Figure 3.8 A show a sharp endothermic melting peak of crystalline paracetamol powder at 171.9 °C and a glass transition temperature (T_g) of pure HPMC at 133.3 °C. The lack of paracetamol melting from the DSC results of the MD-printed and cast ODFs indicated that paracetamol was in an amorphous state. As the T_g of amorphous paracetamol is 23 °C[155], the drug would plasticise the polymer and the T_g of the HPMC-paracetamol dispersion ODF is expected to be below 133 °C. The board peak at about 90 °C from the thermogram of printed and cast ODFs reflects the presence of moisture in the ODFs. The moisture contents could further reduce the T_g of the ODFs to a temperature range that overlaps with the broad moisture loss peak, which may explain the absence of the T_g of the ODF.

3.3.6.3 ATR-FTIR and comparison between printed and cast ODFs

The ATR-FTIR data of the drug-loaded MD-printed with eight printing cycles and cast films, the reference raw materials and their physical mixture are shown in Figure 3.8 B. The characteristic peaks of Form I paracetamol have been well characterised by other literature[156,157] and the obtained IR spectrum of paracetamol matches the reported data. The pure HPMC shows characteristic peaks at 3449 cm^{-1} (O-H stretching), 2903 cm^{-1} (C-H stretching), 1453 cm^{-1} (C-H scissoring), 1374 cm^{-1} (O-H bending) and 1053 cm^{-1} (C-O stretching). The spectrum of the physical mixture is a simple sum of the spectra of crystalline paracetamol and HPMC. The broadened characteristic crystalline paracetamol peaks at 3321 cm^{-1} (N-H stretching) and 3108 cm^{-1} (O-H stretching) in the spectra of the cast and MD-printed films indicate that paracetamol is in its amorphous state and consistent with molecular dispersion[158]. The shift of peak from 1505 cm^{-1} (aromatic ring mode) to 1514 cm^{-1} in the cast film and MD-printed film has been reported previously and is consistent with the molecular dispersion of the drug in the polymer[157]. No apparent shifts of HPMC characteristic peaks are observed; thus, minimal drug-polymer interaction is indicated. Three random locations on the cast and MD-printed ODFs were examined by ATR-FTIR to access the evenness of drug distribution. The relative intensities of the peaks at 1514 cm^{-1} were used as the signature peaks of the concentration of paracetamol contents. No significant difference was observed in the spectra of different locations within the films (see supplementary data in the appendix, Figure A.2.), indicating paracetamol is evenly distributed in the printed films with eight printing cycles.
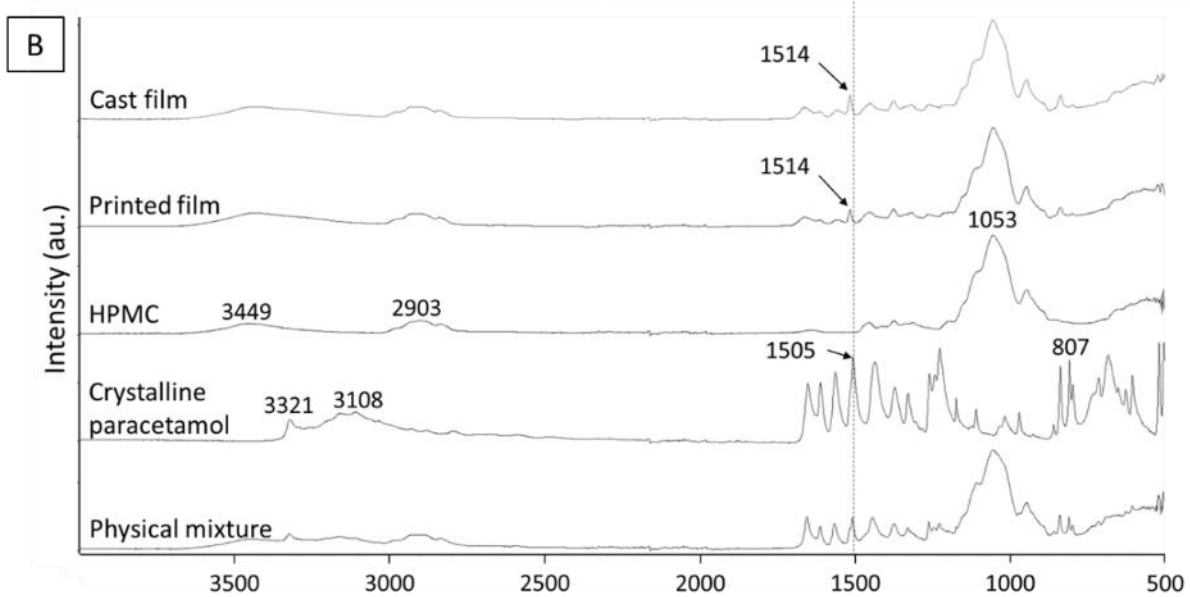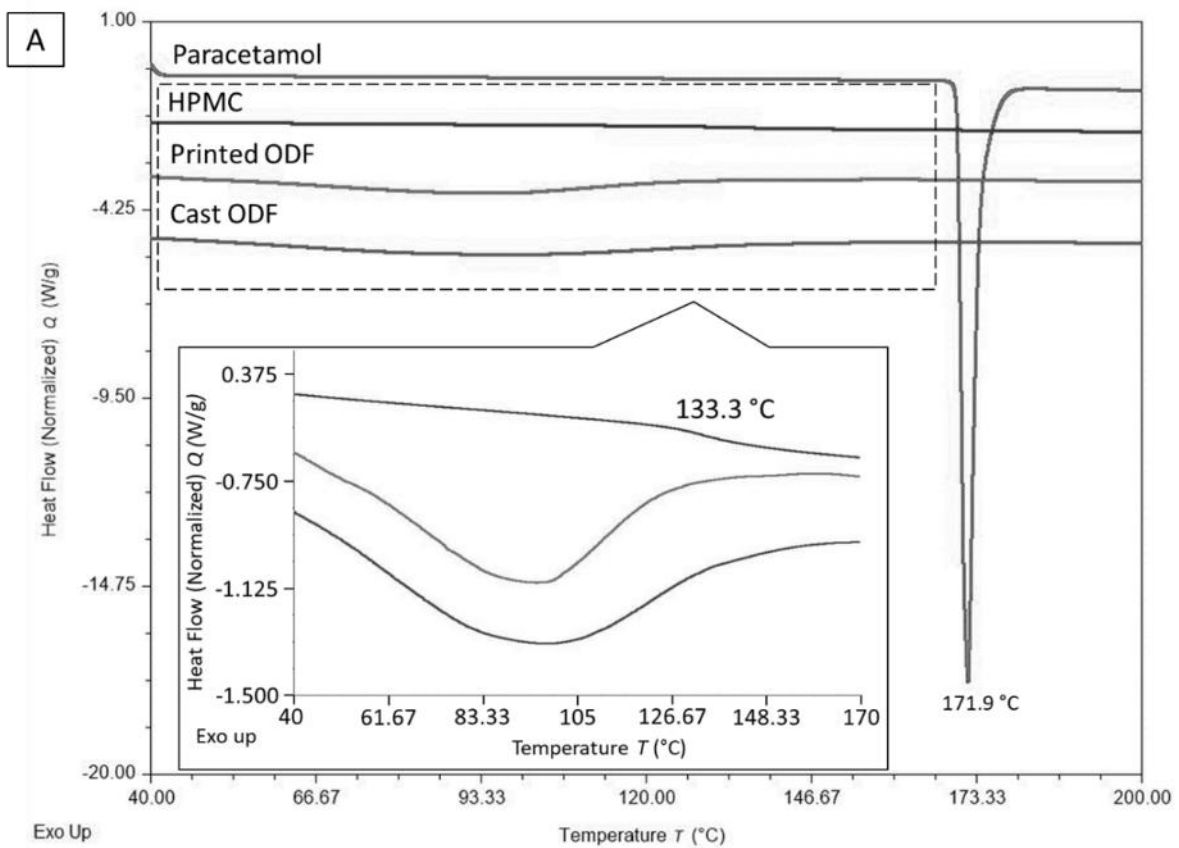
Figure 3.8. *(A) DSC thermograms and (B) ATR-FTIR spectra of the raw materials, the cast drug-loaded ODFs and MD-printed drug-loaded ODFs with eight printing cycles.*

3.3.7 Mechanical properties of drug-loaded ODFs

The ODFs must be strong enough to be handled during the manufacturing process, the packaging process, and administering to patients[152]. Literature suggested that ODFs with a tensile strength higher than 2 N/mm^2 and an elongation at break of more than 10 % are preferable to demonstrate good handling properties[159]. However, there are no official specifications on such parameters available. Therefore, in this study, the commercially available Listerine PocketPaks® ODFs were used as the benchmark comparison to assess the handling properties of the ODFs prepared by MD printing and casting. As Listerine PocketPaks® ODFs is a marketed product and is produced commercially, we assume the product provides sufficient mechanical properties for production, packaging, and handling.

Figure 3.9 shows the mechanical test of MD-printed and cast drug-loaded ODFs compared to the Listerine PocketPaks® ODFs. It is worth noting that for MD-printed films the breakpoints were mostly close to the contact point with the clamps, whereas for the cast films, some broke in the middle and others broke close to the contact point with the clamps. The likely cause of the breaking points of the MD-printed films being closer to the clamps is the lower thickness of the edges than the centres, as illustrated in Figure 3.6 B. The tensile strength and elongation at break for Listerine PocketPaks® films were 29.29 ± 2.39 N/mm^2 and 0.99 ± 0.14 %, respectively; both parameters were statistically significantly lower than the cast ($p = 0.008 < 0.05$. and $p = 0.001 < 0.05$) and MD-printed ODFs ($p = 0.008 < 0.05$. and $p = 0.001 < 0.05$). Although the Listerine PocketPaks® use pullulan as the primary film-forming polymer, the thickness of Listerine PocketPaks® films is very similar to the MD-printed films (see Figure 3.6 B). As the film thickness has a significant effect on the mechanical properties, it is reasonable to directly compare the mechanical properties of the MD-printed film and Listerine PocketPaks®. The results imply that the MD-printed drug-loaded ODFs have better handling properties than Listerine PocketPaks® ODFs. The tensile strength of the 18 mm x 18 mm MD-printed ODFs and cast ODFs were 60.39 ± 7.43 N/mm^2 and 53.27 ± 2.19 N/mm^2, respectively, which shows no statistical difference ($p = 0.115 > 0.05$). The percentage elongation for the MD-printed ODFs and cast ODFs were 2.50 ± 0.47 % and 7.00 ± 1.51 %, respectively, showing a significant statistical difference ($p = 0.001 < 0.05$). The difference seen in the elongation between cast and MD-printed

drug-loaded ODFs could be due to the difference in the uniformity in thickness of the films made by the two methods. The cast films have highly uniform thickness because they were cut from the centre of a large parent film, whereas the MD-printed films were individually printed with no wastage, but the edges of the films that are directly in contact with the clamps of the texture analyser sample holder were thinner than the centres of the films, and therefore offered a lower cross-sectional area.
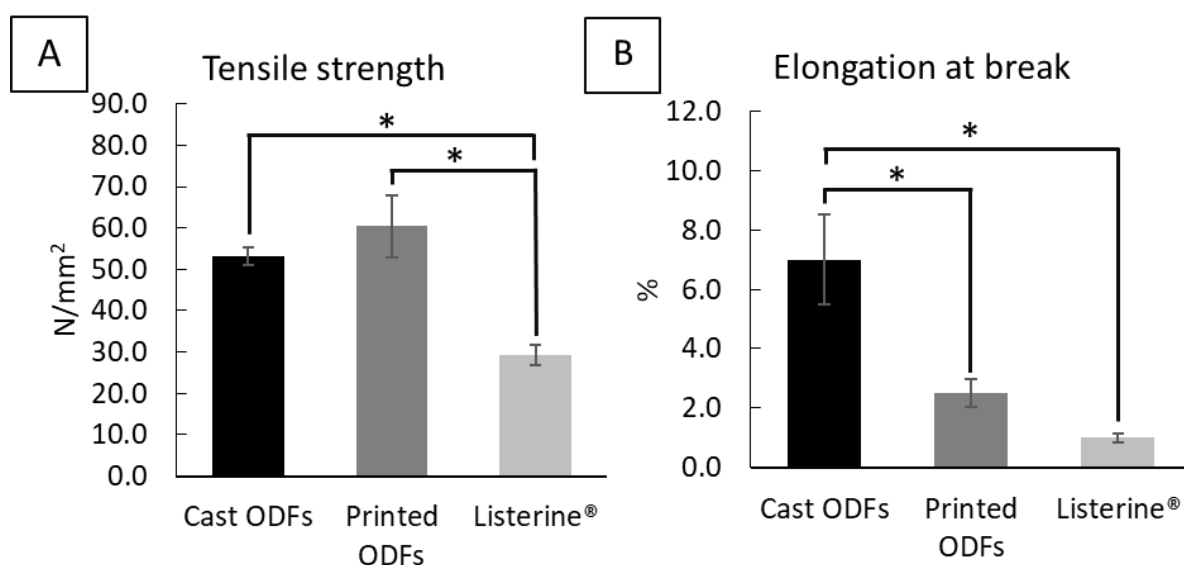
Figure 3.9. *Mechanical properties of drug-loaded ODFs prepared by casting and MD printing, and Listerine PocketPak® films: (A) tensile strength measurements and (B) elongation at break (%). Asterisks refer to a statistically significant difference with cast film.*

3.3.8 Drug content uniformity in MD-printed ODFs

The relationship between the dispensed drug within the MD-printed ODFs and the number of printing cycles ranging from 1 to 8 is shown in Figure 3.10 A. The number of printing cycles showed a highly linear relationship with the amount of paracetamol loaded into the ODFs with an excellent correlation coefficient ($R^2 = 0.995$). When the drug quantity in Table 3.3 is converted into a percentage (% w/w) drug loading (drug content/dry film weight x 100%), with changing the number of printing cycles, the paracetamol loading concentration (% w/w) of the MD-printed ODFs remained relatively constant, ranged from 7.89 to 7.27 % w/w. The concentration difference is

less than 0.36% if the paracetamol concentration in cast ODF (7.63% w/w) is taken as the benchmark. According to the literature, the drug content uniformity of ODFs is suggested to be within 85 – 115% of the average drug content[160]. The drug contents of all MD-printed ODFs fall well within this range. This result indicates a low inter-drop volume variance of the MD printing process. The high accuracy in drop volume and the reproducibility of the printing allows the MD printing to be used as a small-batch manufacturing process to produce ODFs with adjustable doses by simply changing the number of printing cycles.
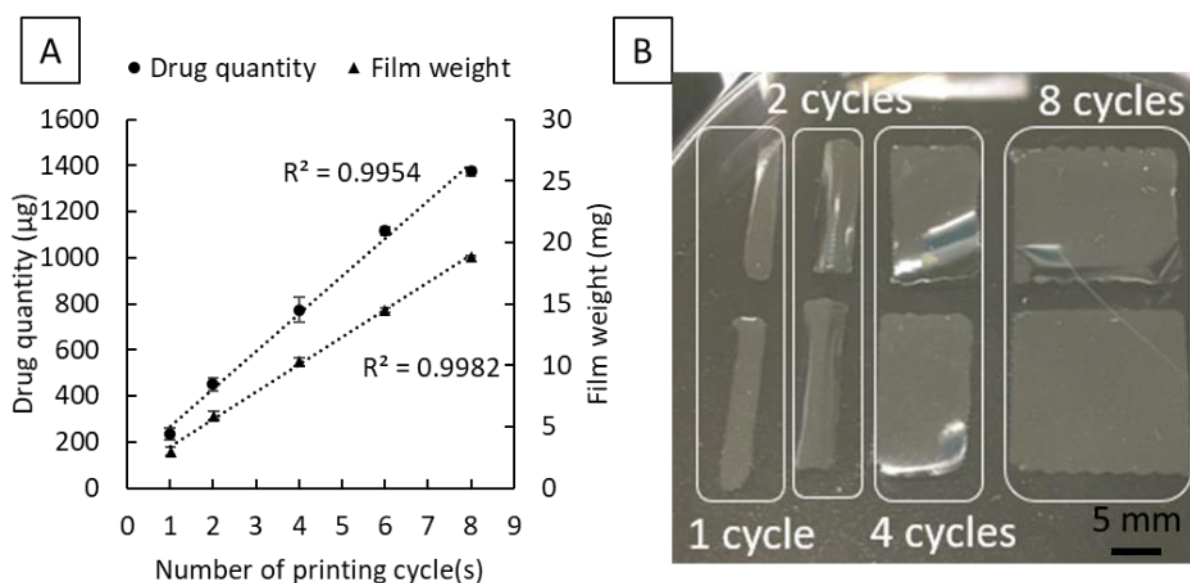
Figure 3.10. *(A) Amount of paracetamol in drug-loaded ODFs prepared by MD printing with different numbers of printing cycles; (B) digital photography of the MD-printed ODFs with different printing cycles.*

3.3.9 Disintegration behaviour of drug-loaded ODFs prepared by MD printing

The disintegration times of drug-loaded ODFs prepared by casting and MD printing are reported in Table 3.3. The disintegration time of the MD-printed films (eight printing cycles) and the cast films are 29.0 ± 3.6 s and 30.0 ± 3.6 s in PBS pH 7.4, respectively. No statistical significance is exhibited by the MD-printed (eight printing cycles) and the cast films. When comparing the disintegration time among different printing cycles, the results show no statistical difference either by the one-way ANOVA test. Disintegration time is one of the critical factors to consider in manufacturing ODFs.

The European Pharmacopeia suggested that the ODF is expected to dissolve in 3 minutes when it is put on the tongue in the oral cavity[161]. The FDA stated that the oral dispersible tablet's disintegration time (which may apply to ODFs) is lower than 30 s in water[162]. However, there are no agreed specifications for the method to determine the disintegration time for ODFs. The printed ODFs were able to fulfil the criteria set by European Pharmacopeia. It has been reported in the literature that the thickness of ODFs can significantly affect the disintegration time[163]. Although the overall thickness of the drug-loaded ODFs prepared by MD printing (eight printing cycles) and casting showed a statistical difference, it may not be significant enough to show a significant difference in disintegration time. The fast disintegration led to the rapid and complete dissolution of the film within 5 minutes.

The number of printing cycles is independent of the disintegration time which is the time taken for the film to disintegrate, but not completely dissolve. This is likely because the film thickness of most of the MD-printed films remained mainly between 40 - 60 µm (Figure 3.11). Although the film dimension increases with printing cycles, the thickness of the film is likely to be the dominating factor in controlling the disintegration time of the film.
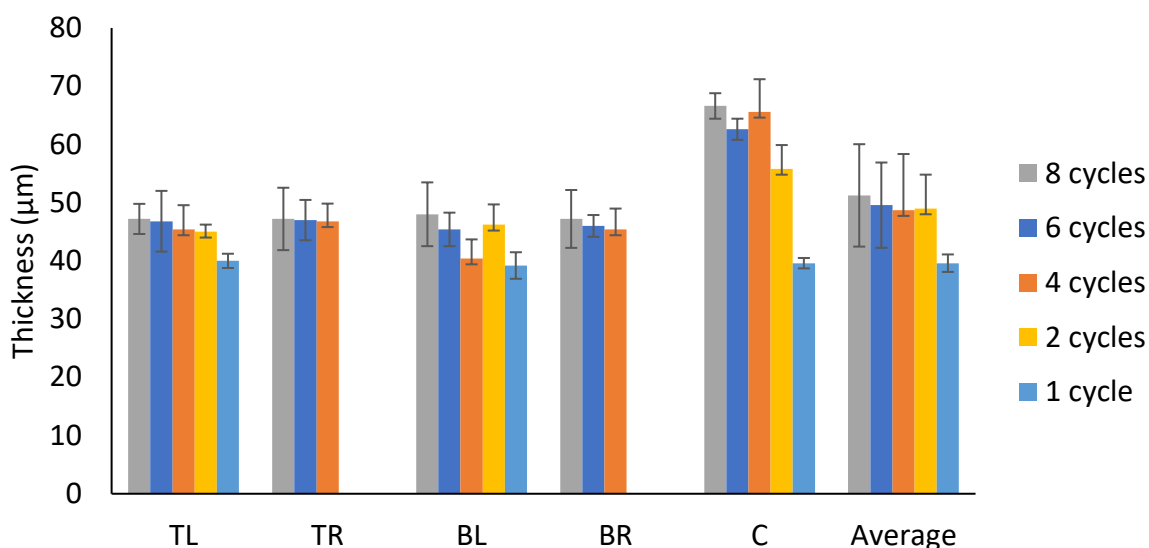
Figure 3.11. *The thickness of all MD printed films with different printing cycles. TL = top left, TR = top right, BL= bottom left, BR = bottom right, C = centre. The small dimension of print films with one cycle and two cycles limits the thickness measurement and therefore, only three measurements were taken.*

3.3.10 Analysis of MD printing as a manufacturing method for drug-loaded ODFs

The concept of individualised medicine was suggested to benefit patients by delivering an appropriate amount of API to avoid adverse side effects and improve patient compliance. The data presented in this study suggested that a MD system could fit well into the point-of-care production of personalised medicine on-demand model for ODFs products. The major advantages of MD printing over inkjet printing are being able to operate on viscous liquid formulations (up to 8000 mPa.s for the printhead used in this study[164]) and produce substrate-free ODFs. ODFs prepared by inkjet printing require an edible substrate to absorb the drug ink[40,41], which is unnecessary for ODFs prepared by MD. The ink absorption kinetic, the thermodynamic changes according to the solvent used in ink formulation and the substrate increase the complexity of the manufacturing process[41]. Inkjet printing ink formulation containing low polymer concentration with high drug concentration is a strategy to overcome low drug loading per drop[51]. However, the high risk of drug recrystallisation over time while printing should not be ignored in such liquid formulations with high drug loading. The accumulation of drug crystals and small nozzles used for inkjet printheads increases the likelihood of nozzle blockage, which

is less likely for the MD since a bigger nozzle is used to deposit viscous ink. MD can also dispense lipid-based formulations such as emulsions to enhance the drug loading of poorly water-soluble drugs in ODFs, which is another advantage compared to inkjet printing.

In terms of the feasibility of the manufacturing process, first, the polymer-drug inks with fixed drug concentrations could be centrally prepared in pharmaceutical manufacturing plants with Good Manufacturing Practices standards. The standardised inks can be distributed to point-of-care manufacturing sites, such as hospital pharmacies, to be printed by a MD system in a clean environment to produce tailored doses of ODFs on-demand for patients. Scaling up the manufacturing would be possible by using multiple print heads simultaneously to increase the production volume.

In this study, a drug-polymer ink was prepared in water to print the ODFs. The solvent system used in this study was limited to APIs with moderate to good aqueous solubility. Hydrophobic APIs require formulation development or the use of a solvent system to improve their solubility in ink. Although using organic solvents in the solvent system can improve the solubility of less-water soluble APIs, the residual solvents in the ODFs could pose safety issues if the solvent evaporation is not completed. If using organic solvents are necessary, those with FDA classification class 3, such as ethanol, acetone, and ethyl acetate, would be preferable. Extended drying time under controlled temperature will be required to avoid incomplete solvent evaporation, which increases the running cost and manufacturing time.

Alternatively, the preparation of an emulation-based ink for hydrophobic APIs could be a solution to improve the drug solubility in ink. The stability of the emulation is critical since it could be stored at the point-of-care for a long period before use. The instability of the emulsion adversely affects the distribution of the drug content in ink and the accuracy of drug loading in printed ODFs.

Printing time is worth considering regarding scaling up the production of personalised ODFs. Currently, the printing time of the eight cycles ODFs takes 131 seconds. The long print time is mainly due to the slow speed of the motorised stage. The print time could be substantially shortened by using fast motorised stages (for example, 50 mm/s) combined with higher printing frequency.

3.4 Conclusions

Overall, on-demand additive printing of fast dissolving ODFs with various doses of paracetamol was demonstrated by the MD system. A viscous polymer-drug ink was used to enable single-pass printing to fabricate ODFs with sufficient thickness for good handling. The dose of paracetamol in ODFs was adjustable linearly by printing ODFs with different printing cycles to change the print area. The deposition of droplets was sequenced to have sufficient overlapping to produce solid ODFs. The surface morphology of printed ODFs was comparable to the cast ODFs, showing a smooth surface without any bubbles. Although the mechanical properties of printed ODFs were statistically different from the cast film, the disintegration time was similar for both fabrication methods. The MD system is designed for depositing viscous liquid with high accuracy, which is suitable for fabricating tailored dose ODFs on-demand. The MD system can avoid issues such as blocked nozzles and recrystallisation of API, which can be an issue for ODFs prepared by inkjet printing. The results of this study demonstrated that the MD printing is an accurate liquid dispensing method for viscous fluids, indicating that the technology has the potential for not only point-of-care ODFs production in small batches but also other liquid dispensing and coating applications for personalised medicine and device fabrications.

Chapter 4 Precision coating of ocular devices/contact lenses by nanoelectrospray additive printing

4.1. Introduction

Eye drops are the most used method of administering ocular medications. It is challenging for patients to use eye drops properly because the drop often runs off the eye. A more critical factor is that bioavailability of eye drops is generally limited to 1 - 5%[165] due to the drug loss through the clearing of tears and drainage of the eye. It is necessary to install eye drops frequently to maintain the drug concentration in the eye at the therapeutic level[166]. Eye drops have also been reported to have poor patient compliance[167], irritation caused by preservatives[168], highly variable dosing[169], and poor drug absorption. Drug-eluting contact lenses (DECLs) were explored as an alternative to eye drops and had been proven to improve treatment efficacy[85]. For the manufacturing of DECLs, various methods have been proposed in the literature, but all techniques have limitations as detailed in Chapter 1[72].

In this study, the design, working principle, characterisation and optimisation of the bespoke nanoelectrospray (nES) system are detailed. A custom-designed nES printing system was built to be a new platform coating technology that can coat contact lenses with polymer/drug formulations to produce DECLs. The nES system enables the on-demand deposition of a thin layer of polymeric coating onto the peripheral area of commercially available contact lenses to preserve the vision zone, aiming to mitigate its influence on the intrinsic physical properties of the contact lens. Zein, the model biopolymer with good film-forming properties, was precisely coated onto the peripheral region of commercially available soft hydrogel contact lenses without blocking the vision zone.

The experiment aimed to investigate the relationship as follows.

- Nozzle substrate distance and spray width
- Dosing speed and the coating thickness
- Layers of overprint and coating thickness

- Location of coating on the contact lens to maintain an unobstructed vision zone
- Prediction of spraying volume using an established scaling law
- Polymer concentrations and the coating morphology

The results showed that the nozzle substrate distance primarily controls the spraying width and it should be considered before adjusting other spraying parameters to build up the required thickness. The coating thickness is subject to the polymer concentration in the formulation, dosing speed and the number of rotations. The polymer concertation can affect the coating morphology significantly; therefore, screening the polymer concentration is necessary for the desire coating morphology. By using the spray current transient and an established scaling law, the predicted spray volume is highly correlated to the experimental results. The findings from this study will be helpful in the next stage of the experiment, where drug-polymer solutions will be sprayed on contact lenses.

4.2. Materials and methods

Unless considered in this chapter, the materials and methods are specified in Chapter 2.

4.2.1. Materials

Purified zein was obtained from Thermo Scientific (Loughborough, UK). Ethanol absolute was sourced from VWR Chemicals (Lutterworth, UK). Milli-Q (Millipore, Merck, USA) ultra-pure water was used as part of the solvent system. Fluorine-doped tin oxide glass slides were purchased from Sigma-Aldrich (Gillingham, UK). All materials were used without further processing. MicroDot Dispense tips with a 50 μm inner diameter (P/N 7364054) were purchased from Nordson EFD (Bedfordshire, UK). Commercial soft contact lenses, Biomedics 1-day extra contact lenses (CooperVision Ltd, USA), with a composition of 45% ocufilcon D/55% water, were used as the model lenses.

4.2.2. Preparation and physical characterisation of zein solutions for nES

The 2.5% w/v and 5% w/v zein solutions were prepared by dissolving the required amount of zein powder in either 70% or 80% w/w aqueous ethanol using a vortex mixer at ambient conditions until all powder dissolved. The details of the formulations are stated in Table 4.3. The resulting solution were then filtered by a 0.45 μm PES syringe filter (Fisher Scientific, Loughborough, UK) before the nES process. The electrical conductivity, viscosity, surface tension, and density of the zein solution were measured according to the methods reported in Chapter 2.

4.2.2.1. Viscosity

The viscosity measurement was done in triplicate to calculate the average viscosity at 80 s^{-1} for comparison between formulations since zein in the aqueous ethanol showed shear thinning behaviour.

4.2.3. Process characterisation and optimisation of the custom-made nES system

A few spraying parameters of the nES system were characterised to understand their influence on the coating quality, and clarification of them is needed. The radius indicates the relative distance between the centre of a circle at the pre-set x, y coordinate to its perimeter, enabling polymer film deposition with varied sizes as rings or dots on the substrate (depending on the spraying mode). The number of rotations controls the number of layers of overprint deposited on the surface. The dosing speed controls the speed of travel for the nozzle relative to the substrate, with a higher number implying a faster moving speed. The nozzle substrate distance (NSD) is the distance between the apex of the nozzle and the substrate, which is controlled by changing the distance travelled on the z-axis.

Three spraying parameters were investigated by the one-factor-at-time approach to understand their influence on the deposited zein film's width and thickness. These are NSD (ranging from 1.5 to 4.5 mm), dosing speeds (ranging from 10 to 40 mm/s) and the number of rotations (ranging from 10 to 40 turns). The characterisations of this section were performed using an electrically conductive fluorine-doped tin oxide glass substrate as the deposition surfaces. Three rings of each experimental setting were prepared for surface profile measurement.

4.2.4. Surface profile measurement of zein films by a stylus profilometer

A Stylus Profilometer (DektakXT, Bruker, MA, USA) was used to measure the surface profile of zein films. The 'Hills and Valleys' profile was used for measurements and the 2 μm radius stylus was set at 1 mg stylus force. Three locations of the zein films were selected as shown in Figure 4.1 to calculate the average spraying width and step height (thickness) of the zein films.

Locations of measurements
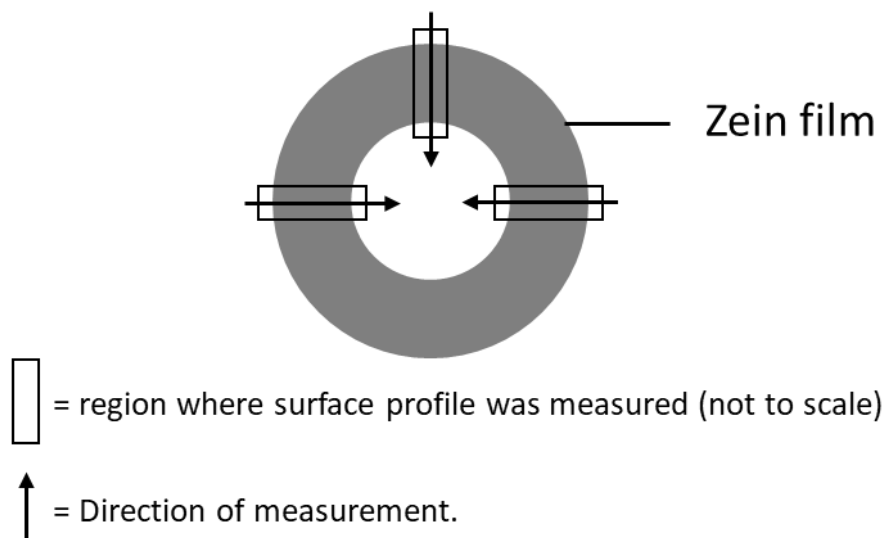
Figure 4.1. *Locations on zine films where surface profile measurements were performed.*

4.2.5. nES printing of a zein solution on the soft hydrogel contact lenses

In the example printing, the solution with 5% w/v zein in 70% w/w aqueous ethanol (Z3) was sprayed on the contact lens using the parameters stated in Table 4.1. The optical transmittance of the nES coated contact lenses (N=3) were measured following the method reported in Chapter 2.2.6 to determine the spraying radius that does not blocks the vision zone. The surface morphology of the coating was imaged using cryo-SEM reported in Chapter 2.2.8.

Table 4.1. *nES spraying parameters of Z3 solution on the contact lens.*

nES condition	1	2	3
Voltage (kV)	1.889	1.889	1.889
NSD (mm)	2.23	2.19	2.22
Spraying radius (mm)	4.5	5	5.5
Dosing speed (mm/s)	30	30	30
Number of revolutions	90	90	90

4.2.6. Calculation of nES deposition volume

In this process, the spray current transient was captured during the printing cycle. An example of a spray current transient is shown in Figure 4.2 below, where $\tau_{on} = (t_2 - t_1)$ and amplitude I_{DC} is the average current in the time frame of τ_{on}.

The value of I_{base} was determined by averaging the current values from just before the steep rise in current at the onset of the transient pulse and was taken from an average of around 20 datasets. Then I_{peak} was measured as the highest current level reached in the transient and taken as the average of 20 measurements. The time threshold for t_1 and t_2 were taken at the points on the rising and falling current transient where the current level satisfied the condition $I > [0.25(I_{peak} - I_{base}) + I_{base}]$.

Three consecutive peaks were taken to calculate the average time required to perform one complete ejection period, τ_p, where $\tau_p = (\tau_{on} + \tau_{off})$. This is then used to calculate the nES pulsation frequency during printing, $f = 1/(\tau_p)$.
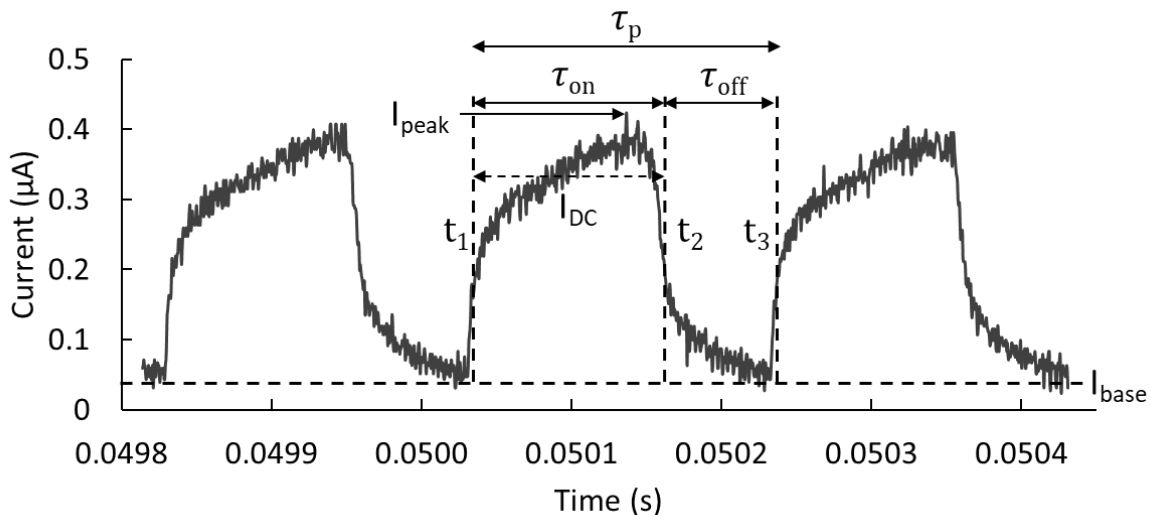
Figure 4.2. *Example current waveform of a 5% w/v zein solution captured during the nES. The waveform is used to calculate the spray volume per unit pulse.*

The procedure for analysis of the nES current transients to estimate the volume of solution deposited during the printing cycle was adapted from earlier work[103] and is briefly described here. An inline flowmeter was not used and instead the flow rate during nES printing was estimated by combining spray current transients, recorded by a fast current amplifier, with the established electrospray scaling laws. According to Fernandez de la Mora[170], the nES transient jet can be considered steady if the jet lifetime, τ_{on}, is longer than the electrical relaxation time, τ, where $\tau = \frac{\varepsilon \varepsilon_o}{K}$ and ε_o is the permittivity of free space, ε is the relative permittivity and K is the electrical conductivity of the solution. For the solutions used in this work, values for τ range from 1.04×10^{-8} s to 1.61×10^{-8} s, far shorter than any jet lifetime observed, which were typically 50 - 100 μS as indicated from the current transients. The second condition is that the jet diameter is less than the nozzle diameter. The jet diameter in the present work was observed to be much smaller than the nozzle diameter. Having satisfied these conditions, the rearranged scaling law expression previously described in equation (4.1)[103] can be used to estimate the volume ejected during a single pulsation, v_{est}.

The volume ejected during a single pulsation event is related to the total charge ejected as described by Paine et al.[103]:

$$v_{est} = \frac{\tau_{on}\epsilon}{\gamma K}\left(\frac{I_{DC}}{f(\epsilon)}\right)^2 \ldots \text{Eqt. (4.1)}$$

, where τ_{on} is the on-time in Figure 4.2, γ is surface tension, K is the electrical conductivity of the solution, I_{DC} is calculated by averaging the current transient to estimate the charge per cycle, then dividing by the number of pulsation events, and $f(\epsilon)$ is a function given by De La Mora and Loscertales[170,171], where $f(\epsilon) = 18$ when the permittivity is greater than 40. All solutions used in this study higher permittivity higher than 40, therefore, $f(\epsilon) = 18$.

Finally, the total printed volume, v_{tot}, can be estimated as follows:

$$v_{tot} = \left(v_{est} \times f \times t_{pnt}\right) \ldots \text{Eqt. (4.2)}$$

, where t_{pnt} is the total spraying time, f is the spray frequency and v_{est} is the estimated spray volume per pulse using equation 4.1.

4.2.7. Determination of spray mass by UV-Vis spectrometry

A stock solution of 5% w/v zein solution in 70% w/w aqueous ethanol was prepared for this experiment. The stock solution was diluted to concentrations ranging from 0.2 mg/ml to 1 mg/ml to build a calibration curve, measured by the UV-Vis spectrophotometer Lambda 35 at 278 nm. The stock solution was nanoelectrosprayed on an aluminium foil according to spraying parameters stated in Table 4.2. Three rings were prepared for each experimental setting. The coated foil was immediately immersed into 1 ml of 70% w/w aqueous ethanol to dissolve the zein coating, followed by quantification using the UV-Vis spectrophotometer. The deposited volume calculated by scaling law was converted to the mass using the density equation, $\rho = m/v$, where ρ is the density, m is the mass and v is the volume. The results were then compared with the UV-Vis spectroscopy method.

Table 4.2. *nES parameter of the 5% w/v zein solution (Z3) on aluminium foils*

nES condition	1	2	3
Voltage (kV)	2.2	2.2	2.2
NSD (mm)	2.5	2.5	2.5
Dosing speed (mm/s)	10	15	30
Number of revolutions	100	100	100
Spraying radius (mm)	5	5	5
Spraying time (s)	266	176	88

4.2.8. Statistical analysis

The basic calculation was performed by Microsoft Excel® (Microsoft Office 365). The data analysis was performed using SPSS statistical program (SPSS 25, IBM, New York, USA). Analysis of variance (ANOVA) and the Tukey test were used to compare the spraying width and thickness. A statistical significance is considered when the p-value is lower than 0.05.

4.3. Results and discussion

4.3.1. Effects of nES parameters on spraying width and film thickness

The physical properties of zein solutions used for nES are reported in Table 4.3. Two concentrations of zein solutions were prepared to understand the influence of polymer concentration on the film quality. The viscosity of Z1-2 (2.5% w/v) and Z3-4 (5% w/v) zein solutions decreased with increased ethanol concentration from 70% w/w to 80% w/w, showing a statistically significant difference ($p < 0.05$). The viscosity of a solution is dependent on the polymer concentration, the polymer's molecular weight and the solvent system[172,173].

The electrical conductivity was found to decrease with higher ethanol concentration in the solution for both concentrations of zein solutions. The electrical conductivity is also subjected to zein concentration, in which the 5 %w/v solutions have higher electrical conductivity than the corresponding 2.5 %w/v solutions. The electrical conductivity can influence the flow rate and ejected volume in nES operation which the electrical conductivity of the precursor solution has an inversely proportional relationship with the ejected volume according to Eqt 4.1[103].

The surface tension for Z1 - 4 solutions is stated in Table 4.3 and shows no statistical difference between solutions. The surface tension primarily affects the strength of the electric potential applied to the solution to break the liquid jet into fine droplets. The results above showed a similar trend in literature that higher ethanol concentration in the zein solution leads to lower electrical conductivity, density, and viscosity[174].

Table 4.3. *Physical properties of zein solutions for nES*

	Formulations			
	Z1	**Z2**	**Z3**	**Z4**
Zein (%w/v)	2.5	2.5	5	5
Ethanol (%w/w)	70	80	70	80
Conductivity (µS/cm)	200.0	186.2	333.0	293.0
Density ± SD (g/ml)	0.87 ± 0.01	0.85 ± 0.01	0.88 ± 0.01	0.86 ± 0.01
Surface tension ± SD (mN/m)	25.7 ± 1.0	24.9 ± 0.8	25.5 ± 1.2	24.7 ± 1.0
Viscosity ± SD (mPa.s)	4.20 ± 0.05	3.87 ± 0.06	5.60 ± 0.09	5.15 ± 0.05

Different nES process parameters were investigated to understand their influence on the spraying width and polymer film thickness. The characterisation results of Z2 and Z4 are present in Figure 4.3 and the rest of the data are included in the appendix Figure A.3. Figure 4.3 A-B shows the results of the influence of dosing speed on Z2 and Z4 solutions at 3.5 mm NSD with ten rotations. The spraying width for Z2 and Z4 solutions ranges from 4.46 to 4.86 mm and 4.74 to 4.96 mm, respectively. The thickness of films for Z2 and Z4 decreased with increasing dosing speed from 10 mm/s to 40 mm/s, showing an excellent fitting to the power-law ($R^2 > 0.99$) (Figure 4.3 B). With the increased dosing speed and the rest of the spraying parameters fixed, the overall spraying time and the total amount of material deposited on the substrate are reduced. The results indicate that the dosing speed primarily controls the thickness of the film and does not significantly affect the spraying width.
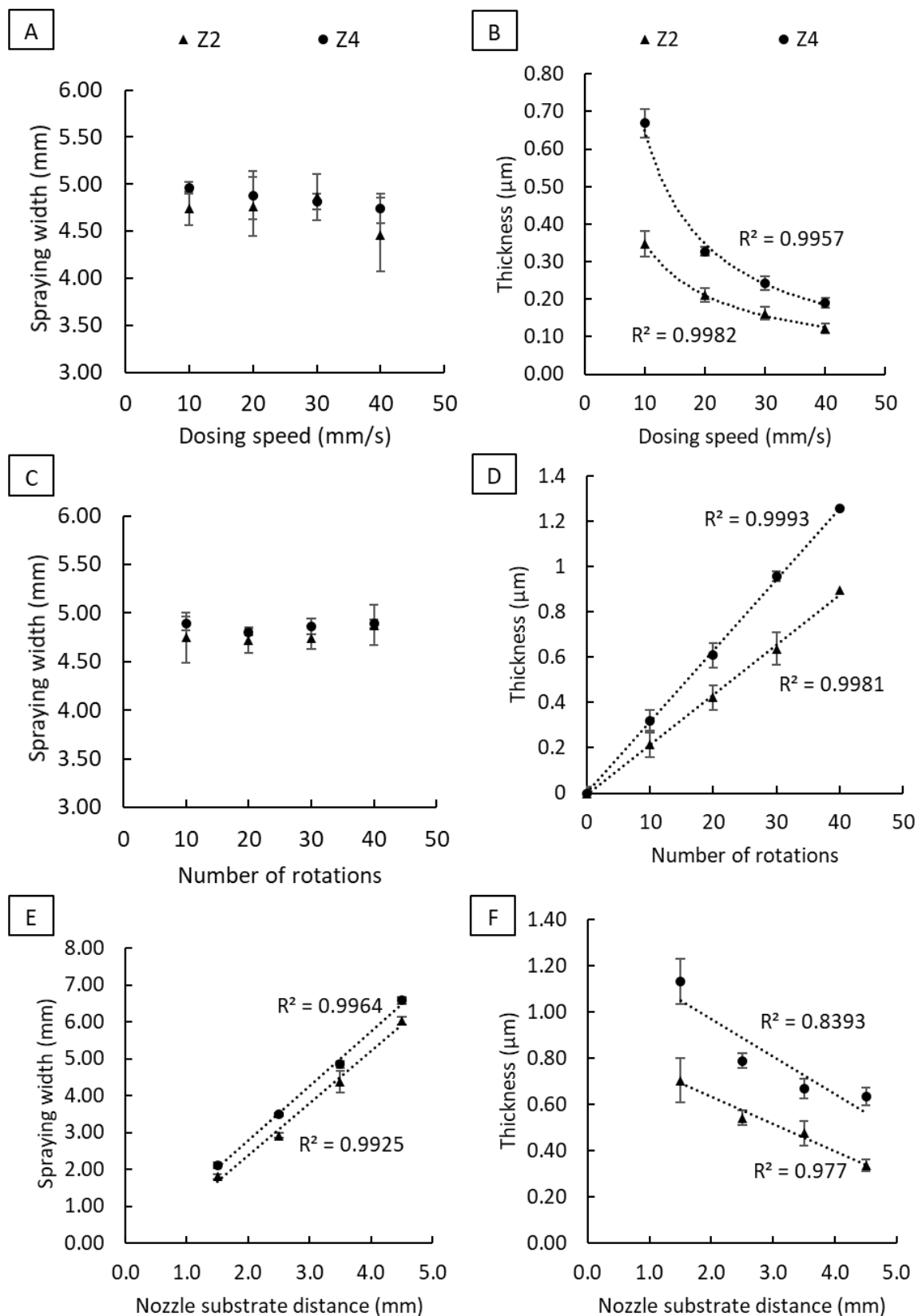
Figure 4.3. *The effect of (A-B) nES dosing speed, (C-D) number of rotations and (E-F) nES NSD on the spraying width and film thickness of Z2 (2.5% w/v) and Z4 (5% w/v).*

For multiple printing rotations, the spraying width and film thickness against the number of rotations for all solutions is shown in Figure 4.3 C-D. The spraying width for both Z2 and Z4 did not show significant changes at different numbers of rotations. The spraying width ranges from 4.72 mm to 4.87 mm and 4.81 mm to 4.89 mm for Z2 and Z4, respectively. The film thickness increases from 0.21 μm (10 turns) to 0.9 μm (40 turns) and 0.32 μm (10 turns) to 1.26 μm (40 turns) for Z2 and Z4, correspondingly. The thickness of zein film for both concentrations shows a linear relationship with the increased number of turns with a good correlation factor ($R^2 > 0.99$).

The effects of NSD on the spraying width and film thickness are shown in Figure 4.3 D-E. The voltage was adjusted accordingly to obtain a stable spray for different NSDs. For Z2, the spraying width increases from 1.81 mm at 1.5 mm NSD to 6.03 mm at 4.5 mm NSD. For Z4, the spraying width increases from 2.11 mm at 1.5 mm NSD to 6.58 mm at 4.5 mm NSD. It is evident that NSD is the main spraying parameter to adjust the spraying width. Increasing NSD resulted in a broader spraying width with a positive linear relationship for both solutions and a good correlation factor ($R^2 > 0.99$). The thickness of films for Z2 and Z4 reduces accordingly with increased NSD and follows a linear relationship.

To optimise the spraying width and film thickness, the NSD is the first operational parameter that should be determined to achieve the desired spraying width according to the required application. With the example of commercially available contact lenses used in the present work, the area for patterning was limited to a peripheral ring of around 3.1 mm width and 8 mm diameter to avoid coating the visual area of the lens. The NSD also controls the drying time of droplets generated by nES, which affects the coating morphology[175]. The higher NSD provides sufficient time for solvent evaporation, resulting in dry particles accumulating on the substrate. The NSD can influence the film morphology from ES deposition due to the solvent evaporation and drying process of in-flight droplets. For example, it has been reported that at a sufficiently large NSD the deposited particles are dry enough to stack on each other to form a rough film[112]. On the other hand, a smooth film can form when the NSD is low enough that the semi-dry nES droplets fuse on the substrate due to insufficient

drying time[112]. Next, the dosing speed should be considered, which primarily controls the coating thickness and might affect the drying time of the nES-deposited droplets. Finally, the film thickness can be built up by changing the number of rotations to achieve the required thickness.

4.3.2. **Effects of nES parameters on the surface profile of zein films**

Two concentrations of zein were nanoelectrosprayed onto an electrically conductive glass substrate to investigate the influence of polymer concentration on the morphology of the film. The general surface profiles of Z1-Z4 on the glass substrate are shown in Figure 4.4**.** Z1 and Z2 solutions (2.5% w/v zein) formed a thin film on a glass substrate with a twin peak pattern and a trough-like centre with relatively low thickness. By doubling the concentration to 5% w/v (Z3 - 4), the deposited material formed a smoother surface profile with the absence of pronounced peaks.

The observed surface profiles can be explained by the spraying and drying processes. With the lower polymer concentration solutions (Z1 and Z2), a lower solution conductivity is observed leading to higher drop volumes and flow rates during deposition. The NSD was set to be reasonably close (3 mm) which does not leave sufficient time for the sprayed particles to dry before landing on the substrate. This results in fluid build-up and a coffee ring-like pattern that the zein molecules coalescence to form the twin peak pattern and a trough-like centre at the central area of the film. The gradual decrease of the thickness of the film from the centre to the edge could be accounted for by the accumulation of satellite droplets after solvent evaporation.
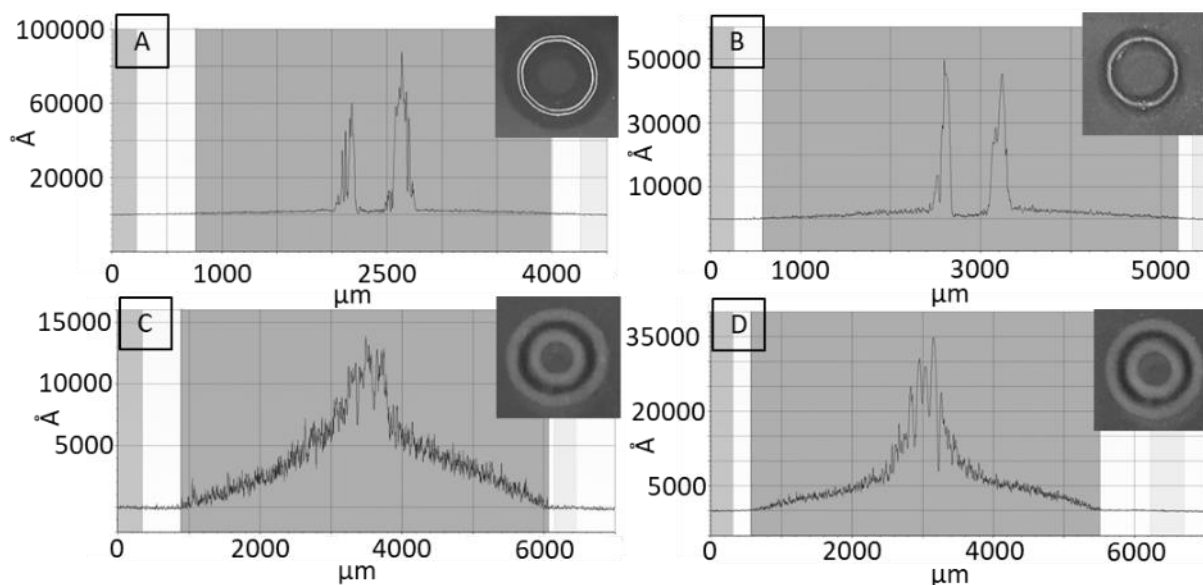
Figure 4.4. *The surface profile and the digital image (top right corner) of zein film deposited on the electrically conductive glass substrate, (A) Z1, (B) Z2, (C) Z3 and (D) Z4.*

As for Z3 - 4, the smoother film thickness profile with increasing thickness towards the centre of the film can be explained by the lower droplet volume and spray flow rate, resulting in the landing of semi-dried droplets without coalescence and bulk wetting. The higher central film thickness can be expected since the spraying solution formed a Taylor cone at the apex of the nozzle, followed by generating a fine plume of particles in a triangle shape. The charged particles/droplets undergo Coulombic fission during the flight to the substrate, producing finer particles/droplets landing further away from the centre of the film due to electrostatic repulsion[111]. The distance from the apex of the nozzle is the shortest distance from the centre of the film. Thus, the thickness of films is expected to be highest at the centre.

The effect of NSD on the observed uneven film thickness profile of the Z2 solution was investigated. The surface profiles of Z2 with NSD from 1.5 mm to 4.5 mm are shown in Figure 4.5. The twin peaks pattern remained in all surface profiles of the tested range of NSD. However, the distance between the peaks reduced gradually from 500 µm at 1.5 mm NSD (Figure 4.5 A) to 287 µm at 4.5 mm (Figure 4.5 D). The observation of a reduction in peak separation distance supports the explanation of a wetted central

band followed by the coffee ring effect during drying as there will be more time for solvent evaporation in flight resulting in the formation of a narrower wetted band.
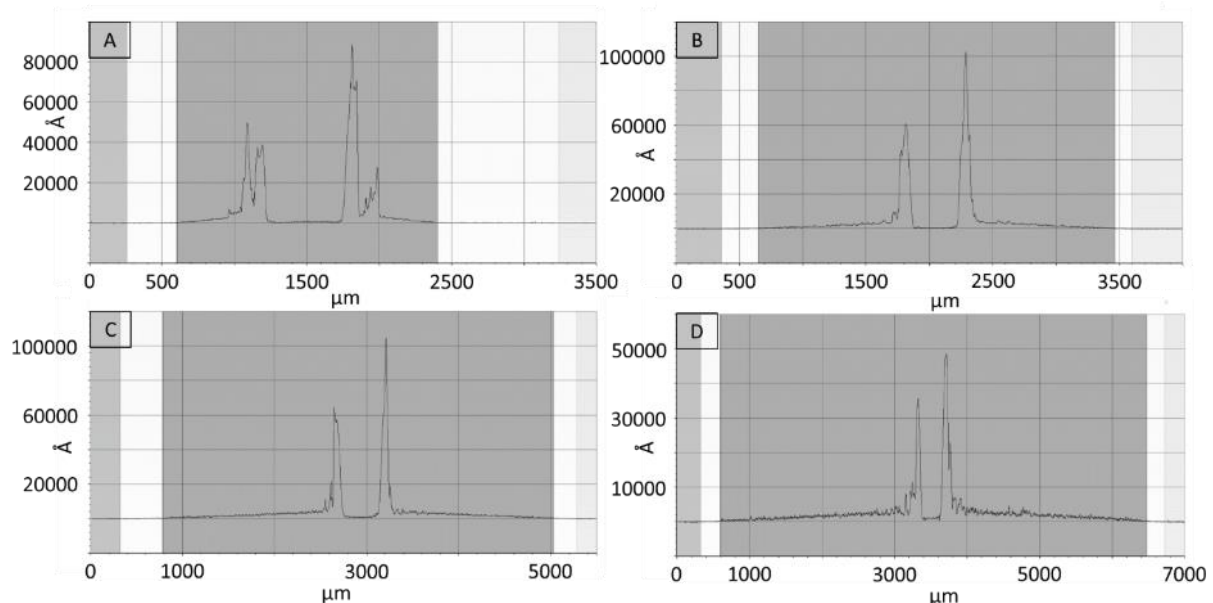
Figure 4.5. *The surface profile of zein films prepared by the Z2 solution at different NSD, (A) 1.5 mm, (B) 2.5 mm, (C) 3.5 mm and (D) 4.5 mm.*

4.3.3. The deposition of a zein solution (Z3) on commercial hydrogel contact lenses via nES

The targeted deposition area of zein (Z3) by nES on a contact lens is shown in Figure 4.6 A. A few factors were considered before coating the soft contact lens. First, the coating area should not cover the vision zone of the contact lens to preserve the optical property of the lens. In general, the optical zone diameter of a contact lens is 8 mm to cover the pupil for all lighting conditions[176]. The vision zone of the contact lens was assumed to be 8 mm in this study, leaving a 3.1 mm width at the peripheral region for coating. The NSD is known to be the main parameter affecting the spraying width and has a linear relationship with the spraying width (Figure 4.3 E). The NSD was set to 2.2 mm from the contact lens surface which had been shown to produce a spray width of approximately 1.2 mm with the tested solution. The radius parameter was then adjusted to avoid coating material deposited unnecessarily on the vision zone. The spraying radius is the distance from the centre of the lens to its perimeter from the top view. The optical transparency of contact lenses coated by zein (Figure 4.6 B) with different spraying radii is shown in Figure 4.6 C. The optical transparency is expected

103

to be at least 95% or above at 600 nm to provide an unobstructed vision. The results show that all coated contact lenses have optical transparency above 95%, whereas the blank contact lens shows 98% transmittance. The optical transparency shows a trend that it reduces with a smaller spraying radius, which is likely caused by the deposition of satellite drops near the centre of the lens, partially blocking light passing through the contact lens. Different printed materials may affect transmittance to a greater extent and perform differently because of the change in electrical conductivity of the spraying solution, which also affects the spray angle and the coverage of deposited material on the substrate. Therefore, the minimum radius needs to be determined. According to the results, it is concluded that the minimum spraying radius should be kept above 4.5 mm at 2.2 mm NSD.
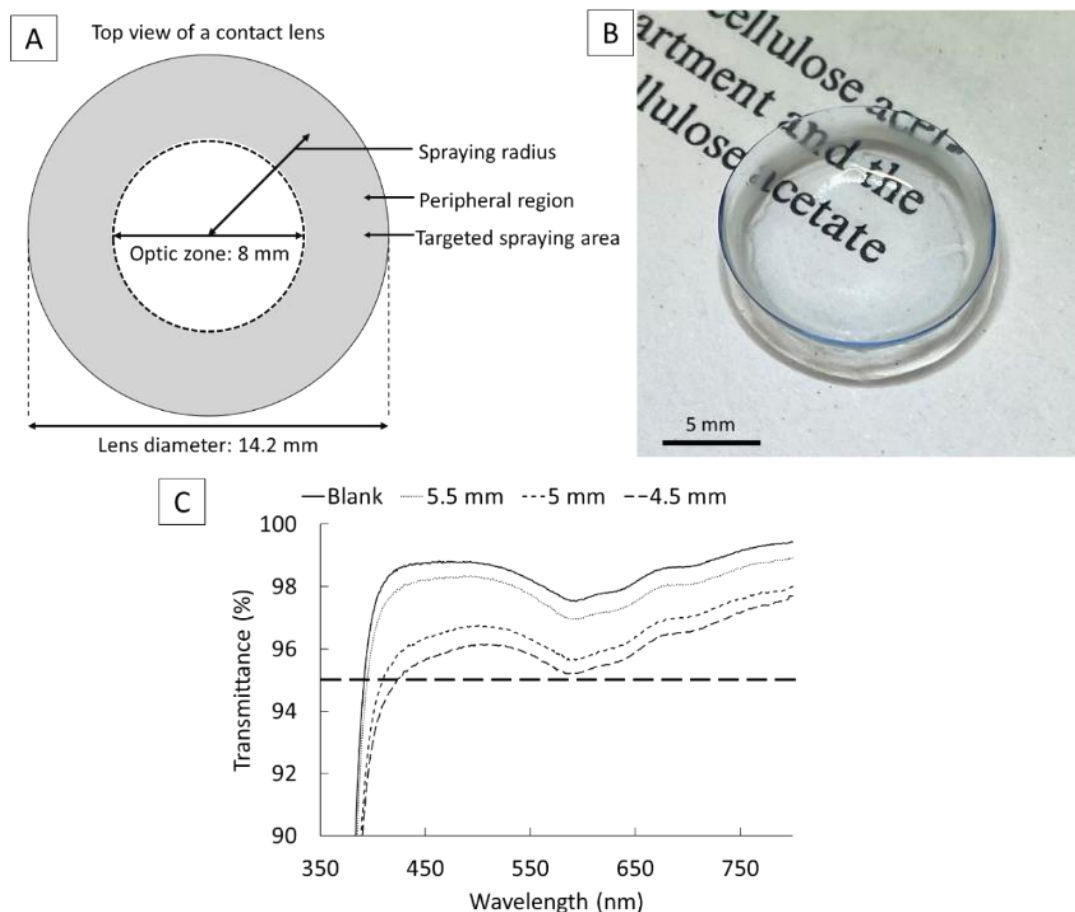
Figure 4.6. *(A) An illustration of the targeted spraying area on the contact lens; (B) a digital image of a Z3-coated contact lens on a piece of newspaper. The white ring at the peripheral region of the contact lens is the zein polymer deposited by nES; (C) optical transparency of blank contact lenses and zein-coated contact lenses with different spraying radii.*

The results of nES 5% w/v zein solution (Z3) on contact lenses with a range of radii are shown in Figure 4.7. Figure 4.7 A, C and E. The white ring indicates the zein coating on contact lenses and the centre of the lens remained free of zein polymer at different spraying radii. The SEM images (Figure 4.7 B, D and F) confirm that no zein polymer was deposited at the centre of the lens and was confined in the peripheral region. Figure 4.7 G shows the cross-sectional image of an example contact lens after coating zein polymer in the peripheral region. A dense film of zein film adhered to the peripheral region of the lens. Overall, the results show that the nES process can deposit the model polymer selectively at the targeted area and avoid coating the visual axis.
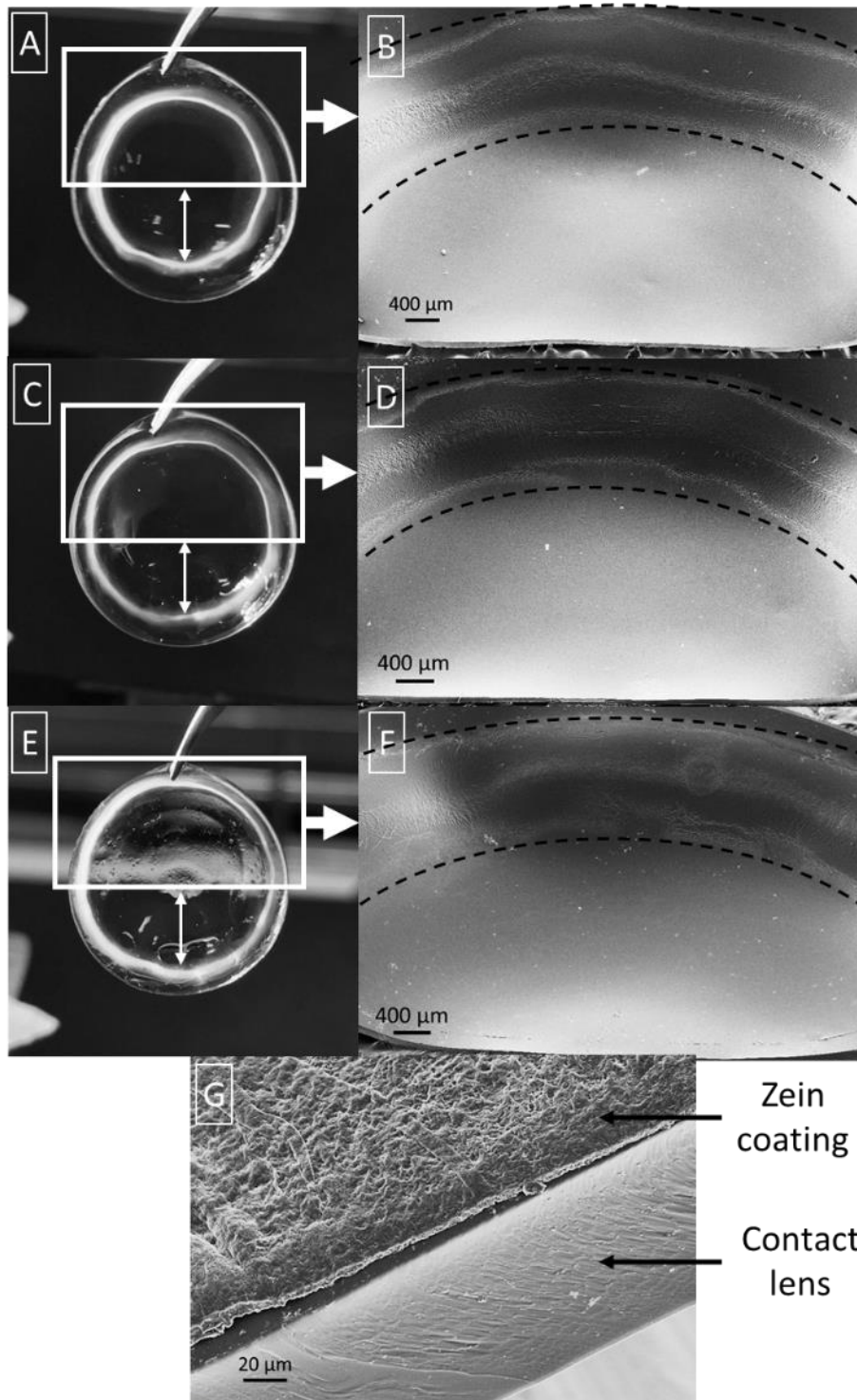
Figure 4.7. Cryo-SEM images of 5% w/v zein (Z3) coated lenses with different spraying radii (indicated by the white arrows); (A) 4.5 mm spraying radius, (C) 5 mm spraying radius and (E) 5.5 mm spraying radius. B, D and E are the magnified images to show the zein coating at the peripheral region (dotted lines) and a clear vision zone at the centre (G) Example of the cross-sectional SEM image of the zein-coated contact lens.

4.3.4. nES deposited volume measurement: Comparison of experimental data and theoretical prediction

The quantity of zein deposited on aluminium foil substrates was compared with the theoretically predicted quantity, yielded from the processing of current transients captured during the spraying process as described in method section 4.2.6. A UV-Vis spectrometer was used to quantify the amount of zein deposited on the substrate independently. Results from testing solution Z3 are presented as deposited solution volume against total spray time in Figure 4.8. As shown, both the experimentally measured and theoretically estimated printed zein volumes are linearly proportional to the total spray time with a good correlation factor (R^2 > 0.99), however, the amount of zein quantified by the UV-Vis method is found to be consistently lower than the amount from the transient estimation method.
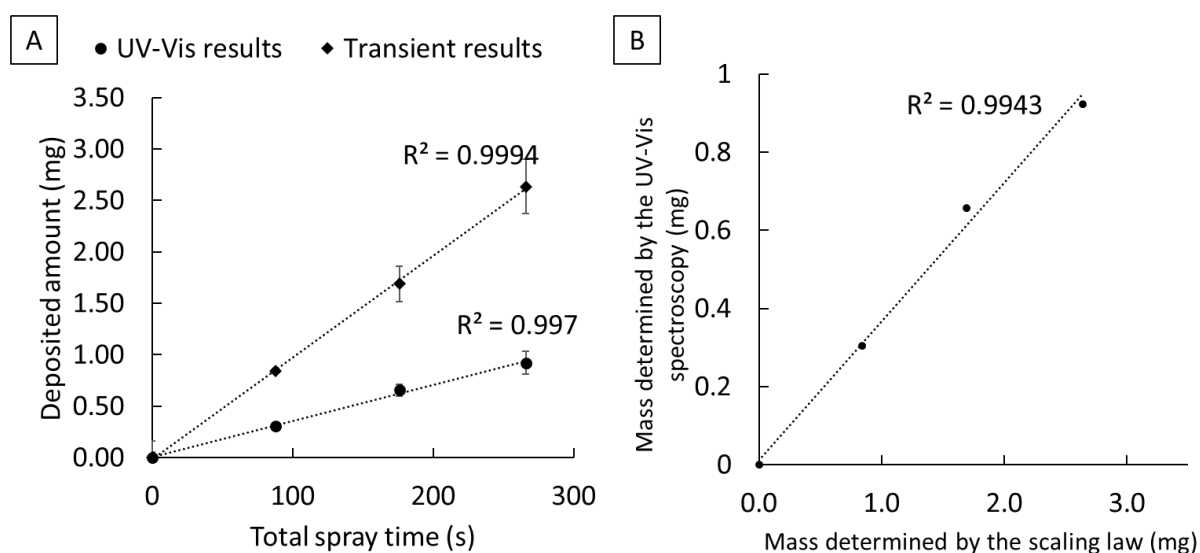
Figure 4.8. *Amount of zein quantified by the UV-Vis spectroscopy compared with the estimated mass calculated by the scaling law: A) each method against time and B) UV-Vis against the scaling law.*

The scaling law by De La Mora[29,30], which is then adapted by Paine et al.[22] in equation 4.1, provides a good scaling of spray current with a volumetric flow rate in ES but for a particular spray fluid only gives an order of magnitude estimation of the absolute spray current values at a particular flow rate. Therefore, in order to improve

the accuracy of material/drug dosing in the printed coating in the present work, it was necessary to include an empirically derived constant, A, to enable an accurate correlation of ejected charge measurements to deposit volume. For this reason, equation 4.2 is modified to include constant A, an experimentally derived constant from best-fit trendlines, to give an accurate volume estimate from the transient technique:

$$v_{tot} = A. v_{est}. f. t_{pnt} \quad ...\text{Eqt. (4.3)}$$

For the zein solutions evaluated in this study, the experimentally determined value of A, to give a correlation between the transient technique and UV-Vis measurements, was found to be 0.36. The theoretical data with and without experiment constant are shown in Table 4.4. The spray volume of zein measured by UV-Vis was found to range from 1.049 – 0.346 µl over the range of spraying time. Applying the experimental constant to the transient data, the spray volume is estimated to range from 1.079 – 0.344 µl. In these cases, equation (4.3) can be helpful in predicting the spray volume by using the current waveform captured during the spraying process.

Table 4.4. Theoretical and experimental calculations of the deposited mass of zein with different total spraying time

	Total spraying time (s)		
	266	**176**	**88**
UV-Vis results (mg)	0.923 ± 0.054	0.656 ± 0.109	0.305 ± 0.058
Transient results before correction (mg)	2.637 ± 0.160	1.690 ± 0.262	0.840 ± 0.171
Transient results after correction (mg)	0.949 ± 0.057	0.606 ± 0.094	0.302 ± 0.062

It is worth mentioning that there is no upper limit on the maximum coating thickness that can be deposited. The technique enables multiple print layers, and the thickness can be adjusted by changing the polymer concentration, dosing speed, NSD and the number of print rotations. The maximum deposition volume in a single experiment is controlled by the volume of the precursor liquid reservoir, which is 2.5 ml. From the

result of this study, the lowest and highest deposition volume for a single layer of zein coating was 3.46 nl and 10.49 nl, respectively. When depositing drug-containing formulas, as the processability is controlled by the electrical conductivity and viscosity of the spraying solution, the polymer can be replaced entirely by the drug as far as the spraying solution has suitable physical properties.

Although the nES system could precisely deposit a low volume of solution, a few limitations are worth discussing. For the use of the current transient to estimate the total spray volume, the precursor solution has to be electrically conductive. The oscilloscope will not be able to detect the current transient when the solvent system has extremely low electrical conductivity, such as organic solvents. Adding organic salts could provide adequate electrical conductivity to the precursor solution mainly containing organic solvents. However, many organic salts are toxic to humans and may not be suitable for biomedical applications. Using a precursor solution with extremely low electrical conductivity is possible for nES, but an alternative method is necessary to determine the quantity of materials deposited on the surface. On the other hand, the nature of the substrate plays a vital role in the spraying efficiency. Electrospray and nES require an electrically conductive substrate to establish a cathode or anode to generate the electric field. The glass substrate and contact lenses used in the study are considered electrically conductive substrates and thus, a smooth spraying process was observed as expected. Using nES to deposit coatings on non-electroconductive surfaces is possible with special substrate surface treatment[177]. Otherwise, the accumulation of charge on the surface will reduce the spraying efficiency with time and terminate the spray eventually.

4.4. Conclusions

This study demonstrated for the first time the highly controllable deposition of polymeric liquid formulations on soft and curved hydrogel-based substrates using nES in pre-defined shape patterns at pre-determined locations. Using commercial soft contact lenses as a challenging example with wet and curved surfaces, the controlled deposition of model polymer zein solution in a ring shape at the peripheral region of the contact lens without blocking the vision zone was demonstrated. The NSD is the

most significant factor controlling the coating coverage. It should be considered first for the process optimisation, followed by adjusting the polymer concentration, dosing time, and the number of revolutions to increase the coating thickness. The deposition volume was shown to be highly predictable using spray current transients with the established electrospray scaling law, which is critical for precise drug dosing for medical applications. The on-demand nature of nES minimises the waste of materials compared to other methods to prepare DECLs while maintaining a clear optical zone. The present study shows the potential of nES as a platform technology for material deposition on medical devices with challenging features such as wet, soft, and curved surfaces. It is envisaged that the applications are primarily for functional coating of medical devices, with examples of drug delivery and anti-microbial surface treatment. For drug delivery applications, the drug candidates for coating range from small molecules to macromolecules, including peptides and proteins as far as a suitable solvent can be used to ensure the stability of the drug molecules. This study built a firm technological foundation for using nES as a novel additive manufacturing method to produce DECLs with drug coating at the surfaces of contact lenses in pre-defined patterns and locations.

Chapter 5 Selectively coated contact lenses by nanoelectrospray to fabricate drug-eluting contact lenses for treating ocular diseases

5.1 Introduction

Most ophthalmic drugs are given as eye drops. Eye drops are self- administrative directly to the eye, but many patients struggle to use them properly. More importantly, the bioavailability of eye drops is often limited to 5%[165] due to drug loss via tear clearance and drainage from the eye[178]. The tear clearance leads to frequent instillation of eye drops to maintain the drug concentration at the therapeutic level[166]. Additionally, eye drops have been reported to have poor patient adherence[167,179], preservative-induced eye irritation and intolerance[168], highly variable dosing[180,181] and poor drug absorption[178].

Innovative drug delivery systems are being explored to increase ophthalmic drug bioavailability. The target of the novel drug delivery systems aims to prolong the drug release in the eye and reduce the administration frequency. Among the novel drug delivery systems for ocular purposes, drug-eluting contact lenses (DECLs) have drawn much attention as a non-invasive method to deliver ophthalmic drugs. DECLs are estimated to improve bioavailability by 50%, compared to 5% by eye drops[85]. The concept of DECLs was first established in the 1960s, and since then, various methods have been reported in the literature to fabricate DECLs[82,182]. Methods to load ophthalmic drugs in contact lenses include molecular imprinting[69], encapsulating drug-loaded polymer films in the polymer matrix of the contact lens[90], and immersion of contact lenses into supercritical fluid[183]. These methods require either developing new polymer chemistry or implementing a new and complex multi-step manufacturing process. The above methods often affect the intrinsic physical properties of contact lenses[72]. Far-field electrospinning was reported to coat drug layers non-selectively on the lens surface and, therefore, required masking the vision zone[70]. Currently, there is no reported effective additive manufacturing method that can be readily adopted by the existing contact lens manufacturing process and is suitable for large-

scale production of DECLs.

The study aims to use the nanoelectrospray (nES) system reported in Chapter 4 to produce DECLs by depositing the model polymer and different model drugs selectively on the commercially available contact lenses[184].

The model polymer, polylactic-co-glycolic acid (PLGA), is a biodegradable and biocompatible polymer that has been well-studied. It is also an FDA-approved material and is commonly used for implants. A few studies reported using PLGA as the drug carrier to prolong the release of ocular medications[89,185]. The molecular weight of PLGA is known to affect the drug release kinetic; therefore, a PLGA with a relatively high molecular weight was chosen in this study to prolong drug release of the model drugs.

Model drugs with a range of hydrophobicity were used in this study. The hydrophilic model drug, ketotifen, is an anti-allergic medication for controlling symptoms associated with allergic conjunctivitis. It is an H1 histaminic receptor antagonist and a mast cell stabiliser, alleviating symptoms such as ocular itching and tearing[186]. The other two hydrophobic model drugs used in this study, bimatoprost and latanoprost, are prostaglandin analogues licensed to treat open-angle glaucoma by reducing intraocular pressure[187].

To evaluate the feasibility of using the nES system to fabricate DECLs, the investigation was made into the following aspects:

1. The quality of the coating on commercially available contact lenses.

2. The effect of sterilisation on DECLs prepared by nES.

3. The *in vitro* release of the model drugs from DECLs prepared by nES.

5.2 Materials and methods

Unless considered in this chapter, the materials and methods are specified in Chapter 2.

5.2.1 Materials

Ketotifen fumarate (KF), bimatoprost (BIM) and latanoprost (LN) were purchased from Molekula (UK). Phosphate buffer saline (PBS) solution tablets (pH 7.4), triethylamine (≥99.5%), phosphoric acid (≥85%) and PLGA Resomer® RG 756 S (M_w 76k - 115k Da, lactide:glycolide 75:25) were obtained from Sigma-Aldrich (Gillingham, UK). Methanol and acetonitrile, high-performance liquid chromatography grade, were purchased from Fisher Scientific (Leicestershire, UK). The ceramic MicroDot tips with a 50 μm inner diameter (P/N 7364054) were purchased from Nordson EFD (Bedfordshire, UK). Commercial soft contact lenses, Biomedics 1-day extra contact lenses (CooperVision Ltd, USA), with a composition of 45% ocufilcon D/55% water, were used as the model lenses. All materials were obtained from suppliers without further processing.

5.2.2 DECLs prepared by nES

Before the nES coating process, commercial contact lenses were removed from their original packaging and equilibrated in PBS pH 7.4 for 30 minutes. Excess liquid on the lens was removed by a lint-free wipe before the nES coating process. To maintain the hydration of contact lenses during the coating process, 10 μl of PBS pH 7.4 was pipetted onto the silver region of the 3D-printed lens holder before positioning the semi-dry contact lens on it (Figure 2.10C).

The solvent system to solubilise PLGA alone was explored to assess the coating quality on contact lenses. The drug-loaded spraying solutions were then prepared as outlined in Table 5.1. The model drugs were dissolved individually in a 2.5% w/v PLGA solution using the optimised solvent system. The resulting solution was filtered via a PTFE syringe filter with 0.2 μm pore size (Fisher Scientific, Loughborough, UK).

Polymer-drug solutions with different drug loadings were prepared to investigate the influence of drug loading on the *in vitro* drug release kinetic.

A custom-made machine (PCE Automation, Beccles, UK) was used to automate the spraying process. Details of the nES system can be found in the literature[184]. Preliminary studies were carried out to determine the spraying parameters to ensure proper deposition of polymer and model drugs on contact lenses without blocking the vision zone. . The vision zone is assumed to be 8 mm diameter of the contact lens from the top view (Figure 2A). The polymer-drug solution was sprayed onto the peripheral region (Figure 2.10A) of contact lenses (N=3) with the parameters specified in Table 5.1. The resulting DECLs were stored in a container with a lint-free dry wipe moistened with PBS 7.4 to maintain hydration before other measurements.

5.2.3 Coating thickness of nES-coated contact lenses

The coating thickness was measured by the electronic thickness gauge ET-3 (Rehder-dev, Greenville, USA) with an accuracy of ±2 μm. The instrument measures the sample thickness by lowering a sensor onto the sample, which is positioned on a steel ball carrier, and calculates the difference in distance relative to the zero point. Prior to measurement, the contact lenses were removed from their original packaging and allowed to equilibrate in PBS 7.4 for 30 minutes. The thickness measurement was taken at three predetermined locations in the peripheral region of each blanked contact lens . The thickness of the marked locations was remeasured after nES to calculate the difference in thickness. Three contact lenses were used for each spraying solution to calculate the average thickness.

Table 5.1. *Composition of the nES spraying solutions and the associated spraying parameters.*

Spraying solutions	PLGA concentration (%w/v)	Model drug concentration (% relative to the polymer weight)			Conductivity (µS/cm)	Applied voltage (kV)
		LN	BIM	KF		
KF1	2.5	-	-	1	3.83	2.7
KF2	2.5	-	-	3	5.13	2.7
KF3	2.5	-	-	5	7.53	2.7
BIM1	2.5	-	1.5	-	6.94	2.8
BIM2	2.5	-	5	-	8.05	2.8
BIM3	2.5	-	15	-	10.20	2.8
LN1	2.5	2.5	-	-	2.20	2.7
LN2	2.5	5	-	-	2.88	2.7
LN3	2.5	15	-	-	5.07	2.7

All nES-coated lenses were prepared with the following spraying parameters:

Nozzle substrate distance (mm)	2.99
Dosing speed (mm/s)	15
Number of revolutions	90
Spraying radius (mm)	5

5.2.4 *In vitro* drug release of nES-coated contact lenses

The *in vitro* drug release of non-sterilised and sterile nES-coated lenses was performed in glass vials containing 2 ml of PBS 7.4. The vials were placed in a shaking incubator set at 35 °C with 125 rpm. All *in vitro* experiments were performed under the sink condition, except LN3 (15% LN). A 1.5 ml aliquot was replaced at regular intervals with fresh PBS 7.4, followed by validated HPLC methods to quantify drug release[126,188,189]. The drug recovery was performed to calculate the amount of model drugs deposited onto the contact lenses since the electrical conductivity of the precursor solutions was too low to capture the current transients. Once the coating process was done, 100 µl of acetone was pipetted to the lens to dissolve the PLGA

coating, followed by pipetting 1.9 ml PBS to solubilise the model drugs and performing sonication for 5 minutes. The amount of model drugs deposited was quantified by validated HPLC methods mentioned below.

The model drugs were assayed by a HPLC system (Jasco, Japan) consisting of a pump (PU-1580), an autosampler (AS-2055 Plus) and a 4-channel UV detector (UV-1570M). A Waters C_{18} column (250 x 4.6 mm i.d., 5 μm particle size) connected with a HC-C_{18} guard column (Agilent, California, USA) was used under ambient condition to assay all model drugs. All methods were operating at a flow rate of 1 ml/min. The mobile phase for KF included methanol to 0.2% triethylamine in water in an 80 to 20 ratio (v/v). The detection wavelength was set at 300 nm. Stock solutions of KF in PBS pH 7.4 were diluted with the mobile phase in 1:1 ratio to produce a calibration curve of 0.78 – 12.5 μg/ml. The mobile phase for BIM consisted of acetonitrile, methanol and 0.1% phosphoric acid (v/v/v) (30:30:40). The detection wavelength was set at 210 nm. Stock solutions of BIM in PBS pH 7.4 were diluted with the mobile phase in 1:1 ratio to produce a calibration curve of 0.63 – 10 μg/ml. The mobile phase for LN comprised acetonitrile and water (v/v) (60:40). The detection wavelength was set at 210 nm. Stock solutions of LN in mobile phase were diluted with the PBS pH 7.4 in 1:1 ratio to produce a calibration curve of 0.63 – 10 μg/ml.

The aliquots of all model drugs collected from *in vitro* experiment was mixed with the associated mobile phase in 1:1 ratio, followed by filtration through a 0.2 μm PTFE syringe filter (15141499, Fisher scientific, UK) before assay.

5.2.5 Steam sterilisation of nES-coated lenses

One formulation of each model drug was selected to investigate the effect of sterilisation on the drug loading and coating on the coated DECLs. The DECLs prepared by nES were stored in a vial containing 2 ml PBS 7.4 for steam sterilisation at 121 °C, 15 psi for 30 minutes in an autoclave (Systec DB-100, Deutschland, Germany)[190]. The amount of drug leaching was assayed by validated HPLC methods mentioned above[126,188,189]. The *in vitro* release of sterile DECLs was performed using the abovementioned method.

5.2.6 Statistical analysis

The mean value of coating thickness and in vitro drug release results were analysed by one-way ANOVA and Tukey test (SPSS 25, IBM, New York, USA). A p-value lower than 0.05 is considered to show statistical significance. The coefficient of variance (CV) was calculated to evaluate the reproducibility of the drug loading to the contact lenses and expressed as percentage.

5.3 Results and discussion

5.3.1 Optical transmittance (OT) and drug loading of nES-coated DECLs

The nES system was designed to deposit materials precisely at the selected locations. Figure 5.1 shows the typical contact lenses before (3A) and after nES (3B) coating. Only the peripheral region of the contact lenses has been coated by the formulation, and the vision zone remains clear as intended. The high transmittance of contact lenses is an essential factor in providing clear vision to contact lens users. The OT of the DECLs prepared by nES is shown in Table 5.2. The OT of all coated lenses is above the acceptable target (>95%) at 600 nm, indicating the coating did not cover the vision zone (7.5 mm) as intended.
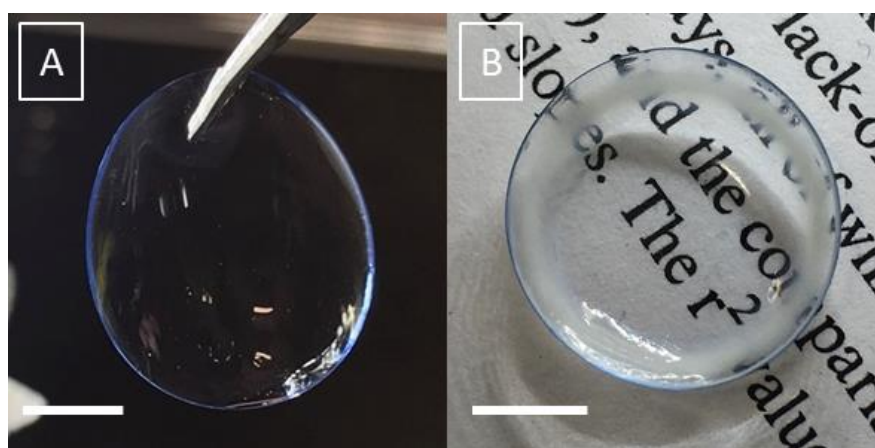
Figure 5.1. *Digital photography of a contact lens before (A) and after nES (B) in general, scale bar in the figure = 5 mm.*

Taking 5% bioavailability into consideration, the required daily dose for KF, BIM, and LN are 1.25 µg, 0.25 µg and 0.125 µg, respectively, when eye drop is used as the drug delivery system[191–193]. All coated lenses show drug loading above the therapeutic

dose, and it is possible to personalise the dose by changing the drug loading in the precursor liquid and/or the spraying parameters. For example, the number of rotations and the dosing speed[184].

Table 5.2. *The optical transmittance of DECLs at the vision zone and the coating thickness.*

	OT (%)	Coating thickness (μm)
Blank lenses	97.6 ± 0.3	-
KF1	96.4 ± 0.3	44 ± 4
KF2	95.9 ± 0.8	45 ± 4
KF3	96.2 ± 1.2	43 ± 5
BIM1	95.9 ± 1.6	41 ± 4
BIM2	96.3 ± 0.4	44 ± 3
BIM3	96.7 ± 0.4	41 ± 4
LN1	96.8 ± 0.3	45 ± 3
LN2	97.0 ± 0.4	44 ± 4
LN3	96.0 ± 0.5	43 ± 3

5.3.2 Morphology of coating on contact lenses

With a relatively short nozzle to substrate distance to limit the spraying width, a solvent system containing fast-drying solvents was chosen. Acetone was selected as the primary solvent in the solvent system since it is an excellent solvent to solubilise PLGA. It also has high vapour pressure and is classified by FDA as a class lll solvent. However, the use of acetone alone destabilised the spraying cone, leading to poor film morphology (Figure 5.2 A). It was reported that the solvent system with a lower vapour pressure generates smooth particles instead of a texture one[194]. Ethanol was added to the solvent system to reduce the vapour pressure without precipitating PLGA in the spraying solution, resulting in a smooth coating on the contact lens (Figure 5.2 B). Further increase the acetone:ethanol ratio to 8:2 precipitated PLGA, and therefore, the solvent ratio stopped at 9:1.
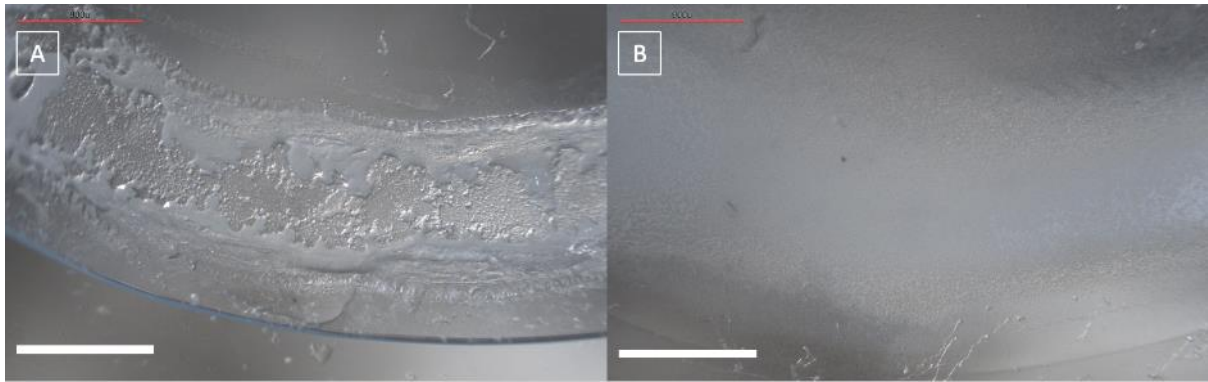
Figure 5.2. *Microscopic image of nES-coated contact lenses using 2.5%w/v PLGA in acetone alone (A) and in acetone to ethanol (9:1) (B). The scale bar is 1 mm.*

Cryo-SEM images in Figure 5.3 show the typical surface morphology of the PLGA films with the model drugs. Similar surface features are shared by DECLs loaded with KF, BIM and LN, and a dense and continuous layer of the drug-loaded polymer film was deposited on the peripheral region of the contact lens. The PLGA coating of all model drugs was a mix of fibres and particles, indicating the molecular weight of PLGA could be high enough to initiate fibre formation. The fusion of nES PLGA particles with adjacent particles occurred on the contact lens to form a solid film when the nozzle substrate distance and dosing speed were sufficiently low.
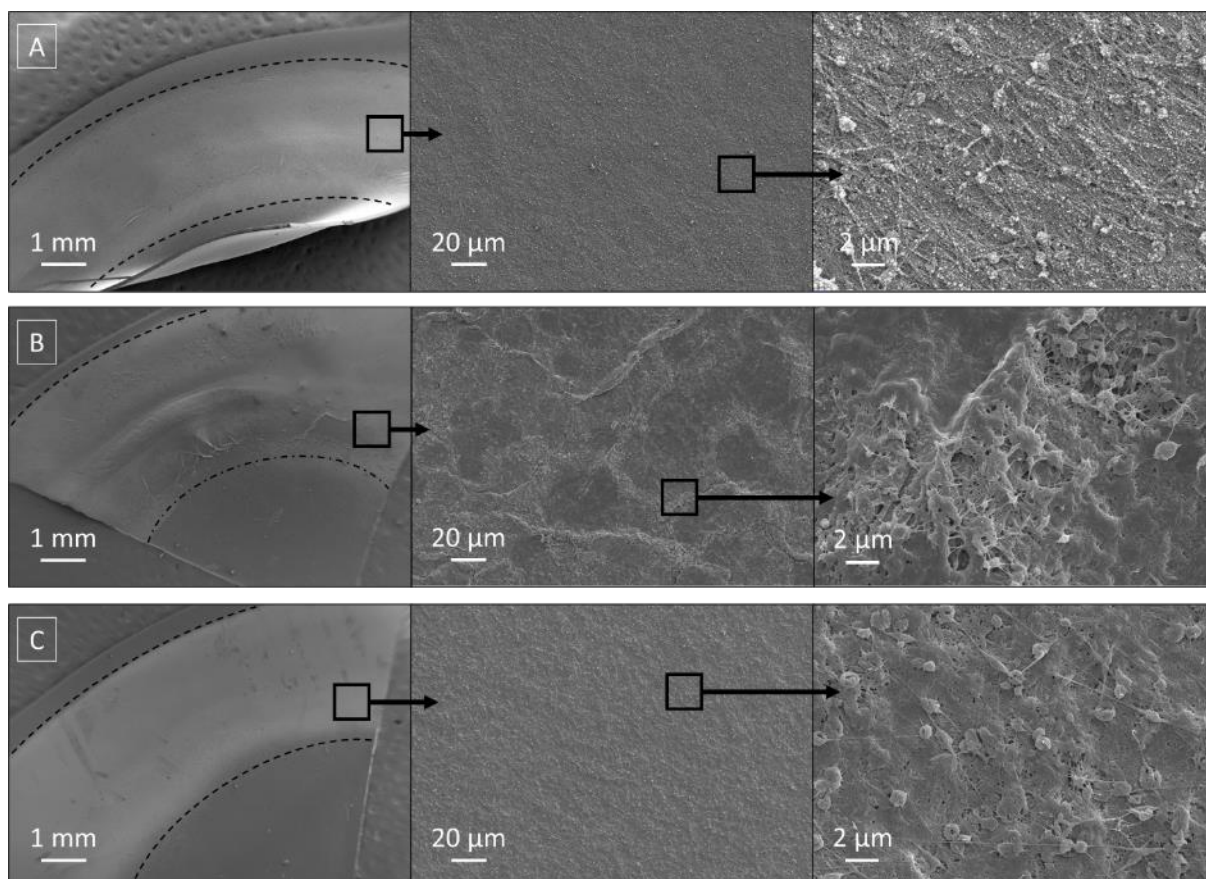
Figure 5.3. *Typical cryo-SEM images of DECLs with different model drugs prepared by nES, A: KF, B: BIM and C: LN. The dashed line indicates the coated region. The black boxes in the figure show the images of higher magnifications of the area of interest.*

5.3.3 *In vitro* drug release of nES-coated lenses

Figure 5.4 and Figure 5.5 show the *in vitro* drug release of the model drugs from DECLs prepared by the nES method with different presentations of the cumulative release of the model drugs. For the KF-loaded contact lenses, a rapid release of ketotifen in the first 30 minutes was observed for all drug loadings (Figure 5.4 A). The release of K3 reached nearly the plateau at 6 hours, whereas K1 and K2 showed no further drug release after 24 hours. For BIM-coated lenses, the results showed that burst release of BIM presented for all levels of drug loading in the first 30 minutes (Figure 5.4 B). No further drug release at 24 hours was observed for BIM1 – BIM3. Compared with KF and BIM, the *in* vitro drug release of LN shows a longer duration of drug release in general. Burst release of LN was observed within the first 2 hours for

all the drug loading levels (Figure 5.4 C). The duration of drug release is dependent on the drug loading. The release of LN from LN1 and L2 stopped at 24 hours and 120 hours, respectively. LN3 shows the most extended drug release until 216 hours. The hydrophobicity of the model drugs plays a role in the release duration, as suggested by the *in vitro* results. The log P of LN is the highest and is expected to have stronger interaction with PLGA than the other two model drugs. Meanwhile, the LN has the lowest aqueous solubility among the model drugs, implying it has the lowest thermodynamic driving force to dissociate into the drug release media.
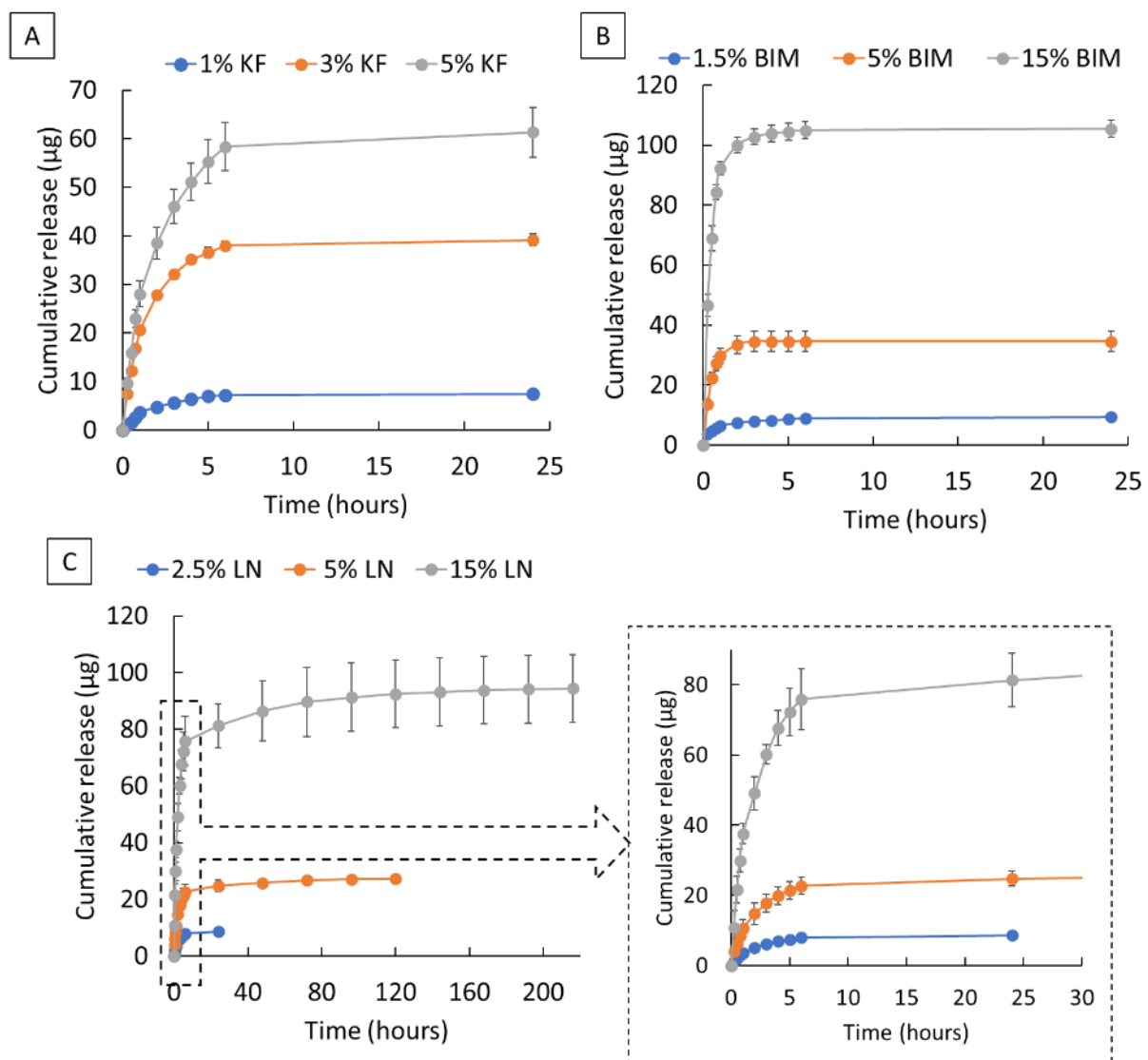
Figure 5.4. *In vitro drug release of KF (A), BIM (B) and LN (C) from DECLs prepared by the nES method.*

The processing method likely accounts for the rapid release of the model drugs from the PLGA film. By nanoelectrospray, the polymer and drug were deposited homogeneously on the substrate, implying some drug molecules were exposed on the surface of the PLGA film. A substantial amount of model drugs on the surface was released as soon as the coated lens was immersed into release media, which explains the burst release phenomenon. The coating thickness of all nES lens samples ranges from 41 to 45 µm on average (p = 0.184) (Table 5.2). The low thickness of the PLGA coating could be another reason for the quick release of the model drugs KF and BIM, because of the short distance required for the drug molecules to travel to the surface of the coating.

It was assumed that the drug loading in the coating could affect the *in vitro* drug release rate. The lower drug loading may show a slower drug release kinetic. However, the *in vitro* results for all levels of KF and BIM loading showed no difference in the drug release rate regardless of the drug loading (Figure 5.5**)**. The low thickness of the PLGA coating may be the reason why no difference in release kinetic was observed. Further lowering the drug-polymer ratio and increasing the thickness of the film may enable modulation of the drug release rate by prolonging the diffusion path.

Interestingly, LN showed different *in vitro* results compared with KF and BIM. The lower drug loading of LN (1.5%) shows a faster drug release kinetic from 5 hours onwards, compared to the 5% (p = 0.036) and 15% (p = 0.019) drug loading. There may have a local surface effect for 5% and 15% LN loading where the concentration of LN is higher at the surface of the coating and reduce the concentration gradient between the coating and the PBS. On the other hand, the 15% LN loading was not performed under sink condition, which may contribute to the longer duration of drug release observed in Figure 5.5 C.
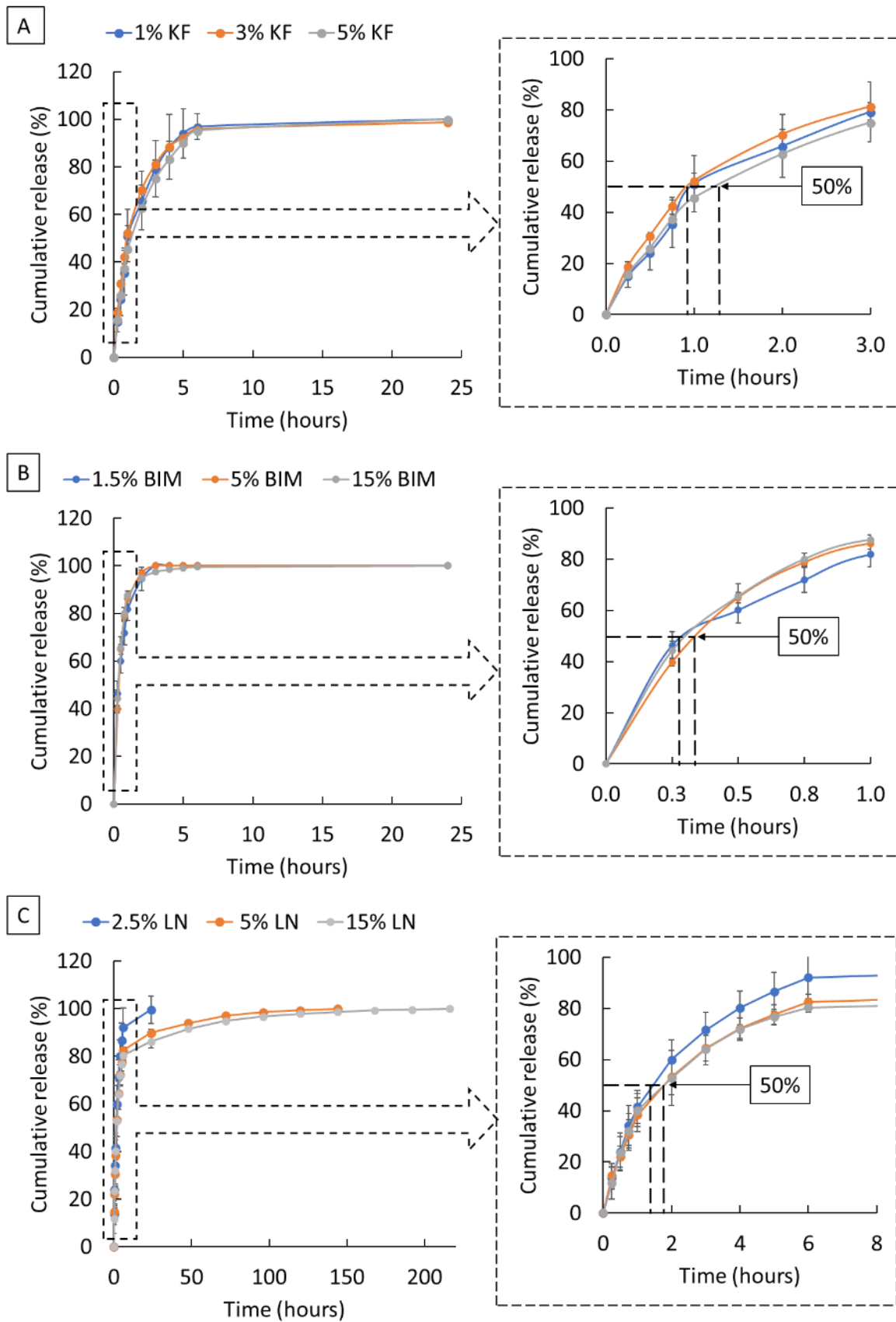
Figure 5.5. *Percentage cumulative in vitro drug release of KF (A), BIM (B) and LN (C) from DECLs prepared by the nES method.*

Table 5.3 shows the comparison between the quantity of model drugs deposited onto the contact lenses and the amount released from the in vitro experiment. It is assumed that the amount released from the nES-coated lenses should fall between 85% and 115% of the deposited amount. The results indicate that all formulations, except LN2, have ratios that are either higher than 115% or lower than 85%. To evaluate the reproducibility of drug deposition to the contact lenses, the coefficient of variation (CV) was calculated. The CV for all formulations remains within 15%, indicating that the data is tightly clustered around the mean.

Several factors could contribute to the deviation between the expected and actual drug loading. One potential factor is batch-to-batch variation, where different batches of the precursor solution may have varying drug concentrations. One batch of the precursor solution was prepared to determine the total amount of model drugs deposited on the contact lens, while another batch was prepared for the in vitro experiment. Using a highly volatile organic solvent system for the percussor solution could introduce variation during sample preparation through pipetting, resulting in deviating drug concentration from the expected value. Additionally, the variation in drug loading could be attributed to the different moisture content of the contact lenses. Despite blotting the wet lenses on a lint-free cloth to remove excess liquid before nES, the exact amount of liquid on the lens remains unknown. The difference in moisture content might alter the electrical conductivity of the contact lens, which affects the spray current and flow rate[195].

The *in vitro* release data of DECLs should be carefully interpreted since there is currently no universally accepted standard method to measure it. The 2 ml of PBS used in the *in vitro* release study was adapted from the literature as a simple approach. The relatively large volume of release media used in this method (2 ml) provided the sink condition for the *in vitro* drug release set-up, thereby maintaining a sufficient concentration gradient to drive the drug molecules out from the coating. However, it should be noted that sink conditions are rarely achieved in real-life scenarios due to the low tear volume (7 - 30 μl)[83]. The *in vitro* results are, therefore, expected to demonstrate a faster drug release kinetic, which is demonstrated from the comparison

of in vitro and in vivo result of the same DECLs[196]. To address this issue, alternative devices that uses 3D printing and microfluidic technology to assess the *in vitro* drug release of DECLs were reported in the literature[83,197]. With the validation of these flow cell models, the *in vitro* release result will be more relevant to the actual drug release on the corner surface.

Table 5.3. *Drug-loaded nES-coated DECLs and the amount of model drugs released from the in vitro drug release experiment*

	Drug loading (µg)	CV(%)	*in vitro* experiment (µg)	CV(%)	Ratio(%)
KF1	7.03 ± 1.07	15	7.48 ± 0.87	12	106 ± 25
KF2	30.72 ± 3.22	10	39.13 ± 1.20	3	127 ± 11
KF3	59.34 ± 5.87	10	61.3 ± 5.19	8	103 ± 18
BIM1	10.55 ± 0.85	8	9.35 ± 0.86	9	89 ± 19
BIM2	40.63 ± 2.58	6	34.55 ± 3.28	9	85 ± 19
BIM3	93.17 ± 11.3	12	105.44 ± 2.86	3	113 ± 13
LN1	8.60 ± 1.02	12	8.56 ± 0.50	6	100 ± 18
LN2	25.07 ± 0.45	2	27.32 ± 2.18	8	106 ± 9
LN3	82.47 ± 4.71	6	94.45 ± 11.95	13	115 ± 16

The *in vitro* drug release from the drug-loaded coating on contact lenses shows burst release for all the model drugs used in this study. High molecular weight PLGA was chosen in this study because it is well-known for its controlled release characteristic[198]. It was shown that PLGA could slow down the release kinetic of fluorescein when the drug-loaded film was encapsulated in the pHEMA contact lens[89]

The *in vitro* release experimental setup used in this study was simple and commonly reported in the literature. Briefly, for the vial method, the DECLs are placed in a vial containing a small volume (2-10 ml) of dissolution media (PBS or tear-simulate fluid) and introduced some forms of agitation such as stirring or shaking[73,199,200]. The physiological structure of the eye is hugely different from the in vitro setup that only about 10 µl of tear fluid stays at the posterior eye segment. The high tear turnover rate is another characteristic often neglected in the vial method. Therefore, the in vitro result herein is limited to comparing the drug release kinetics for the tested formulations. To provide a more realistic eye model for in vitro drug release experiments, researchers have explored using flow cell devices to mimic the low liquid capacity of the posterior eye and the high tear turnover rate[179,183]. Validation of the in vitro release with in vivo results will be helpful to standardise the drug release method.

5.3.4 Effect of steam sterilisation on the nES-coated lenses

Steam sterilisation is standard practice to sterilise contact lenses before being used. Therefore, it was adopted to evaluate the influence of sterilisation on the nES-coated contact lenses. The image in Figure 5.6 shows the drug-loaded PLGA coating before and after the steam autoclave. In general, the coated lenses curled up for all model drugs, with LN lenses having the most apparent curling. The curling effect seen in nES DECLs is likely related to the hydrogel nature of soft contact lenses. Excess liquid on the blank contact lenses was blotted on a lint-free cloth before the nES coating process. The semi-wet contact lenses started to shrink with time during the nES coating process, which took about 2 minutes to complete. During the spraying process, the PBS in the contact lens matrix may evaporate with time or be displaced by the solvent in the precursor solution, leading to lens shrinkage. When the nES-coated lens was introduced into PBS 7.4, the lens swelled to the original dimension. However, the PLGA ring restricted the swelling of the contact lenses in the peripheral region, and the lens curled up as a result. Although 10 µl of PBS was pipetted to the peripheral region to mitigate the shrinkage of contact lenses during the coating process, the spraying chamber was not a closed system, and the dehydration of lenses was not controlled. The shrinkage of contact lenses was also subjected to environmental

factors such as temperature and humidity. A closed spraying chamber with controlled humidity may reduce the curling issue.

After treating the nES-coated lenses in the autoclave, the PLGA coating detached from the lens surface to different extents. Almost all nES-coated contact lenses returned to their original shape after steam autoclave. The change in lens shape is likely attributed to the change in the physical state of PLGA. The PLGA used in the study has a glass transition temperature of 46.63 °C (data not shown). The behaviour of PLGA coating changed from glassy to plastic during the autoclave process and gained flexibility like a rubber. However, this also could cause delamination of the coating as seen for ketotifen. The PLGA coating with ketotifen delaminated completely in all samples as seen in Figure 5.6. The hydrophilic nature of ketotifen fumarate might facilitate the delamination. The strong affinity of KF to PBS may create hydrophilic channels in the coating, which facilitates the delamination of the PLGA coating. The PLGA coating with BIM showed the best result after the autoclave that only one lens showed the sign of partial delamination of the coating from the lens surface. Upon close inspection using cryo-SEM, the coating morphology for both BIM and LN show comparable results (Figure 5.8). The PLGA coating shows a fragmented surface with some holes penetrating the coating.
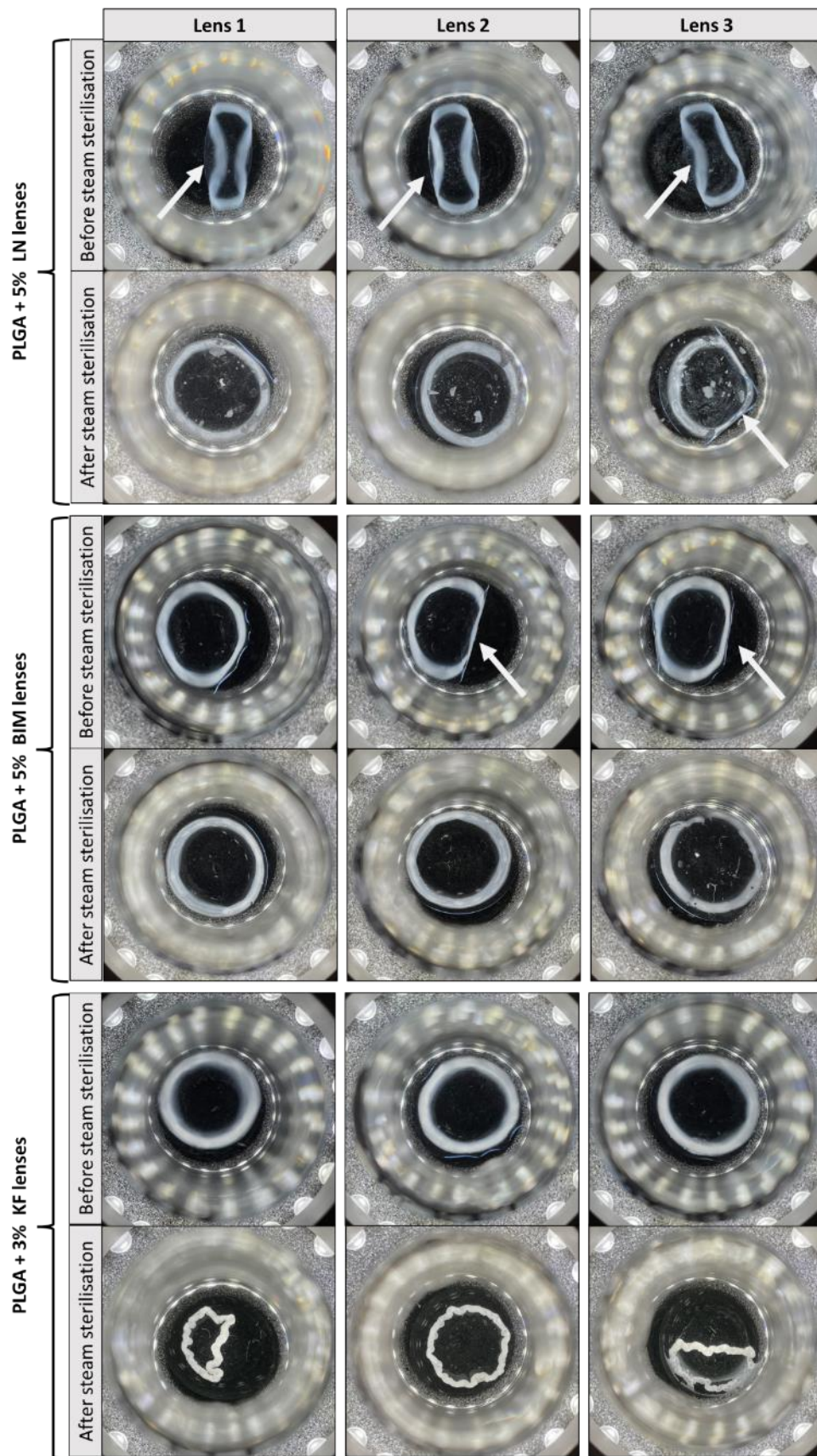
Figure 5.6. *Digital images of nES-coated DECLs before and after steam sterilisation.*
The white arrow indicates the curling issue of contact lenses after nES.

The *in vitro* drug release of LN and BIM from DECLs with and without steam autoclave is shown in Figure 5.7. The amount of LN loaded to the contact lenses after autoclave was 9.71 ± 0.21 µg and the amount of LN found in the PBS solution was 15.35 ± 1.21 µg. The % LN leaching in the PBS 7.4 was 61.17 ± 1.79%. The *in vitro* drug release of autoclaved LN-coated lenses showed burst release in the first hour and reached the plateau at 24 hours. BIM-coated lenses showed a total drug loading of 11.35 ± 2.1 µg and 37.68 ± 8.68 µg in the PBS solution. A 76.4 ± 5.97% of BIM leached in the buffer solution during the autoclave process. The release kinetic of BIM before and after the autoclave showed no difference in that the burst release happened in the first 0.25 hours and plateaued at 3 hours.
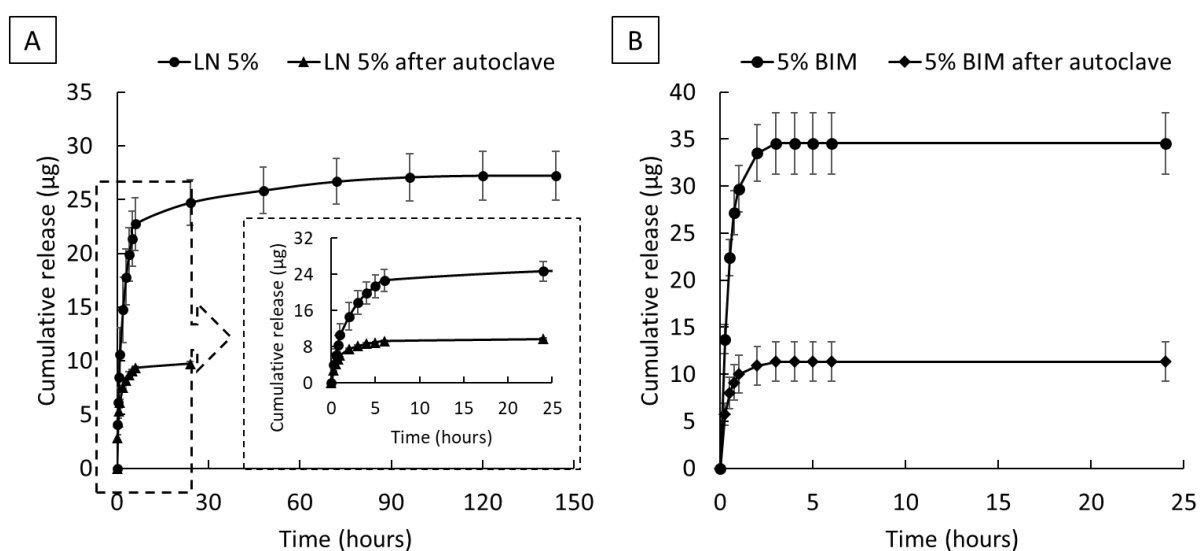
Figure 5.7. *The in vitro release of LN(A) and BIM (B) from nES-coated lenses after autoclave.*

Some extent of drug leaching from the nES-coated lenses was expected because of the nature of the coating. The nES generates a thin coating with uniform distribution of drug molecules through the film where drug molecules on the surface of the coating are expected to dissolve quickly from the coating into the PBS. One approach to limit drug leaching would be using pH-sensitive polymers to produce the coating. The ideal pH for the eye is pH 7.4. The use of pH-sensitive polymers such as Eudragit S100 degrades above pH 7.0[201]

The sterilisation step of contact lenses is necessary to prevent potential microbes from causing eye infections during application. Although the nES could coat the PLGA polymer and model drugs onto the lens surface, the steam sterilisation method limits the choice of polymers that can be used. Both BIM and LN autoclaved lenses show apparent damage on the coating after the steam autoclave. The fibre structure observed in Figure 5.3 disappeared, but many tiny pores were observed on the coating surface as seen in Figure 5.8. For the steam sterilisation method, the polymer ideally has a glass transition temperature higher than 121 °C to reduce the likelihood of the damaged coating or delamination. Alternatively, gamma ray sterilisation could be used if the polymer has a glass transition temperature lower than 121 °C. The typical dose of gamma irradiation for medical devices is 25 kGy[202]
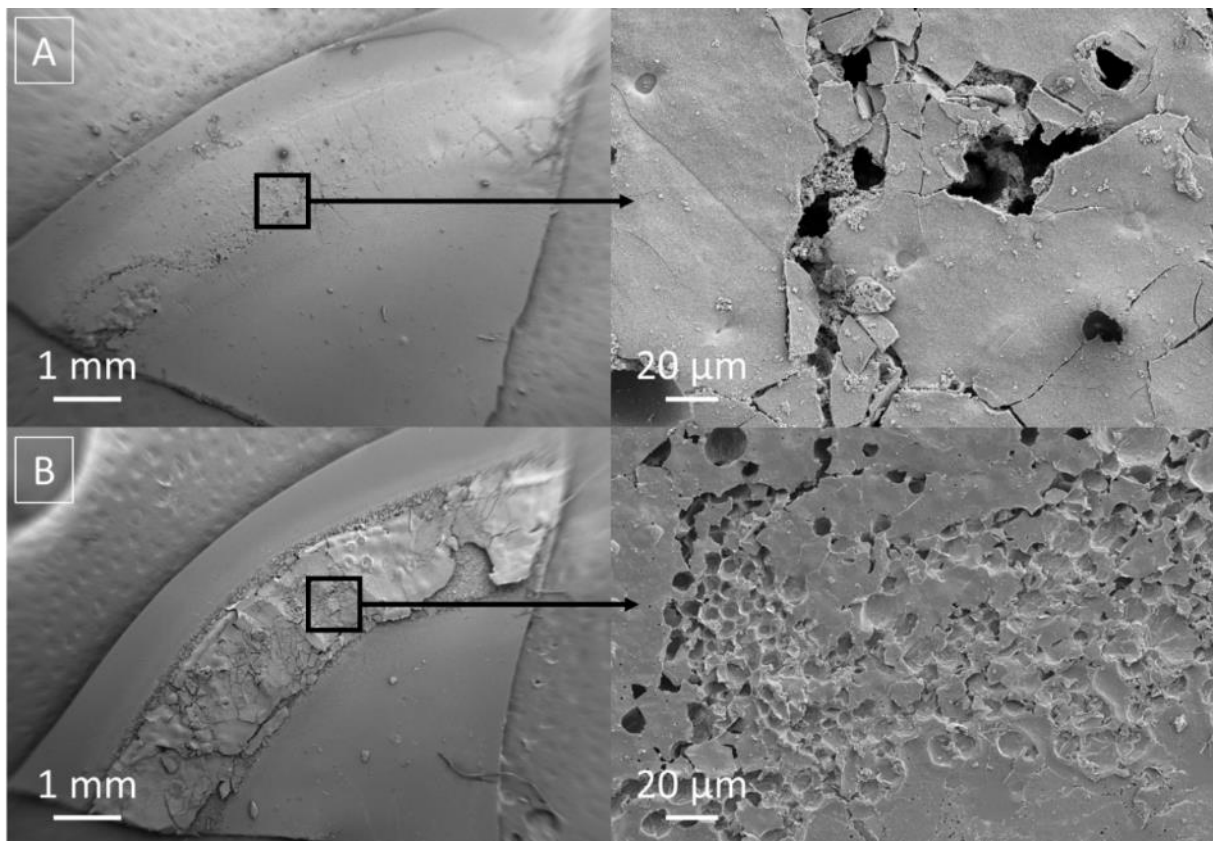
Figure 5.8. *Typical cryo-SEM images of DECLs with A: BIM and B: LN, after autoclave.*

The study aimed to evaluate the novel method to prepare DECLs by nES. To the best of our knowledge, this is the first study using nES to prepare DECLs. The rationale

was based on using additive printing technology to prepare polymer-drug coated contact lenses on demand to produce a personalised drug delivery system. The results suggested that solid, continuous coatings with different model drugs were deposited on the peripheral region of commercially available contact lenses to maintain a clear vision zone as intended.

As shown in the previous chapter, the nES technique makes tailoring dosage possible. By changing the drug loading with fixed spraying parameters, it is possible to build a calibration curve for a specific range of drug loading and prepare the tailored dosed lenses accordingly. Other spraying parameters such as applied voltages, nozzle substrate distance and nozzle diameter are known to affect the coating morphology and the quantity of drug deposited on the lens surface[112]. These parameters should be optimised to avoid the polymer-drug coating covering the vision zone and deposit required amount of drug onto the contact lenes.

A potential application of the nES system is its integration into the production of contact lenses. The production of contact lenses involves crosslinking monomers and crosslinkers to form dry lenses, which are then hydrated in saline solution and sealed in final packaging for sterilisation. The nES system could be integrated as an additional step at the end of the manufacturing process to coat the contact lenses with polymers and APIs, prior to sterilisation. By employing multiple nozzles in parallel during the nES coating step, the production rates of DECLs could be increased, paving the way for large-scale manufacturing.

5.4 Conclusions

In this study, DECLs with a range of drug loading of the model drugs were prepared by nES. All DECLs showed excellent optical transmittance at the optical zone, implying that the coating method will not interfere with the vision. It was found that the swelling of hydrogel contact lenses poses challenges in returning to the original curvature of the lenses after the nES coating. Further study is needed to control the shrinkage during the nES process. The *in vitro* release of the model drug showed that the

hydrophobicity of the model drug plays a vital role in the duration of drug release, of which the 15% LN lenses showed the longest duration of drug release. The drug loadings showed no difference in the release kinetics for BIM and KF, except LN. Similar to many reported methods to prepare DECLs, drug leaching was unavoidable using the nES method. Adding a small quantity of the ophthalmic drug into the saline solution may be the solution, as demonstrated by the first commercially available DECL. Steam sterilisation is a harsh method for sterile DECLs prepared by nES, even though it is the standard method for sterilising contact lenses. Alternative sterilisation methods like gamma rays can minimise damage to the coating.

Chapter 6 Conclusion and future outlook

The present works characterised two additive printing technologies and demonstrated their potential to fabricate personalised medicines for different drug delivery systems. It is concluded that no single additive printing method can accommodate all dosage forms.

Chapter 3 discussed the characterisation of the piezoelectric MD system built in-house using a range of viscous inks containing HPMC. The sequence of optimisation of the printing parameter for an ink should start from adjusting the applied pressure to ensure proper ejection of ink, followed by changing the opening height to generate bubbles-free droplets. Subsequently, the opening time was adjusted to dispense the targeted volume, followed by modification of the delay time to achieve the targeted droplet pitch. Altering the printing cycles allowed for linear adjustment of paracetamol dosage in ODFs with increased film dimension. The dimension of ODFs should be limited to a reasonable size (18 mm x 18 mm) to make it clinically practical, implying limited amount of APIs can be loaded to the ODFs. The development of emulsion-based formulation enables higher drug loading to expend the range of printable APIs. The piezoelectric MD technology enables single-pass printing without extra edible substrates, achieving sufficient ODF thickness for good handling. The printing of ODFs could be done on the final packaging materials, such as aluminium foil, before sealing and dispensing to the patients at the point-of-care to streamline the dispensing process.

Chapter 4 presented a novel approach for controlled deposition of polymeric liquid formulations on soft and curved hydrogel-based substrates using a bespoke nES system. The nozzle substrate distance should be considered first to determine the spray area, followed by the dosing speed and the number of overcoats for required thickness. The deposition volume of zein was predictable using spray current transients and the established electrospray scaling law and the results was highly correlated to the spectroscopic results. The results in chapter 4 provided fundamental

understanding of the nES system's spraying parameters' effect on coating quality, highlighting optimization priorities. The on-demand nature of nES reduces material waste compared to other methods to prepare DECLs, which could be beneficial when the formulation contains expensive APIs. The study suggested that nES has the potential to be a platform technology for depositing materials on medical devices with challenging features such as soft, wet, and curved surfaces. While the transient measurement is limited to the precursor solution with good electrical conductivity, it is not suitable for formulations containing mainly organic solvents. Adding organic salt to an organic solvent system will provide adequate electrical conductivity to enable the monitoring of the stability of spray and the deposition volume.

In Chapter 5, the preparation of DECLs containing three model drugs with varying hydrophobicity was explored using the bespoke nES system. The nES system was able to coat all formulations on the contact lenses to produce DECLs with an excellent optical transmittance at the optical zone. However, the shrinkage of hydrogel contact lenses during nES costing presented challenges. Further investigation is required to control the shrinkage during the nES process by monitor the shrinkage of contact lenses at specific temperature and humidity using an optical camera system. The *in vitro* drug release results revealed that the duration of drug release was highly dependent on the hydrophobicity of the model drug, with 15% LN lenses showing the longest duration of drug release. However, drug loading did not significantly impact the release kinetics of BIM and KF, with the exception of LN. Steam sterilisation, which is the standard method for sterilising contact lenses, was found to be a harsh method that could damage the PLGA coating. Gamma rays could be used as an alternative sterilisation method that minimises coating damage. The spraying volume was unable to be monitored using the oscilloscope due to the low electrical conductivity of the precursor solutions. Adding organic salts that are safe to human, would be helpful to predict the spraying volume using the transient captured during the spray.

The development of personalized medicines at the point-of-care is an emerging field that holds great promise for improving therapeutic outcomes. While there are machines capable of printing medications with various doses, their operation requires

highly skilled personnel. Ideally, these machines should come with user-friendly software that enables healthcare professionals to operate them with minimal training. However, the regulatory barrier is a significant challenge to overcome for the widespread adoption of printing personalized medicines. Many additive printers in the literature have not been validated or performed printing under Good Manufacturing Practices, making it essential to develop comprehensive guidelines for the development of validated equipment for printing personalized medicine at the point of care. It is believed that additive printing technologies will provide highly versatile tooling to improve therapeutic outcomes for patients in the near future once sophisticated guidelines are provided by regulatory bodies.

To advance the printing of ODFs using MD technology, there are several areas of further research that could be pursued. First and foremost, developing high drug loading formulations should be explored in order to expand the range of APIs that can be printed. In addition, a thorough stability study of the formulation and the crystal state of the APIs in the printed films should be conducted to examine the feasibility of high drug loading. Furthermore, examination of the stability of the high drug-loaded printed films is necessary to determine the optimal storage conditions after on-demand printing. These areas of investigation will contribute to a more comprehensive understanding of the capabilities and limitations of MD technology for the printing of personalized medicines at the point-of-care.

In order to further advance the development of controlled deposition of polymeric liquid formulations on hydrogel-based substrates using a bespoke nES system, several future directions were identified. One approach is to address the drug leaching issue during storage by utilizing pH-sensitive polymer. Additionally, depositing the coating between contact lens layers could also prove beneficial, as it has the potential to prolong the diffusion distance for drug molecules. Another important direction is to better understand the rate of shrinkage of contact lenses on the lens holder at varying temperatures and humidity levels, which can be achieved through the use of an optical camera system to monitor the changes in lens diameter from the top view of the lens holder in both the x and y axes. To achieve high precision in coating thickness on the

contact lens, a more precise imaging method is needed. For example, Ross et al. used the anterior segment ocular coherence tomography to measure the thickness of coating inside the contact lens matrix from the cross-sectional images[203]. Finally, it is essential to evaluate the *in vitro* release of DECLs using flow cell devices to assess their performance similar to physiological conditions.

References

[1]   J. Norman, R.D. Madurawe, C.M.V. Moore, M.A. Khan, A. Khairuzzaman, A new chapter in pharmaceutical manufacturing: 3D-printed drug products, Adv Drug Deliv Rev 108 (2017) 39–50. https://doi.org/10.1016/j.addr.2016.03.001.

[2]   N. Sandler, M. Preis, Printed Drug-Delivery Systems for Improved Patient Treatment, Trends Pharmacol Sci 37 (2016) 1070–1080. https://doi.org/10.1016/j.tips.2016.10.002.

[3]   A. Goldhirsch, E.P. Winer, A.S. Coates, R.D. Gelber, M. Piccart-Gebhart, B. Thürlimann, H.J. Senn, K.S. Albain, F. André, J. Bergh, H. Bonnefoi, D. Bretel-Morales, H. Burstein, F. Cardoso, M. Castiglione-Gertsch, A.S. Coates, M. Colleoni, A. Costa, G. Curigliano, N.E. Davidson, A. di Leo, B. Ejlertsen, J.F. Forbes, R.D. Gelber, M. Gnant, P. Goodwin, P.E. Goss, J.R. Harris, D.F. Hayes, C.A. Hudis, J.N. Ingle, J. Jassem, Z. Jiang, P. Karlsson, S. Loibl, M. Morrow, M. Namer, C.K. Osborne, A.H. Partridge, F. Penault-Llorca, C.M. Perou, M.J. Piccart-Gebhart, K.I. Pritchard, E.J.T. Rutgers, F. Sedlmayer, V. Semiglazov, Z.M. Shao, I. Smith, B. Thürlimann, M. Toi, A. Tutt, M. Untch, G. Viale, T. Watanabe, N. Wilcken, E.P. Winer, W.C. Wood, Personalizing the treatment of women with early breast cancer: Highlights of the st gallen international expert consensus on the primary therapy of early breast Cancer 2013, Annals of Oncology 24 (2013) 2206–2223. https://doi.org/10.1093/annonc/mdt303.

[4]   A.T. Florence, V.H.L. Lee, Personalised medicines: More tailored drugs, more tailored delivery, Int J Pharm 415 (2011) 29–33. https://doi.org/10.1016/j.ijpharm.2011.04.047.

[5]   V.M. Vaz, L. Kumar, 3D Printing as a Promising Tool in Personalized Medicine, AAPS PharmSciTech 22 (2021). https://doi.org/10.1208/s12249-020-01905-8.

[6]   D.R. Serrano, A. Kara, I. Yuste, F.C. Luciano, B. Ongoren, B.J. Anaya, G. Molina, L. Diez, B.I. Ramirez, I.O. Ramirez, S.A. Sánchez-Guirales, R. Fernández-García, L. Bautista, H.K. Ruiz, A. Lalatsa, 3D Printing Technologies in Personalized Medicine, Nanomedicines, and Biopharmaceuticals, Pharmaceutics 15 (2023). https://doi.org/10.3390/pharmaceutics15020313.

[7]   K. Grießmann, J. Breitkreutz, M. Schubert-Zsilavecz, M. Abdel-Tawab, Dosing accuracy of measuring devices provided with antibiotic oral suspensions, Paediatr Perinat Drug Ther 8 (2007) 61–70. https://doi.org/10.1185/146300907X178950.

[8]   J. Walsh, D. Bickmann, J. Breitkreutz, M. Chariot-Goulet, Delivery devices for the administration of paediatric formulations: Overview of current practice, challenges and recent developments, Int J Pharm 415 (2011) 221–231. https://doi.org/10.1016/j.ijpharm.2011.05.048.

[9]   J. Madathilethu, M. Roberts, M. Peak, J. Blair, R. Prescott, J.L. Ford, Content uniformity of quartered hydrocortisone tablets in comparison with mini-tablets for paediatric dosing, BMJ Paediatr Open 2 (2018) 1–7. https://doi.org/10.1136/bmjpo-2017-000198.

[10]   W.A. Habib, A.S. Alanizi, M.M. Abdelhamid, F.K. Alanizi, Accuracy of tablet splitting: Comparison study between hand splitting and tablet cutter, Saudi Pharmaceutical Journal 22 (2014) 454–459. https://doi.org/10.1016/j.jsps.2013.12.014.

[11]   R. Varghese, S. Salvi, P. Sood, J. Karsiya, D. Kumar, Recent advancements in additive manufacturing techniques employed in the pharmaceutical industry: A bird's eye view, Annals of 3D Printed Medicine 8 (2022) 100081. https://doi.org/10.1016/j.stlm.2022.100081.

[12]   N. Gottschalk, A. Burkard, J. Quodbach, M. Bogdahn, Drop-on-powder 3D printing of amorphous high dose oral dosage forms: Process development, opportunities and printing limitations, Int J Pharm X 5 (2023) 100151. https://doi.org/10.1016/j.ijpx.2022.100151.

[13]   W. Jamróz, M. Kurek, E. Łyszczarz, J. Szafraniec, J. Knapik-Kowalczuk, K. Syrek, M. Paluch, R. Jachowicz, 3D printed orodispersible films with Aripiprazole, Int J Pharm 533 (2017) 413–420. https://doi.org/10.1016/j.ijpharm.2017.05.052.

[14]   D.N. Heo, S.J. Lee, R. Timsina, X. Qiu, N.J. Castro, L.G. Zhang, Development of 3D printable conductive hydrogel with crystallized PEDOT:PSS for neural

tissue engineering, Materials Science and Engineering C 99 (2019) 582–590. https://doi.org/10.1016/j.msec.2019.02.008.

[15] E. Sjöholm, N. Sandler, Additive manufacturing of personalized orodispersible warfarin films, Int J Pharm 564 (2019) 117–123. https://doi.org/10.1016/j.ijpharm.2019.04.018.

[16] A. Pharmaceuticals, FDA APPROVES THE FIRST 3D PRINTED DRUG PRODUCT, (2015). https://www.aprecia.com/news/fda-approves-the-first-3d-printed-drug-product (accessed August 20, 2023).

[17] Fitzgerald S, FDA Approves First 3D-Printed Epilepsy Drug, Neurology Today (2015) 26.

[18] R. Parhi, G.K. Jena, An updated review on application of 3D printing in fabricating pharmaceutical dosage forms, Drug Deliv Transl Res 12 (2022) 2428–2462. https://doi.org/10.1007/s13346-021-01074-6.

[19] B.J. Park, H.J. Choi, S.J. Moon, S.J. Kim, R. Bajracharya, J.Y. Min, H.K. Han, Pharmaceutical applications of 3D printing technology: current understanding and future perspectives, J Pharm Investig 49 (2019) 575–585. https://doi.org/10.1007/s40005-018-00414-y.

[20] W. Jamróz, J. Szafraniec, M. Kurek, R. Jachowicz, 3D Printing in Pharmaceutical and Medical Applications – Recent Achievements and Challenges, Pharm Res 35 (2018). https://doi.org/10.1007/s11095-018-2454-x.

[21] K. Ilyés, N.K. Kovács, A. Balogh, E. Borbás, B. Farkas, T. Casian, G. Marosi, I. Tomuță, Z.K. Nagy, The applicability of pharmaceutical polymeric blends for the fused deposition modelling (FDM) 3D technique: Material considerations–printability–process modulation, with consecutive effects on in vitro release, stability and degradation, European Journal of Pharmaceutical Sciences 129 (2019) 110–123. https://doi.org/10.1016/j.ejps.2018.12.019.

[22] O. Jennotte, N. Koch, A. Lechanteur, B. Evrard, Three-dimensional printing technology as a promising tool in bioavailability enhancement of poorly water-soluble molecules: A review, Int J Pharm 580 (2020) 119200. https://doi.org/10.1016/j.ijpharm.2020.119200.

[23] C. Planchette, H. Pichler, M. Wimmer-Teubenbacher, M. Gruber, H. Gruber-Woelfler, S. Mohr, C. Tetyczka, W.K. Hsiao, A. Paudel, E. Roblegg, J. Khinast, Printing medicines as orodispersible dosage forms: Effect of substrate on the printed micro-structure, Int J Pharm 509 (2016) 518–527. https://doi.org/10.1016/j.ijpharm.2015.10.054.

[24] U.M. Musazzi, G.M. Khalid, F. Selmin, P. Minghetti, F. Cilurzo, Trends in the production methods of orodispersible films, Int J Pharm 576 (2020) 118963. https://doi.org/10.1016/j.ijpharm.2019.118963.

[25] M.S. Gupta, T.P. Kumar, D.V. Gowda, Orodispersible Thin Film: A new patient-centered innovation, J Drug Deliv Sci Technol 59 (2020) 101843. https://doi.org/10.1016/j.jddst.2020.101843.

[26] C. Lau, Development of suck and swallow mechanisms in infants, Ann Nutr Metab 66 (2015) 7–14. https://doi.org/10.1159/000381361.

[27] A.F. Borges, C. Silva, J.F.J. Coelho, S. Simões, Oral films: Current status and future perspectives: I-Galenical development and quality attributes, Journal of Controlled Release 206 (2015) 1–19. https://doi.org/10.1016/j.jconrel.2015.03.006.

[28] M.S. Gupta, D.V. Gowda, T.P. Kumar, J.M. Rosenholm, A Comprehensive Review of Patented Technologies to Fabricate Orodispersible Films: Proof of Patent Analysis (2000–2020), Pharmaceutics 14 (2022). https://doi.org/10.3390/pharmaceutics14040820.

[29] E.M. Hoffmann, A. Breitenbach, J. Breitkreutz, Advances in orodispersible films for drug delivery, Expert Opin Drug Deliv 8 (2011) 299–316. https://doi.org/10.1517/17425247.2011.553217.

[30] Y. Thabet, J. Breitkreutz, Orodispersible films: Product transfer from lab-scale to continuous manufacturing, Int J Pharm 535 (2018) 285–292. https://doi.org/10.1016/j.ijpharm.2017.11.021.

[31] D. Steiner, J.H. Finke, A. Kwade, Instant ODFs – Development of an intermediate, nanoparticle-based product platform for individualized medication,

European Journal of Pharmaceutics and Biopharmaceutics 126 (2018) 149–158. https://doi.org/10.1016/j.ejpb.2017.04.014.

[32]   E. Turković, I. Vasiljević, M. Drašković, J. Parojčić, Orodispersible films — Pharmaceutical development for improved performance: A review, J Drug Deliv Sci Technol 75 (2022). https://doi.org/10.1016/j.jddst.2022.103708.

[33]   S. Karki, H. Kim, S.J. Na, D. Shin, K. Jo, J. Lee, Thin films as an emerging platform for drug delivery, Asian J Pharm Sci 11 (2016) 559–574. https://doi.org/10.1016/j.ajps.2016.05.004.

[34]   R. Jani, D. Patel, Hot melt extrusion: An industrially feasible approach for casting orodispersible film, Asian J Pharm Sci 10 (2014) 292–305. https://doi.org/10.1016/j.ajps.2015.03.002.

[35]   U.M. Musazzi, F. Selmin, M.A. Ortenzi, G.K. Mohammed, S. Franzé, P. Minghetti, F. Cilurzo, Personalized orodispersible films by hot melt ram extrusion 3D printing, Int J Pharm 551 (2018) 52–59. https://doi.org/10.1016/j.ijpharm.2018.09.013.

[36]   Q. Song, X. Guo, Y. Sun, M. Yang, Anti-solvent Precipitation Method Coupled Electrospinning Process to Produce Poorly Water-Soluble Drug-Loaded Orodispersible Films, AAPS PharmSciTech 20 (2019). https://doi.org/10.1208/s12249-019-1464-2.

[37]   M. Birer, F. Acartürk, Electrospun orally disintegrating film formulation of telmisartan, Pharm Dev Technol 26 (2021) 661–672. https://doi.org/10.1080/10837450.2021.1916031.

[38]   S.L. Shenoy, W.D. Bates, H.L. Frisch, G.E. Wnek, Role of chain entanglements on fiber formation during electrospinning of polymer solutions: Good solvent, non-specific polymer-polymer interaction limit, Polymer (Guildf) 46 (2005) 3372–3384. https://doi.org/10.1016/j.polymer.2005.03.011.

[39]   H. Wickström, M. Palo, K. Rijckaert, R. Kolakovic, J.O. Nyman, A. Määttänen, P. Ihalainen, J. Peltonen, N. Genina, T. De Beer, K. Löbmann, T. Rades, N. Sandler, Improvement of dissolution rate of indomethacin by inkjet printing,

European Journal of Pharmaceutical Sciences 75 (2015) 91–100. https://doi.org/10.1016/j.ejps.2015.03.009.

[40] N. Genina, E.M. Janßen, A. Breitenbach, J. Breitkreutz, N. Sandler, Evaluation of different substrates for inkjet printing of rasagiline mesylate, European Journal of Pharmaceutics and Biopharmaceutics 85 (2013) 1075–1083. https://doi.org/10.1016/j.ejpb.2013.03.017.

[41] N. Sandler, A. Määttänen, P. Ihalainen, L. Kronberg, A. Meierjohann, T. Viitala, J. Peltonen, Inkjet printing of drug substances and use of porous substrates-towards individualized dosing, J Pharm Sci 100 (2011) 3386–3395. https://doi.org/10.1002/jps.22526.

[42] H. Öblom, E. Sjöholm, M. Rautamo, N. Sandler, Towards printed pediatric medicines in hospital pharmacies: Comparison of 2d and 3d-printed orodispersiblewarfarin films with conventional oral powders in unit dose sachets, Pharmaceutics 11 (2019). https://doi.org/10.3390/pharmaceutics11070334.

[43] T. Ehtezazi, M. Algellay, Y. Islam, M. Roberts, N.M. Dempster, S.D. Sarker, The Application of 3D Printing in the Formulation of Multilayered Fast Dissolving Oral Films, J Pharm Sci 107 (2018) 1076–1085. https://doi.org/10.1016/j.xphs.2017.11.019.

[44] M. Slavkova, J. Breitkreutz, Orodispersible drug formulations for children and elderly, European Journal of Pharmaceutical Sciences 75 (2015) 2–9. https://doi.org/10.1016/j.ejps.2015.02.015.

[45] S.J. Trenfield, A. Awad, A. Goyanes, S. Gaisford, A.W. Basit, 3D Printing Pharmaceuticals: Drug Development to Frontline Care, Trends Pharmacol Sci 39 (2018) 440–451. https://doi.org/10.1016/j.tips.2018.02.006.

[46] M. Preis, J. Breitkreutz, N. Sandler, Perspective: Concepts of printing technologies for oral film formulations, Int J Pharm 494 (2015) 578–584. https://doi.org/10.1016/j.ijpharm.2015.02.032.

[47] N. Scoutaris, S. Ross, D. Douroumis, Current Trends on Medical and Pharmaceutical Applications of Inkjet Printing Technology, Pharm Res 33 (2016) 1799–1816. https://doi.org/10.1007/s11095-016-1931-3.

[48] Ronan Daly, T.S. Harrington, G.D. Martin, Ian M. Hutchings, Ronan Daly a, * T.S.H. b, Graham D. Martin a, Ian M. Hutchings a, Inkjet printing for pharmaceutics – A review of research and manufacturing, Int J Pharm 494 (2015) 554–567.

[49] M.A. Alhnan, T.C. Okwuosa, M. Sadia, K.W. Wan, W. Ahmed, B. Arafat, Emergence of 3D Printed Dosage Forms: Opportunities and Challenges, Pharm Res 33 (2016) 1817–1832. https://doi.org/10.1007/s11095-016-1933-1.

[50] P.A. Meléndez, K.M. Kane, C.S. Ashvar, M. Albrecht, P.A. Smith, Thermal inkjet application in the preparation of oral dosage forms: Dispensing of prednisolone solutions and polymorphic characterization by solid-state spectroscopic techniques, J Pharm Sci 97 (2008) 2619–2636. https://doi.org/10.1002/jps.21189.

[51] P.R. Vuddanda, M. Alomari, C.C. Dodoo, S.J. Trenfield, S. Velaga, A.W. Basit, S. Gaisford, Personalisation of warfarin therapy using thermal ink-jet printing, European Journal of Pharmaceutical Sciences 117 (2018) 80–87. https://doi.org/10.1016/j.ejps.2018.02.002.

[52] M. Alomari, A.W. Basit, S. Gaisford, S. Velaga, P.R. Vuddanda, C.C. Dodoo, S.J. Trenfield, Printing T3 and T4 oral drug combinations as a novel strategy for hypothyroidism, Int J Pharm 549 (2018) 363–369. https://doi.org/10.1016/j.ijpharm.2018.07.062.

[53] O. Kiefer, B. Fischer, J. Breitkreutz, Fundamental investigations into metoprolol tartrate deposition on orodispersible films by inkjet printing for individualised drug dosing, Pharmaceutics 13 (2021) 1–16. https://doi.org/10.3390/pharmaceutics13020247.

[54] M. Edinger, J. Jacobsen, D. Bar-Shalom, J. Rantanen, N. Genina, Analytical aspects of printed oral dosage forms, Int J Pharm 553 (2018) 97–108. https://doi.org/10.1016/j.ijpharm.2018.10.030.

[55] H.K. Cader, G.A. Rance, M.R. Alexander, A.D. Gonçalves, C.J. Roberts, C.J. Tuck, R.D. Wildman, Water-based 3D inkjet printing of an oral pharmaceutical dosage form, Int J Pharm 564 (2019) 359–368. https://doi.org/10.1016/j.ijpharm.2019.04.026.

[56] M. Edinger, D. Bar-Shalom, N. Sandler, J. Rantanen, N. Genina, QR encoded smart oral dosage forms by inkjet printing, Int J Pharm 536 (2018) 138–145. https://doi.org/10.1016/j.ijpharm.2017.11.052.

[57] I.M. Hutchings, G. Martin, Inkjet technology for digital fabrication, 1st ed., Wiley, Chichester, West Sussex, United Kingdom, 2013.

[58] Vermes GmbH, The MDS 3000 Series, (2020). https://www.vermes.com/en/micro-dispensing-systems/mds-micro-dispensing-systems/ (accessed July 5, 2021).

[59] Y.S. Wong, J. Sun, H.T. Loh, Y.H. Fuh, Q. Xu, J.H. Ng, Comparison of micro-dispensing performance between micro-valve and piezoelectric printhead, Microsystem Technologies 15 (2009) 1437–1448. https://doi.org/10.1007/s00542-009-0905-3.

[60] B. Bonhoeffer, A. Kwade, M. Juhnke, Alternative Manufacturing Concepts for Solid Oral Dosage Forms From Drug Nanosuspensions Using Fluid Dispensing and Forced Drying Technology, J Pharm Sci 107 (2018) 909–921. https://doi.org/10.1016/j.xphs.2017.11.007.

[61] J. Jimenez, M. Sakthivel, K.K. Nischal, M. v. Fedorchak, Drug delivery systems and novel formulations to improve treatment of rare corneal disease, Drug Discov Today 24 (2019) 1564–1574. https://doi.org/10.1016/j.drudis.2019.03.005.

[62] Y. Yang, A. Lockwood, Topical ocular drug delivery systems: Innovations for an unmet need, Exp Eye Res 218 (2022) 109006. https://doi.org/10.1016/j.exer.2022.109006.

[63] S. Gause, K.H. Hsu, C. Shafor, P. Dixon, K.C. Powell, A. Chauhan, Mechanistic modeling of ophthalmic drug delivery to the anterior chamber by eye drops and contact lenses, Adv Colloid Interface Sci 233 (2016) 139–154. https://doi.org/10.1016/j.cis.2015.08.002.

[64] R. Gupta, B. Patil, B.M. Shah, S.J. Bali, S.K. Mishra, T. Dada, Evaluating Eye Drop Instillation Technique in Glaucoma Patients, J Glaucoma 21 (2012) 189–192. https://doi.org/10.1097/IJG.0b013e31820bd2e1.

[65] O. Wichterle, Hydrophilic Gels for Biological Use, Nature 185 (1960) 117–118. https://doi.org/10.1038/185063a0.

[66] J. Vision, Johnson & Johnson Vision Care Receives FDA Approval for ACUVUE® Theravision[TM] with Ketotifen – World's First and Only Drug-Eluting Contact Lens, (2022). https://www.jjvision.com/press-release/johnson-johnson-vision-care-receives-fda-approval-acuvuer-theravisiontm-ketotifen (accessed April 24, 2022).

[67] A. Soluri, A. Hui, L. Jones, Delivery of ketotifen fumarate by commercial contact lens materials, Optometry and Vision Science 89 (2012) 1140–1149. https://doi.org/10.1097/OPX.0b013e3182639dc8.

[68] F.A. Maulvi, R.J. Patil, A.R. Desai, M.R. Shukla, R.J. Vaidya, K.M. Ranch, B.A. Vyas, S.A. Shah, D.O. Shah, Effect of gold nanoparticles on timolol uptake and its release kinetics from contact lenses: In vitro and in vivo evaluation, Acta Biomater 86 (2019) 350–362. https://doi.org/10.1016/j.actbio.2019.01.004.

[69] F. Yan, Y. Liu, S. Han, Q. Zhao, N. Liu, Bimatoprost Imprinted Silicone Contact Lens to Treat Glaucoma, AAPS PharmSciTech 21 (2020). https://doi.org/10.1208/s12249-020-1622-6.

[70] P. Mehta, A.A. Al-Kinani, M.S. Arshad, M.W. Chang, R.G. Alany, Z. Ahmad, Development and characterisation of electrospun timolol maleate-loaded polymeric contact lens coatings containing various permeation enhancers, Int J Pharm 532 (2017) 408–420. https://doi.org/10.1016/j.ijpharm.2017.09.029.

[71] Y. Yokozaki, J. Sakabe, B. Ng, Y. Shimoyama, Effect of temperature, pressure and depressurization rate on release profile of salicylic acid from contact lenses prepared by supercritical carbon dioxide impregnation, Chemical Engineering Research and Design 100 (2015) 89–94. https://doi.org/10.1016/j.cherd.2015.05.008.

[72] O. L. Lanier, K.G. Christopher, R.M. Macoon, Y. Yu, P. Sekar, A. Chauhan, Commercialization challenges for drug eluting contact lenses, Expert Opin Drug Deliv 00 (2020) 1–17. https://doi.org/10.1080/17425247.2020.1787983.

[73] A. el Shaer, S. Mustafa, M. Kasar, S. Thapa, B. Ghatora, R.G. Alany, Nanoparticle-laden contact lens for controlled ocular delivery of prednisolone: Formulation optimization using statistical experimental design, Pharmaceutics 8 (2016). https://doi.org/10.3390/pharmaceutics8020014.

[74] J.& J. Vision, Johnson & Johnson Vision Receives Approval in Canada for World's First and Only Drug-Releasing Contact Lens for Vision Correction and Allergic Eye Itch: ACUVUE® Theravision™ with Ketotifen, (2021). https://www.jjvision.com/press-release/johnson-johnson-vision-receives-approval-canada-worlds-first-and-only-drug-releasing.

[75] C.C.S. Karlgard, N.S. Wong, L.W. Jones, C. Moresoli, In vitro uptake and release studies of ocular pharmaceutical agents by silicon-containing and p-HEMA hydrogel contact lens materials, Int J Pharm 257 (2003) 141–151. https://doi.org/10.1016/S0378-5173(03)00124-8.

[76] F.A. Maulvi, T.G. Soni, D.O. Shah, Extended release of hyaluronic acid from hydrogel contact lenses for dry eye syndrome, J Biomater Sci Polym Ed 26 (2015) 1035–1050. https://doi.org/10.1080/09205063.2015.1072902.

[77] L.D. Wuchte, S.A. Dipasquale, M.E. Byrne, B. Materials, B. Devices, D.D. Laboratories, M. Hill, In vivo drug delivery via contact lenses: The current state of the field from origins to present, J Drug Deliv Sci Technol. (2021) 1–33. https://doi.org/10.1016/j.jddst.2021.102413.In.

[78] P. Sekar, A. Chauhan, Effect of vitamin-E integration on delivery of prostaglandin analogs from therapeutic lenses, J Colloid Interface Sci 539 (2019) 457–467. https://doi.org/10.1016/j.jcis.2018.12.036.

[79] C. Torres-Luna, N. Hu, T. Tammareddy, R. Domszy, J. Yang, N.S. Wang, A. Yang, Extended delivery of non-steroidal anti-inflammatory drugs through contact lenses loaded with Vitamin E and cationic surfactants, Contact Lens and Anterior Eye 42 (2019) 546–552. https://doi.org/10.1016/j.clae.2019.04.011.

[80] D. Lee, S. Cho, H.S. Park, I. Kwon, Ocular drug delivery through pHEMA-Hydrogel contact lenses Co-loaded with lipophilic vitamins, Sci Rep 6 (2016) 1–8. https://doi.org/10.1038/srep34194.

[81] C.C. Peng, J. Kim, A. Chauhan, Extended delivery of hydrophilic drugs from silicone-hydrogel contact lenses containing Vitamin E diffusion barriers, Biomaterials 31 (2010) 4032–4047. https://doi.org/10.1016/j.biomaterials.2010.01.113.

[82] J. Xu, Y. Xue, G. Hu, T. Lin, J. Gou, T. Yin, H. He, Y. Zhang, X. Tang, A comprehensive review on contact lens for ophthalmic drug delivery, Journal of Controlled Release 281 (2018) 97–118. https://doi.org/10.1016/j.jconrel.2018.05.020.

[83] A. Tieppo, K.M. Pate, M.E. Byrne, In vitro controlled release of an anti-inflammatory from daily disposable therapeutic contact lenses under physiological ocular tear flow, European Journal of Pharmaceutics and Biopharmaceutics 81 (2012) 170–177. https://doi.org/10.1016/j.ejpb.2012.01.015.

[84] B. Malaekeh-Nikouei, F.A. Ghaeni, V.S. Motamedshariaty, S.A. Mohajeri, Controlled release of prednisolone acetate from molecularly imprinted hydrogel contact lenses, J Appl Polym Sci 126 (2012) 387–394. https://doi.org/10.1002/app.36625.

[85] K.H. Hsu, S. Gause, A. Chauhan, Review of ophthalmic drug delivery by contact lenses, J Drug Deliv Sci Technol 24 (2014) 123–135. https://doi.org/10.1016/S1773-2247(14)50021-4.

[86] F.H. Nasr, S. Khoee, M.M. Dehghan, S.S. Chaleshtori, A. Shafiee, Preparation and Evaluation of Contact Lenses Embedded with Polycaprolactone-Based Nanoparticles for Ocular Drug Delivery, Biomacromolecules 17 (2016) 485–495. https://doi.org/10.1021/acs.biomac.5b01387.

[87] G. Behl, J. Iqbal, N.J. O'Reilly, P. McLoughlin, L. Fitzhenry, Synthesis and Characterization of Poly(2-hydroxyethylmethacrylate) Contact Lenses Containing Chitosan Nanoparticles as an Ocular Delivery System for Dexamethasone Sodium Phosphate, Pharm Res 33 (2016) 1638–1648. https://doi.org/10.1007/s11095-016-1903-7.

[88]   F.A. Maulvi, D.T. Desai, K.H. Shetty, D.O. Shah, M.D.P. Willcox, Advances and challenges in the nanoparticles-laden contact lenses for ocular drug delivery, Int J Pharm 608 (2021) 121090. https://doi.org/10.1016/j.ijpharm.2021.121090.

[89]   J.B. Ciolino, T.R. Hoare, N.G. Iwata, I. Behlau, C.H. Dohlman, R. Langer, D.S. Kohane, A drug-eluting contact lens, Invest Ophthalmol Vis Sci 50 (2009) 3346–3352. https://doi.org/10.1167/iovs.08-2826.

[90]   A.R. Desai, F.A. Maulvi, D.M. Desai, M.R. Shukla, K.M. Ranch, B.A. Vyas, S.A. Shah, S. Sandeman, D.O. Shah, Multiple drug delivery from the drug-implants-laden silicone contact lens: Addressing the issue of burst drug release, Materials Science and Engineering C 112 (2020) 110885. https://doi.org/10.1016/j.msec.2020.110885.

[91]   J.B. Ciolino, S.P. Hudson, A.N. Mobbs, T.R. Hoare, N.G. Iwata, G.R. Fink, D.S. Kohane, A prototype antifungal contact lens, Invest Ophthalmol Vis Sci 52 (2011) 6286–6291. https://doi.org/10.1167/iovs.10-6935.

[92]   M.S. Wilm, M. Mann, Electrospray and Taylor-Cone theory, Dole's beam of macromolecules at last?, Int J Mass Spectrom Ion Process 136 (1994) 167–180.

[93]   A. Pawar, S. Thakkar, M. Misra, A bird's eye view of nanoparticles prepared by electrospraying: advancements in drug delivery field, Journal of Controlled Release 286 (2018) 179–200. https://doi.org/10.1016/j.jconrel.2018.07.036.

[94]   S.K. Boda, X. Li, J. Xie, Electrospraying an enabling technology for pharmaceutical and biomedical applications: A review, J Aerosol Sci 125 (2018) 164–181. https://doi.org/10.1016/j.jaerosci.2018.04.002.

[95]   P. Davoodi, F. Feng, Q. Xu, W. Yan, Y. Wah, M.P. Srinivasan, Coaxial electrohydrodynamic atomization : Microparticles for drug delivery applications, Journal of Controlled Release 205 (2015) 70–82. https://doi.org/10.1016/j.jconrel.2014.12.004.

[96]   D.G. Yu, X.Y. Li, X. Wang, J.H. Yang, S.W.A. Bligh, G.R. Williams, Nanofibers Fabricated Using Triaxial Electrospinning as Zero Order Drug Delivery Systems, ACS Appl Mater Interfaces 7 (2015) 18891–18897. https://doi.org/10.1021/acsami.5b06007.

[97]   A. Balogh, R. Cselkó, B. Démuth, G. Verreck, J. Mensch, G. Marosi, Z.K. Nagy, Alternating current electrospinning for preparation of fibrous drug delivery systems, Int J Pharm 495 (2015) 75–80. https://doi.org/10.1016/j.ijpharm.2015.08.069.

[98]   A. Balogh, B. Farkas, G. Verreck, J. Mensch, E. Borbás, B. Nagy, G. Marosi, Z.K. Nagy, AC and DC electrospinning of hydroxypropylmethylcellulose with polyethylene oxides as secondary polymer for improved drug dissolution, Int J Pharm 505 (2016) 159–166. https://doi.org/10.1016/j.ijpharm.2016.03.024.

[99]   A. Balogh, B. Farkas, Á. Pálvölgyi, A. Domokos, B. Démuth, G. Marosi, Z.K. Nagy, Novel Alternating Current Electrospinning of Hydroxypropylmethylcellulose Acetate Succinate (HPMCAS) Nanofibers for Dissolution Enhancement: The Importance of Solution Conductivity, J Pharm Sci 106 (2017) 1634–1643. https://doi.org/10.1016/j.xphs.2017.02.021.

[100] M. Wilm, M. Mann, Analytical properties of the nanoelectrospray ion source, Anal Chem 68 (1996) 1–8. https://doi.org/10.1021/ac9509519.

[101] G.T.T. Gibson, S.M. Mugo, R.D. Oleschuk, Nanoelectrospray emitters: Trends and perspective, Mass Spectrom Rev 28 (2009) 918–936. https://doi.org/10.1002/mas.20248.

[102] M.S. Alexander, M.D. Paine, J.P.W. Stark, Pulsation modes and the effect of applied voltage on current and flow rate in nanoelectrospray, Anal Chem 78 (2006) 2658–2664. https://doi.org/10.1021/ac0520036.

[103] M.D. Paine, M.S. Alexander, K.L. Smith, M. Wang, J.P.W. Stark, Controlled electrospray pulsation for deposition of femtoliter fluid droplets onto surfaces, J Aerosol Sci 38 (2006) 315–324. https://doi.org/10.1016/j.jaerosci.2006.12.004.

[104] C. Wei, H. Qin, C.P. Chiu, Y.S. Lee, J. Dong, Drop-on-demand E-jet printing of continuous interconnects with AC-pulse modulation on highly insulating substrates, J Manuf Syst 37 (2015) 505–510. https://doi.org/10.1016/j.jmsy.2014.07.005.

[105] H. Qin, Y. Cai, J. Dong, Y.S. Lee, Direct printing of capacitive touch sensors on flexible substrates by additive e-jet printing with silver nanoinks, Journal of

Manufacturing Science and Engineering, Transactions of the ASME 139 (2017) 1–7. https://doi.org/10.1115/1.4034663.

[106] H. Chen, J. Zhong, J. Wang, R. Huang, X. Qiao, H. Wang, Z. Tan, Enhanced growth and differentiation of myoblast cells grown on E-jet 3D printed platforms, Int J Nanomedicine 14 (2019) 937–950. https://doi.org/10.2147/IJN.S193624.

[107] M.J. Poellmann, K.L. Barton, S. Mishra, A.J.W. Johnson, Patterned Hydrogel Substrates for Cell Culture with Electrohydrodynamic Jet Printing, Macromol Biosci 11 (2011) 1164–1168. https://doi.org/10.1002/mabi.201100004.

[108] K. Kim, G. Kim, B.R. Lee, S. Ji, S.Y. Kim, B.W. An, M.H. Song, J.U. Park, High-resolution electrohydrodynamic jet printing of small-molecule organic light-emitting diodes, Nanoscale 7 (2015) 13410–13415. https://doi.org/10.1039/c5nr03034j.

[109] D.A. Kovacevich, L. Lei, D. Han, C. Kuznetsova, S.E. Kooi, H. Lee, J.P. Singer, Self-Limiting Electrospray Deposition for the Surface Modification of Additively Manufactured Parts, ACS Appl Mater Interfaces 12 (2020) 20901–20911. https://doi.org/10.1021/acsami.9b23544.

[110] Y. Liu, S. Li, H. Li, M. Alomgir Hossen, D.E. Sameen, J. Dai, W. Qin, K.J. Lee, Synthesis and properties of core-shell thymol-loaded zein/shellac nanoparticles by coaxial electrospray as edible coatings, Mater Des 212 (2021) 110214. https://doi.org/10.1016/j.matdes.2021.110214.

[111] E. Bodnár, J. Grifoll, J. Rosell-Llompart, Polymer solution electrospraying: A tool for engineering particles and films with controlled morphology, J Aerosol Sci 125 (2018) 93–118. https://doi.org/10.1016/j.jaerosci.2018.04.012.

[112] A. Jaworek, Electrospray droplet sources for thin film deposition, J Mater Sci 42 (2007) 266–297. https://doi.org/10.1007/s10853-006-0842-9.

[113] D.N. Nguyen, C. Clasen, G. Van den Mooter, Pharmaceutical Applications of Electrospraying, J Pharm Sci 105 (2016) 2601–2620. https://doi.org/10.1016/j.xphs.2016.04.024.

[114] Paracetamol, British National Formulary (2022). https://bnf.nice.org.uk/drugs/paracetamol/ (accessed November 18, 2022).

[115] Ketotifen, British National Formulary (2022). https://bnf.nice.org.uk/drug/ketotifen.html (accessed October 3, 2022).

[116] D.F. Woodward, A.H.P. Krauss, J. Chen, R.K. Lai, C.S. Spada, R.M. Burk, S.W. Andrews, L. Shi, Y. Liang, K.M. Kedzie, R. Chen, D.W. Gil, A. Kharlamb, A. Archeampong, J. Ling, C. Madhu, J. Ni, P. Rix, J. Usansky, H. Usansky, A. Weber, D. Welty, W. Yang, D.D.S. Tang-Liu, M.E. Garst, B. Brar, L.A. Wheeler, L.J. Kaplan, The pharmacology of bimatoprost (Lumigan™), Surv Ophthalmol 45 (2001). https://doi.org/10.1016/S0039-6257(01)00224-7.

[117] P.E. Sirinek, M.M. Lin, Intracameral sustained release bimatoprost implants (Durysta), Semin Ophthalmol 37 (2022) 385–390. https://doi.org/10.1080/08820538.2021.1985145.

[118] Bimatoprost, British National Formulary (2022). https://bnf.nice.org.uk/drugs/bimatoprost/ (accessed October 3, 2022).

[119] S.S. Patel, C.M. Spencer, Latanoprost, Drugs Aging 9 (1996) 363–378. https://doi.org/10.2165/00002512-199609050-00007.

[120] Latanoprost, British National Formulary (2022). https://bnf.nice.org.uk/drugs/latanoprost/ (accessed October 3, 2022).

[121] Drugbank, Acetaminophen, (2022). https://go.drugbank.com/drugs/DB00316 (accessed December 15, 2022).

[122] Drugbank, Ketotifen, (2022). https://go.drugbank.com/drugs/DB00920 (accessed December 15, 2022).

[123] Drugbank, Bimatoprost, (2022). https://go.drugbank.com/drugs/DB00905 (accessed December 15, 2022).

[124] Drugbank, Latanoprost, (2022). https://go.drugbank.com/drugs/DB00654 (accessed December 15, 2022).

[125] PubChem, Acetaminophen, (2023). https://pubchem.ncbi.nlm.nih.gov/compound/1983 (accessed March 25, 2023).

[126] A.A. Abd El-Bary, H.F. Salem, R.M. Kharshoum, 2-Hydroxypropyl-ß-cyclodextrin complex with ketotifen fumerate for eye drops preparations,

International Journal of Drug Delivery 1 (2011) 228–240. https://doi.org/10.5138/ijdd.v3i2.217.

[127] P. Jansook, T. Loftsson, Aqueous Prostaglandin Eye Drop Formulations, Pharmaceutics 14 (2022) 1–13. https://doi.org/10.3390/pharmaceutics14102142.

[128] C.L. Li, L.G. Martini, J.L. Ford, M. Roberts, The use of hypromellose in oral drug delivery, Journal of Pharmacy and Pharmacology 57 (2010) 533–546. https://doi.org/10.1211/0022357055957.

[129] E. Mašková, K. Kubová, B.T. Raimi-Abraham, D. Vllasaliu, E. Vohlídalová, J. Turánek, J. Mašek, Hypromellose – A traditional pharmaceutical excipient with modern applications in oral and oromucosal drug delivery, Journal of Controlled Release 324 (2020) 695–727. https://doi.org/10.1016/j.jconrel.2020.05.045.

[130] R. Shukla, M. Cheryan, Zein: The industrial protein from corn, Ind Crops Prod 13 (2001) 171–192. https://doi.org/10.1016/S0926-6690(00)00064-9.

[131] J. Gomez-Estaca, M.P. Balaguer, R. Gavara, P. Hernandez-Munoz, Formation of zein nanoparticles by electrohydrodynamic atomization: Effect of the main processing variables and suitability for encapsulating the food coloring and active ingredient curcumin, Food Hydrocoll 28 (2012) 82–91. https://doi.org/10.1016/j.foodhyd.2011.11.013.

[132] V.A. Gaona-Sánchez, G. Calderón-Domínguez, E. Morales-Sánchez, J.J. Chanona-Pérez, G. Velázquez-de la Cruz, J. v. Méndez-Méndez, E. Terrés-Rojas, R.R. Farrera-Rebollo, Preparation and characterisation of zein films obtained by electrospraying, Food Hydrocoll 49 (2015) 1–10. https://doi.org/10.1016/j.foodhyd.2015.03.003.

[133] H.J. Wang, S.J. Gong, Z.X. Lin, J.X. Fu, S.T. Xue, J.C. Huang, J.Y. Wang, In vivo biocompatibility and mechanical properties of porous zein scaffolds, Biomaterials 28 (2007) 3952–3964. https://doi.org/10.1016/j.biomaterials.2007.05.017.

[134] FDA, Food Additive Status List - Zein, (2022). https://www.fda.gov/food/food-additives-petitions/food-additive-status-list.

[135] L. Li, S.H. Yang, K. Lemr, V. Havlicek, K.A. Schug, Continuous flow-extractive desorption electrospray ionization: Analysis from " non-electrospray ionization-friendly" solvents and related mechanism, Anal Chim Acta 769 (2013) 84–90. https://doi.org/10.1016/j.aca.2013.01.018.

[136] D.N. Kapoor, A. Bhatia, R. Kaur, R. Sharma, G. Kaur, S. Dhawan, PLGA: A unique polymer for drug delivery, Ther Deliv 6 (2015) 41–58. https://doi.org/10.4155/tde.14.91.

[137] Y. Xu, C.S. Kim, D.M. Saylor, D. Koo, Polymer degradation and drug delivery in PLGA-based drug–polymer applications: A review of experiments and theories, J Biomed Mater Res B Appl Biomater 105 (2017) 1692–1716. https://doi.org/10.1002/jbm.b.33648.

[138] M. Hirenkumar, S. Steven, Poly Lactic-co-Glycolic Acid (PLGA) as Biodegradable Controlled Drug Delivery Carrier, Polymers (Basel) 3 (2012) 1–19. https://doi.org/10.3390/polym3031377.Poly.

[139] H.F. George, F. Qureshi, Newton's Law of Viscosity, Newtonian and Non-Newtonian Fluids BT - Encyclopedia of Tribology, in: Q.J. Wang, Y.-W. Chung (Eds.), Springer US, Boston, MA, 2013: pp. 2416–2420. https://doi.org/10.1007/978-0-387-92897-5_143.

[140] M. Wagner, Thermal analysis in practice : fundamental aspects, First edit, Hanser Publications, 2018.

[141] M.E. Brown, Determination of purity by Differential Scanning Calorimetry (DSC), J Chem Educ 56 (1979) 310–313. https://doi.org/10.1021/ed056p310.

[142] D.G. Watson, Infrared spectrophotometry, in: Pharmaceutical Analysis, 5th ed., Elsevier Ltd, 2021: pp. 114–136.

[143] D.G. Watson, Ultraviolet and visible spectroscopy, in: Pharmaceutical Analysis, 5th ed., Elsevier Ltd, 2021: pp. 89–113.

[144] N.M. Quesnel, P. Simonet, Spectral transmittance of UV-absorbing soft and rigid gas permeable contact lenses, Optometry and Vision Science 72 (1995) 2–10. https://doi.org/10.1097/00006324-199501000-00002.

[145] D.G. Watson, High-performance liquid chromatography, in: Pharmaceutical Analysis, 5th ed., Elsevier Ltd, 2021: pp. 295–349.

[146] N. Raval, R. Maheshwari, D. Kalyane, S.R. Youngren-Ortiz, M.B. Chougule, R.K. Tekade, Importance of physicochemical characterization of nanoparticles in pharmaceutical product development, Elsevier Inc., 2018. https://doi.org/10.1016/B978-0-12-817909-3.00010-8.

[147] Y. Thabet, D. Lunter, J. Breitkreutz, Continuous inkjet printing of enalapril maleate onto orodispersible film formulations, Int J Pharm 546 (2018) 180–187. https://doi.org/10.1016/j.ijpharm.2018.04.064.

[148] B. Bonhoeffer, A. Kwade, M. Juhnke, Impact of Formulation Properties and Process Parameters on the Dispensing and Depositioning of Drug Nanosuspensions Using Micro-Valve Technology, J Pharm Sci 106 (2017) 1102–1110. https://doi.org/10.1016/j.xphs.2016.12.019.

[149] A. Alhayali, P.R. Vuddanda, S. Velaga, Silodosin oral films: Development, physico-mechanical properties and in vitro dissolution studies in simulated saliva, J Drug Deliv Sci Technol 53 (2019) 101122. https://doi.org/10.1016/j.jddst.2019.06.019.

[150] A.D. Chonkar, J.V. Rao, R.S. Managuli, S. Mutalik, S. Dengale, P. Jain, N. Udupa, Development of fast dissolving oral films containing lercanidipine HCl nanoparticles in semicrystalline polymeric matrix for enhanced dissolution and ex vivo permeation, European Journal of Pharmaceutics and Biopharmaceutics 103 (2016) 179–191. https://doi.org/10.1016/j.ejpb.2016.04.001.

[151] M. Preis, K. Knop, J. Breitkreutz, Mechanical strength test for orodispersible and buccal films, Int J Pharm 461 (2014) 22–29. https://doi.org/10.1016/j.ijpharm.2013.11.033.

[152] K. Wasilewska, K. Winnicka, How to assess orodispersible film quality? A review of applied methods and their modifications, Acta Pharmaceutica 69 (2019) 155–176. https://doi.org/10.2478/acph-2019-0018.

[153] A.F. Borges, C. Silva, J.F.J. Coelho, S. Simões, Outlining critical quality attributes (CQAs) as guidance for the development of orodispersible films,

Pharm Dev Technol 22 (2017) 237–245. https://doi.org/10.1080/10837450.2016.1199567.

[154] J.C. Visser, H.J. Woerdenbag, S. Crediet, E. Gerrits, M.A. Lesschen, W.L.J. Hinrichs, J. Breitkreutz, H.W. Frijlink, Orodispersible films in individualized pharmacotherapy: The development of a formulation for pharmacy preparations, Int J Pharm 478 (2015) 155–163. https://doi.org/10.1016/j.ijpharm.2014.11.013.

[155] J. Sibik, M.J. Sargent, M. Franklin, J.A. Zeitler, Crystallization and phase changes in paracetamol from the amorphous solid to the liquid phase, Mol Pharm 11 (2014) 1326–1334. https://doi.org/10.1021/mp400768m.

[156] N. Al-Zoubi, J.E. Koundourellis, S. Malamataris, FT-IR and Raman spectroscopic methods for identification and quantitation of orthorhombic and monoclinic paracetamol in powder mixes, J Pharm Biomed Anal 29 (2002) 459–467. https://doi.org/10.1016/S0731-7085(02)00098-5.

[157] S.L. Wang, S.Y. Lin, Y.S. Wei, Transformation of metastable forms of acetaminophen studied by thermal Fourier transform infrared (FT-IR) microspectroscopy, Chem Pharm Bull (Tokyo) 50 (2002) 153–156. https://doi.org/10.1248/cpb.50.153.

[158] S. Qi, A. Gryczke, P. Belton, D.Q.M. Craig, Characterisation of solid dispersions of paracetamol and EUDRAGIT® E prepared by hot-melt extrusion using thermal, microthermal and spectroscopic analysis, Int J Pharm 354 (2008) 158–167. https://doi.org/10.1016/j.ijpharm.2007.11.048.

[159] J.C. Visser, W.M.C. Dohmen, W.L.J. Hinrichs, J. Breitkreutz, H.W. Frijlink, H.J. Woerdenbag, Quality by design approach for optimizing the formulation and physical properties of extemporaneously prepared orodispersible films, Int J Pharm 485 (2015) 70–76. https://doi.org/10.1016/j.ijpharm.2015.03.005.

[160] R.P. Dixit, S.P. Puthli, Oral strip technology: Overview and future potential, Journal of Controlled Release 139 (2009) 94–107. https://doi.org/10.1016/j.jconrel.2009.06.014.

[161] Ph.Eur., European Pharmacopoeia Version 8., 8 (2013).

[162] FDA, Guidance for Industry Orally Disintegrating Tablets, (2008). https://www.fda.gov/regulatory-information/search-fda-guidance-documents/orally-disintegrating-tablets (accessed July 29, 2021).

[163] L. Zhang, M. Aloia, B. Pielecha-Safira, H. Lin, P.M. Rajai, K. Kunnath, R.N. Davé, Impact of Superdisintegrants and Film Thickness on Disintegration Time of Strip Films Loaded With Poorly Water-Soluble Drug Microparticles, J Pharm Sci 107 (2018) 2107–2118. https://doi.org/10.1016/j.xphs.2018.04.006.

[164] Microdrop Technologies, Nanojet Piezovalve NJ-K-4, (2019). https://www.microdrop.de/piezovalve.html (accessed January 30, 2019).

[165] I.P. Kaur, S. Kakkar, Nanotherapy for posterior eye diseases, Journal of Controlled Release 193 (2014) 100–112. https://doi.org/10.1016/j.jconrel.2014.05.031.

[166] R. Kholdebarin, R.J. Campbell, Y.P. Jin, Y.M. Buys, G. Beiko, C. Birt, K. Damji, F. Feldman, C. Lajaoie, S. Kulkarni, J. Martow, T. Sakamoto, J. Spencer, G.E. Trope, Multicenter study of compliance and drop administration in glaucoma, Canadian Journal of Ophthalmology 43 (2008) 454–461. https://doi.org/10.3129/I08-076.

[167] P.A. Newman-Casey, L.M. Niziol, B.W. Gillespie, N.K. Janz, P.R. Lichter, D.C. Musch, The Association between Medication Adherence and Visual Field Progression in the Collaborative Initial Glaucoma Treatment Study, Ophthalmology 127 (2020) 477–483. https://doi.org/10.1016/j.ophtha.2019.10.022.

[168] J. Thygesen, Glaucoma therapy: Preservative-free for all?, Clinical Ophthalmology 12 (2018) 707–717. https://doi.org/10.2147/OPTH.S150816.

[169] D.L.B. Scott A. Davis, Betsy Sleath, Delesha M. Carpenter, Susan J. Blalock, Kellu W. Muri, S.A. Davis, B. Sleath, D.M. Carpenter, S.J. Blalock, K.W. Muir, D.L. Budenz, Drop instillation and glaucoma, Curr Opin Ophthalmol. 29 (2018) 171–177. https://doi.org/10.1097/ICU.0000000000000451.

[170] J. Fernández De La Mora, On the outcome of the Coulombic fission of a charged isolated drop, J Colloid Interface Sci 178 (1996) 209–218. https://doi.org/10.1006/jcis.1996.0109.

[171] J.F. de la Mora, I.G. Loscertales, The current emitted by highly conducting Taylor cones, J Fluid Mech 260 (1994) 155–184. https://doi.org/10.1017/S0022112094003472.

[172] Y. Wu, J. Du, J. Zhang, Y. Li, Z. Gao, pH Effect on the Structure, Rheology, and Electrospinning of Maize Zein, Foods 12 (2023). https://doi.org/10.3390/foods12071395.

[173] F. Tivano, V. Chiono, Zein as a renewable material for the preparation of green nanoparticles for drug delivery, Frontiers in Biomaterials Science 2 (2023) 1–21. https://doi.org/10.3389/fbiom.2023.1156403.

[174] F. Rodríguez-Félix, C.L. Del-Toro-Sánchez, F. Javier Cinco-Moroyoqui, J. Juárez, S. Ruiz-Cruz, G.A. López-Ahumada, E. Carvajal-Millan, D.D. Castro-Enríquez, C.G. Barreras-Urbina, J.A. Tapia-Hernández, Preparation and Characterization of Quercetin-Loaded Zein Nanoparticles by Electrospraying and Study of In Vitro Bioavailability, J Food Sci 84 (2019) 2883–2897. https://doi.org/10.1111/1750-3841.14803.

[175] N. Bock, T.R. Dargaville, M.A. Woodruff, Electrospraying of polymers with therapeutic molecules: State of the art, Prog Polym Sci 37 (2012) 1510–1551. https://doi.org/10.1016/j.progpolymsci.2012.03.002.

[176] A. Abass, S. Stuart, B.T. Lopes, D. Zhou, B. Geraghty, R. Wu, S. Jones, I. Flux, R. Stortelder, A. Snepvangers, R. Leca, A. Elsheikh, Simulated optical performance of soft contact lenses on the eye, PLoS One 14 (2019) 1–17. https://doi.org/10.1371/journal.pone.0216484.

[177] S.J. Lee, S.M. Park, S.J. Han, D.S. Kim, Electrolyte solution-assisted electrospray deposition for direct coating and patterning of polymeric nanoparticles on non-conductive surfaces, Chemical Engineering Journal 379 (2020) 122318. https://doi.org/10.1016/j.cej.2019.122318.

[178] V. Agrahari, A. Mandal, V. Agrahari, H.M. Trinh, M. Joseph, A. Ray, H. Hadji, R. Mitra, D. Pal, A.K. Mitra, A comprehensive insight on ocular pharmacokinetics, Drug Deliv Transl Res 6 (2016) 735–754. https://doi.org/10.1007/s13346-016-0339-2.

[179] P.A. Newman-Casey, A.L. Robin, T. Blachley, K. Farris, M. Heisler, K. Resnicow, P.P. Lee, The Most Common Barriers to Glaucoma Medication Adherence: A Cross-Sectional Survey, Ophthalmology 122 (2015) 1308–1316. https://doi.org/10.1016/j.ophtha.2015.03.026.

[180] S.A. Davis, B. Sleath, D.M. Carpenter, S.J. Blalock, K.W. Muir, D.L. Budenz, Drop instillation and glaucoma., Curr Opin Ophthalmol 29 (2018) 171–177. https://doi.org/10.1097/ICU.0000000000000451.

[181] R. Gupta, B. Patil, B.M. Shah, S.J. Bali, S.K. Mishra, T. Dada, Evaluating Eye Drop Instillation Technique in Glaucoma Patients, J Glaucoma 21 (2012).

[182] O. Wichterle, O. Lim, Cross-linked hydrophilic polymers and articles made therefrom, 1965. https://doi.org/US3220960A.

[183] J.H. Choi, Y. Li, R. Jin, T. Shrestha, J.S. Choi, W.J. Lee, M.J. Moon, H.T. Ju, W. Choi, K.C. Yoon, The Efficiency of Cyclosporine A-Eluting Contact Lenses for the Treatment of Dry Eye, Curr Eye Res 44 (2019) 486–496. https://doi.org/10.1080/02713683.2018.1563702.

[184] Chak.Hin. Tam, M.S. Alexander, S. Qi, Precision coating of ocular devices/contact lenses by nanoelectrospray additive printing, Mater Des 219 (2022) 110782. https://doi.org/10.1016/j.matdes.2022.110782.

[185] S. Soltani, P. Zakeri-Milani, M. Barzegar-Jalali, M. Jelvehgari, Fabrication and in-vitro evaluation of ketotifen fumarate-loaded PLGA nanoparticles as a sustained delivery system, Iranian Journal of Pharmaceutical Research 16 (2017) 22–34.

[186] L. Bielory, K.W. Lien, S. Bigelsen, Efficacy and tolerability of newer antihistamines in the treatment of allergic conjunctivitis, Drugs 65 (2005) 215–228. https://doi.org/10.2165/00003495-200565020-00004.

[187] K.S. Lim, C.B. Nau, M.M. O'Byrne, D.O. Hodge, C.B. Toris, J.W. McLaren, D.H. Johnson, Mechanism of Action of Bimatoprost, Latanoprost, and Travoprost in Healthy Subjects. A Crossover Study, Ophthalmology 115 (2008) 790–795. https://doi.org/10.1016/j.ophtha.2007.07.002.

[188] J.R. Franca, L.D. Batista, T.G. Ribeiro, C. Fernandes, R.O. Castilho, A.A.G. Faraco, Development and Validation of a High Performance Liquid Chromatographic Method for Determination of Bimatoprost in Chitosan-Based Ocular Inserts, Anal Lett 48 (2015) 531–540. https://doi.org/10.1080/00032719.2014.947533.

[189] P.P. Patel, P.P. Patel, P. Giram, Bioanalytical Method Development and Validation for Latanoprost Quantification in Pharmaceutical Opthalmic Microemulsion Formulation by RP-HPLC, J Anal Bioanal Tech 6 (2015). https://doi.org/10.4172/2155-9872.1000284.

[190] F.A. Maulvi, H.H. Choksi, A.R. Desai, A.S. Patel, K.M. Ranch, B.A. Vyas, D.O. Shah, pH triggered controlled drug delivery from contact lenses: Addressing the challenges of drug leaching during sterilization and storage, Colloids Surf B Biointerfaces 157 (2017) 72–82. https://doi.org/10.1016/j.colsurfb.2017.05.064.

[191] Ketotifen, British National Formulary (2022). https://bnf.nice.org.uk/drug/ketotifen.html (accessed October 3, 2022).

[192] Bimatoprost, British National Formulary (2022). https://bnf.nice.org.uk/drugs/bimatoprost/ (accessed October 3, 2022).

[193] Latanoprost, British National Formulary (2022). https://bnf.nice.org.uk/drugs/latanoprost/ (accessed October 3, 2022).

[194] M. Jafari-Nodoushan, J. Barzin, H. Mobedi, Size and morphology controlling of PLGA microparticles produced by electro hydrodynamic atomization, Polym Adv Technol 26 (2015) 502–513. https://doi.org/10.1002/pat.3480.

[195] M.K. Rahman, T.H. Phung, S. Oh, S.H. Kim, T.N. Ng, K.S. Kwon, High-Efficiency Electrospray Deposition Method for Nonconductive Substrates: Applications of Superhydrophobic Coatings, ACS Appl Mater Interfaces 13 (2021) 18227–18236. https://doi.org/10.1021/acsami.0c22867.

[196] A.F. Pereira-da-Mota, C.M. Phan, A. Concheiro, L. Jones, C. Alvarez-Lorenzo, Testing drug release from medicated contact lenses: The missing link to predict in vivo performance, Journal of Controlled Release 343 (2022) 672–702. https://doi.org/10.1016/j.jconrel.2022.02.014.

[197] M. Bajgrowicz, C.M. Phan, L.N. Subbaraman, L. Jones, Release of ciprofloxacin and moxifloxacin from daily disposable contact lenses from an in vitro eye model, Invest Ophthalmol Vis Sci 56 (2015) 2234–2242. https://doi.org/10.1167/iovs.15-16379.

[198] D.N. Kapoor, A. Bhatia, R. Kaur, R. Sharma, G. Kaur, S. Dhawan, PLGA: A unique polymer for drug delivery, Ther Deliv 6 (2015) 41–58. https://doi.org/10.4155/tde.14.91.

[199] Q. Zhu, H. Cheng, Y. Huo, S. Mao, Sustained ophthalmic delivery of highly soluble drug using pH-triggered inner layer-embedded contact lens, Int J Pharm 544 (2018) 100–111. https://doi.org/10.1016/j.ijpharm.2018.04.004.

[200] P. Mehta, A.A. Al-Kinani, R. Haj-Ahmad, M.S. Arshad, M.W. Chang, R.G. Alany, Z. Ahmad, Electrically atomised formulations of timolol maleate for direct and on-demand ocular lens coatings, European Journal of Pharmaceutics and Biopharmaceutics 119 (2017) 170–184. https://doi.org/10.1016/j.ejpb.2017.06.016.

[201] M.Z.I. Khan, Ž. Prebeg, N. Kurjaković, A pH-dependent colon targeted oral drug delivery system using methacrylic acid copolymers. I. Manipulation of drug release using Eudragit® L100-55 and Eudragit® S100 combinations, Journal of Controlled Release 58 (1999) 215–222. https://doi.org/10.1016/S0168-3659(98)00151-5.

[202] C. Martínez-Sancho, R. Herrero-Vanrell, S. Negro, Study of gamma-irradiation effects on aciclovir poly(D,L-lactic-co- glycolic) acid microspheres for intravitreal administration, Journal of Controlled Release 99 (2004) 41–52. https://doi.org/10.1016/j.jconrel.2004.06.004.

[203] A.E. Ross, L.C. Bengani, R. Tulsan, D.E. Maidana, B. Salvador-Culla, H. Kobashi, P.E. Kolovou, H. Zhai, K. Taghizadeh, L. Kuang, M. Mehta, D.G. Vavvas, D.S. Kohane, J.B. Ciolino, Topical sustained drug delivery to the retina

with a drug-eluting contact lens, Biomaterials 217 (2019). https://doi.org/10.1016/j.biomaterials.2019.119285.

Appendix
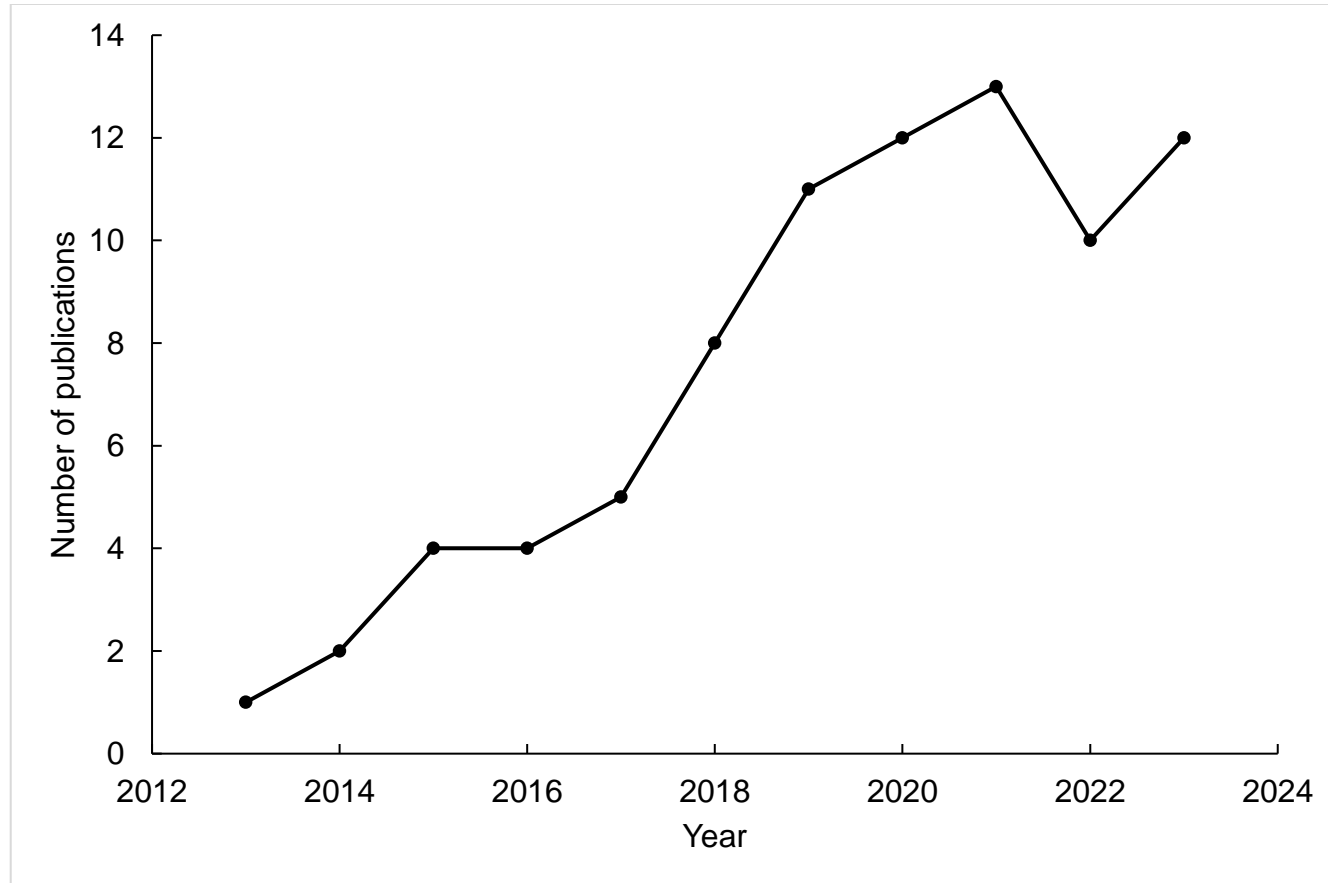
Figure A. 1 *The search result on PubMed of the number of publications of personalised orodispersible films from 2013 to 2023*
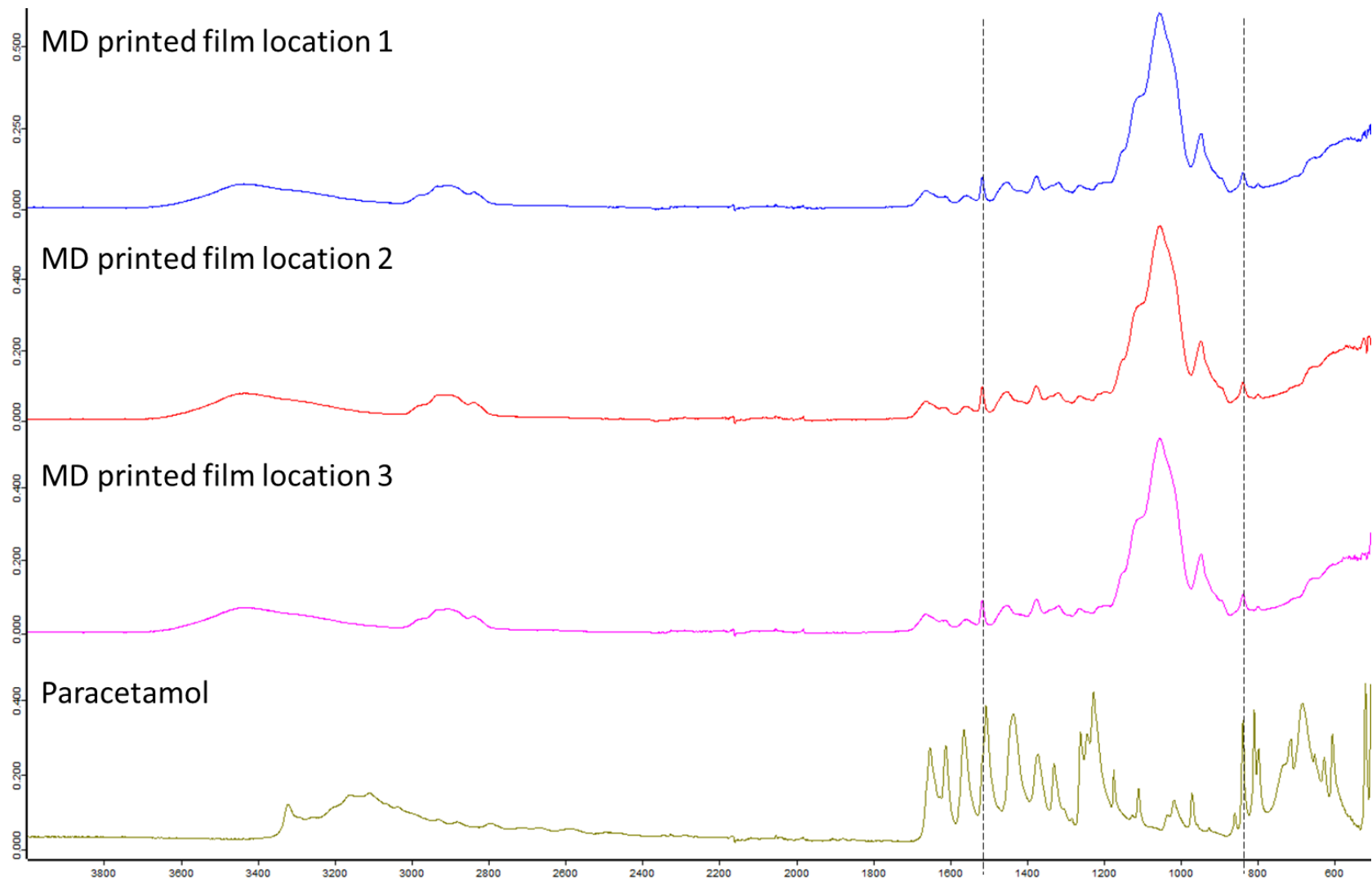
Figure A. 2 *ATR-FTIR spectra of MD printed drug-loaded ODFs with eight printing cycles at random locations. The dash lines indicate the characteristic peaks from paracetamol*
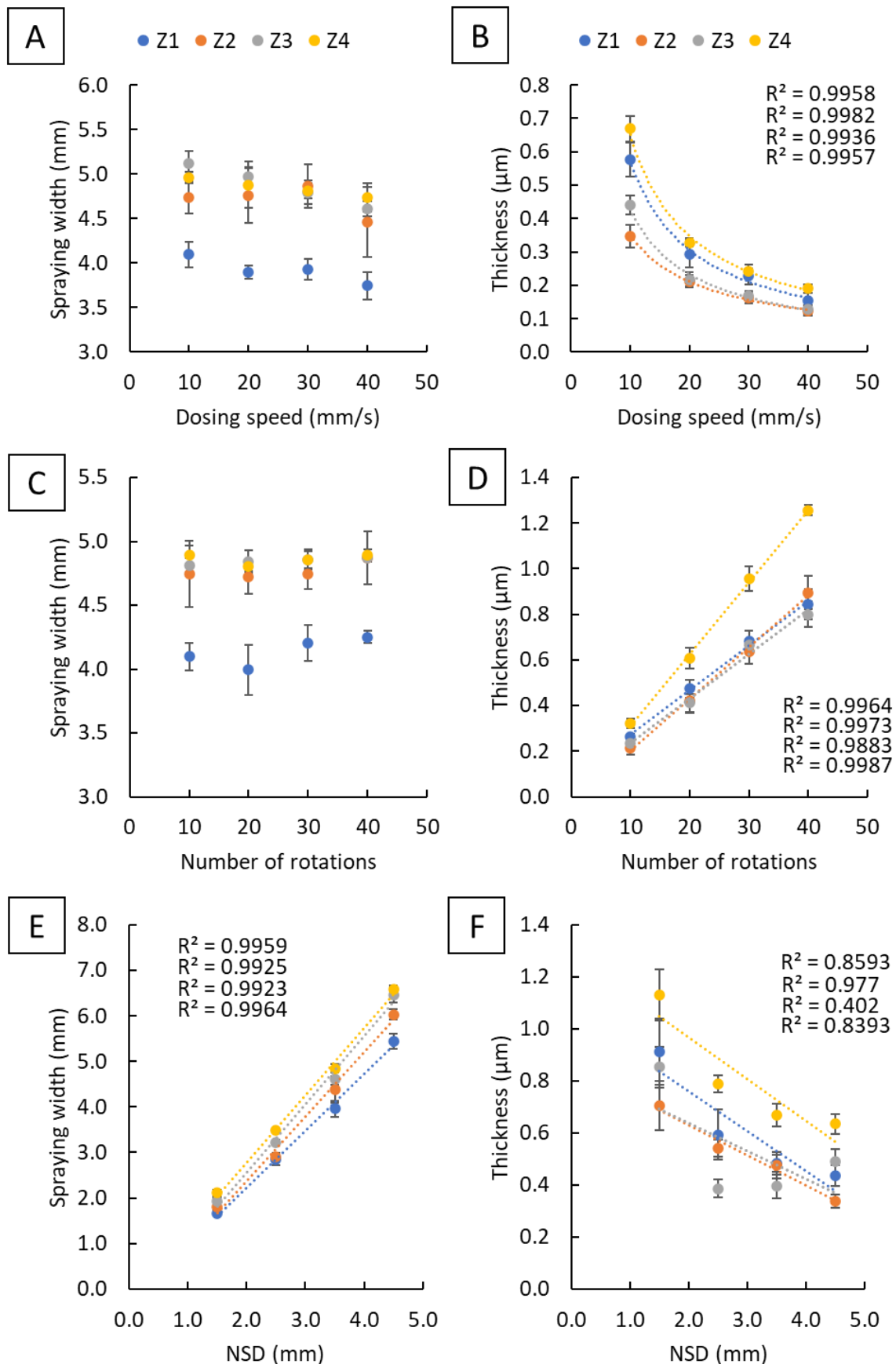
Figure A. 3 The effect of spraying parameters on the spraying width and film thickness of Z1, Z2 (2.5% w/v), Z3 and Z4 (5% w/v). (A-B) nES dosing speed, (C-D) number of rotations and (E-F) nES NSD.